TAMPEREEN TEKNILLINEN YLIOPISTO
TAMPERE UNIVERSITY OF TECHNOLOGY

Jari Leppäaho

MPP-Tracking DC-DC Converters in Photovoltaic Applications

Implementation, Modeling and Analysis

Julkaisu 995 • Publication 995

Tampere 2011

Tampereen teknillinen yliopisto. Julkaisu 995
Tampere University of Technology. Publication 995

Jari Leppäaho

MPP-Tracking DC-DC Converters in Photovoltaic Applications

Implementation, Modeling and Analysis

Thesis for the degree of Doctor of Science in Technology to be presented with due permission for public examination and criticism in Rakennustalo Building, Auditorium RG202, at Tampere University of Technology, on the 18th of November 2011, at 12 noon.

Tampereen teknillinen yliopisto - Tampere University of Technology
Tampere 2011

ISBN 978-952-15-2667-1 (printed)
ISBN 978-952-15-2702-9 (PDF)
ISSN 1459-2045

Abstract

This thesis provides a comprehensive study of switched-mode dc-dc converters in terms of dynamic characterization, implementation and operational constraints. The study concentrates on the maximum-power-point-tracking converters used in photovoltaic interfacing in order to maximize the power generation. The main objective is to emphasize the differences between the four basic conversion schemes and to analyze the dynamical characteristics of the current-fed converters.

Harvesting of solar energy directly into electrical energy is known to be challenging due to the highly varying terminal characteristics of the energy harvesting unit, i.e., generally a photovoltaic generator. The environmental conditions as well as the load determine its characteristics. The operation point of PV generator has to be kept at its maximum-power point in order to maximize the harvested energy. The dc-dc switched-mode converters are conventionally used to interface the energy sources possessing constant-voltage behavior such as batteries or voltage buses but the same converters are also used as a basis for the maximum-power-point-tracking devices. It is observed, however, that such voltage-fed converters are not capable of interfacing a photovoltaic generator optimally because of its current-source nature. Therefore, an additional capacitor is usually added between the source and converter to enhance the constant-voltage properties of the source and to enable the input-voltage-based feedback control. It is known that the dual nature of PV generator enables the use of either input-voltage or input-current feedback control. It is observed, that the input-current control is prone to saturation of the controller and therefore, the input-voltage control is recommended to be used. The use of input-voltage control will, however, force the converter operate as a current-fed converter causing also significant changes to its static and dynamic properties as well as constraints related to the voltage-fed converters in photovoltaic interfacing.

This thesis presents the generalized dynamic representation of a switched-mode dc-dc converter which can be applied to analyze all possible conversion schemes. The representation makes a clear distinction between the voltage-fed and current-fed conversion schemes and their stability assessment. It is also shown that the current-fed converters can be implemented by applying three different methods based either on intuition, explicit duality transformation or adding a capacitor at the input terminal of a conventional voltage-fed converter. The study includes dynamic characterizations that have not been presented earlier.

Preface

This work was carried out at Department of Electrical Energy Engineering at Tampere University of Technology (TUT) during years 2008-2011. The research was funded by TUT, Graduate School in Electrical Engineering and ABB Oy. Financial supports in the form of personal grants from the Finnish Foundation for Economic and Technology Sciences - KAUTE, Fortum Foundation, Emil Aaltonen Foundation and Ulla Tuominen Foundation are greatly appreciated.

First of all, I want to express my greatest gratitude to Professor Teuvo Suntio for supervising my thesis and providing an interesting research topic and inspiring environment to conduct research. It has been a great pleasure to work under his guidance. My colleagues, Juha Huusari, M.Sc., Anssi Mäki, M.Sc., Lari Nousiainen, M.Sc., Joonas Puukko, M.Sc., Tuomas Messo, M.Sc., and Diego Torres Lobera, M.Sc., deserve special thanks for their help in countless professional matters but also for the hilarious moments in the corridors of our department. I am very thankful for Professors Jian Sun and Mummadi Veerachary for examining my thesis and their constructive comments that improved the quality of my thesis. I would also like to thank Matti Karppanen, Dr.Tech., for helping me with the dynamic analyses and practical measurements at the beginning of my research work, Tomi Roinila, Dr.Tech., for the Matlab scripts that helped me with the simulations, Mr. Pentti Kivinen for building the lamp unit used in the experiments, and all the personnel in the Department of Electrical Energy Engineering for the pleasant working environment. I would also like to thank Sirpa Järvensivu for proofreading my thesis.

Finally, I want to thank my parents, sisters and brothers, my parents-in-law and especially my loving wife Iina for all the support, encouragement and patience during my studies and life.

Espoo, October 2011

Jari Leppäaho

Contents

List of Publications

The thesis is based on the following publications, which are referred to as P1, P2, P3, P4, P5, P6, P7 and P8 in the text.

[P1] Suntio, T., Huusari, J., and Leppäaho, J., "Issues on solar-generator-interfacing with voltage-fed MPP-Tracking converter," *European Power Electronics and Drives Association Journal*, vol. 20 no. 3, pp. 40-47, September 2010.

[P2] Suntio, T., Leppäaho, J., Huusari, J., and Nousiainen, L., "Issues on solar-generator-interfacing with current-fed MPP-Tracking converter," *IEEE Transactions on Power Electronics*, vol. 25, no. 9, pp. 2409 - 2419, September 2010.

[P3] Leppäaho, J., Huusari, J., Nousiainen, L., Puukko, J., and Suntio., T., "Dynamic properties and stability assessment of current-fed converters in photovoltaic applications," *IEEJ Transactions on Industry Applications*, vol. 131, no. 8, pp. 976-984, 2011.

[P4] Leppäaho, J., Karppanen, M., and Suntio, T., "Current-sourced buck converter," *Nordic Workshop on Power and Industrial Electronics*, NORPIE'08, Espoo, Finland, 7 p., 2008.

[P5] Leppäaho, J., and Suntio, T., "Solar-generator-interfacing with a current-fed superbuck converter implemented by duality-transformation methods," *International Power Electronics Conference*, IPEC'10, Sapporo, Japan, pp. 680 – 687, 2010.

[P6] Leppäaho, J., and Suntio, T., "Dynamic characteristics of current-fed superbuck converter," *IEEE Transactions on Power Electronics*, vol. 26, no. 1, pp. 200 - 209, January 2011.

[P7] Leppäaho, J., Nousiainen, L., Puukko, J., Huusari J., and Suntio T., "Implementing current-fed converters by adding an input capacitor at the input of voltage-fed converter for interfacing solar generator," *International Power Electronics and Motion Control Conference*, EPE-PEMC'10, Ohrid, Macedonia, pp. T12-81 - T12-88, 2010.

[P8] Leppäaho, J., and Suntio, T., "Dynamic properties of PCM-controlled current-fed boost converter in photovoltaic system interfacing," *European Conference on Power Electronics and Applications*, EPE'11, Birmingham, United Kingdom, 10 p., 2011.

Author's Contribution

The author planned and performed the experimental tests and participated in the dynamic analysis in [P1] and [P2]. Publications [P3] - [P8] are mainly contributed by the author. Professor Teuvo Suntio, the supervisor of the thesis, gave many constructive and important comments regarding these publications. The other co-authors helped with the dynamic analyses and practical experiments.

Symbols and Abbreviations

Symbols

$\mathbf{A}$	Coefficient matrix
$\mathbf{B}$	Coefficient matrix
$\mathbf{C}$	Coefficient matrix
C	Capacitor
C	Capacitance
c	General control variable
c_{pv}	Capacitance of photovoltaic cell
$\hat{c}$	Perturbed control variable
$\mathbf{D}$	Coefficient matrix
D	Diode
D	Average of duty-ratio
D'	Complement of average of duty-ratio, i.e. $D' = 1 - D$
d	Instantaneous duty-ratio
d'	Complement of instantaneous duty-ratio, i.e. $d' = 1 - d$
$\hat{d}$	Perturbed duty-ratio
$\hat{e}_{\text{o}}$	Ideal perturbed voltage
f_{s}	Switching frequency
$\mathbf{G}$	General transfer function matrix
G_{ij}	Entry of general transfer function matrix
G_{a}	Modulator gain factor
$G_{\text{c-in}}$	Input-side controller transfer function
G_{ci}	Control-to-input transfer function
$G_{\text{c-out}}$	Output-side controller transfer function
G_{co}	Control-to-output transfer function
G_{ij}	Entry of general transfer function matrix
G_{io}	Input-to-output transfer function
$G_{\text{io-}\infty}$	Ideal input-to-output transfer function
$G_{\text{s-in}}$	Input sensing gain factor
$G_{\text{s-out}}$	Output sensing gain factor
$\mathbf{I}$	Unit matrix
I	Average current
I_{s}	Average saturation current

i	Instantaneous current
i_{cpv}	Instantaneous current through photovoltaic cell capacitance
i_{d}	Instantaneous diode current
i_{pv}	Instantaneous photovoltaic current
i_{sc}	Instantaneous short-circuit current
i_{rsh}	Instantaneous current through shunt resistor
$\hat{i}$	Perturbed current
$\langle i \rangle$	Time averaged current
$\hat{j}$	Perturbed current of ideal current sink
L	Load subsystem
L	Inductor
L	Inductance
L	Loop gain, entry of load subsystem transfer function matrix
M_{c}	Inductor-current slope compensation
p_{pv}	Power of photovoltaic cell
Q	Transistor (switch) or flip-flop output
!Q	Negation of flip-flop output
R	Flip-flop reset
R, r	Resistor
R, r	Resistance
$\mathrm{R_s}$	Sensing resistor
$\mathrm{r_d}$	Parasitic resistor of diode (dynamic resistance)
$\mathrm{r_{ds}}$	Parasitic resistor of switch (dynamic resistance)
$\mathrm{r_{pv}}$	Dynamic resistance of photovoltaic cell
$\mathrm{r_s}$	Series resistance
$\mathrm{r_{sh}}$	Shunt resistance
S	Source subsystem
S	Flip-flop set
S	Switch, entry of subsystem transfer function matrix
s	Laplace variable
T_{oi}	Output-to-input transfer function
$T_{\mathrm{oi}\text{-}\infty}$	Ideal output-input transfer function
T_{s}	Length of switching period
U	Input variable vector in Laplace domain
u	Input variable vector in time domain
U	Average voltage

U_{mpp}	Maximum power point voltage
U_{pv}	Average photovoltaic voltage
U_{T}	Average thermal voltage
u	Instantaneous voltage
u_{r}	Reference voltage
$\hat{u}$	Perturbed voltage
$\langle u \rangle$	Time averaged voltage
$\mathbf{X}$	State variable vector in Laplace domain
$\mathbf{x}$	State variable vector in time domain
x	General input variable
$\mathbf{Y}$	Output variable vector in Laplace domain
$\mathbf{y}$	Output variable vector in time domain
y	General output variable
Y	Admittance
Y_{in}	Input admittance
$Y_{\mathrm{in\text{-}oco}}$	Input admittance at open-circuited output terminal
$Y_{\mathrm{in\text{-}sco}}$	Input admittance at short-circuited output terminal
$Y_{\mathrm{in\text{-}\infty}}$	Ideal input admittance
Y_{o}	Output admittance
$Y_{\mathrm{o\text{-}oci}}$	Output admittance at open-circuited input terminal
$Y_{\mathrm{o\text{-}sci}}$	Output admittance at short-circuited input terminal
Y_{o}	Output admittance
Y_{S}	Source admittance
Z	Impedance
Z_{in}	Input impedance
$Z_{\mathrm{in\text{-}oco}}$	Input impedance at open-circuited output terminal
$Z_{\mathrm{in\text{-}sco}}$	Input impedance at short-circuited output terminal
$Z_{\mathrm{in\text{-}\infty}}$	Ideal input impedance
Z_{o}	Output impedance
$Z_{\mathrm{o\text{-}oco}}$	Output impedance at open-circuited output terminal
$Z_{\mathrm{o\text{-}sco}}$	Output impedance at short-circuited output terminal
η	Ideality factor, efficiency

Subscripts

-1	Refers to switch position 1
-2	Refers to switch position 2
C	Refers to capacitor
c	Refers to current compensation slope or controller
ci	Refers to control-to-input transfer function
co	Refers to control-to-output transfer function
-c	Refers to closed loop
mpp	Refers to maximum-power point
L	Refers to inductor or load
io	Refers to input-to-output transfer function
in, -in	Refers to input
ins	Refers to ideal input energy source
o, -out	Refers to output
oi	Refers to output-to-input transfer functions
-o	Refers to open loop
-oc , oc	Refers to open circuit
-oco	Refers to open-circuited output terminal
off	Refers to switch off-state
on	Refers to switch on-state
-sc , sc	Refers to short circuit
-sco	Refers to short-circuited output terminal
S	Refers to energy source
s	Refers to sensing element
d	Refers to diode
-∞	Refers to ideal transfer function

Superscripts

-1	Inversed matrix
D	Refers to dual transformation
g	Refers to G parameters or voltage-to-voltage conversion scheme
h	Refers to H parameters or current-to-current conversion scheme
y	Refers to Y parameters or voltage-to-current conversion scheme
z	Refers to Z parameters or current-to-voltage conversion scheme

Abbreviations

AC, ac	Alternating current
CC	Constant current
CF	Current fed
CV	Constant voltage
CCM	Continuous conduction mode
DC, dc	Direct current
DCM	Discontinuous conduction mode
KCL	Kirchhoff's current law
KVL	Kirchhoff's voltage law
MOSFET	Metal-oxide semiconductor field effect transistor
MPP	Maximum power point
MPPT	Maximum power point tracking
OC	Open circuit
PCM	Peak-current mode
PV	Photovoltaic
PWM	Pulse width modulation
RHP	Right-half plane
SC	Short circuit
SMES	Superconductive magnetic energy storage
SSA	State-space averaging
VF	Voltage fed

1 Introduction

This chapter presents the essential background of the thesis and motivation for conducting the research. The configurations and properties of photovoltaic (PV) energy systems and the basic dc-dc interfacing techniques based on switched-mode converters are introduced. The literature survey of previous research is performed and the recent knowledge of the interfacing methods and issues in PV energy systems are discussed. Finally, the structure, objectives and the scientific contribution of the thesis are stated.

1.1 Photovoltaic Energy Systems

The wide utilization of nature's energy reserves has had a very important role in developing our modern civilization. As a consequence, mankind is now more dependent on energy than ever. The development has been extremely fast since the industrial revolution initiated in the 18^{th} century when the non-renewable fossil fuels, such as coal and oil, were started to be exploited more extensively [1]. The unpleasant fact is, however, that such a development would inevitably run our planet out of fossil energy resources. Unfortunately, this was first realized as late as in the 1970s when the first oil crises occurred. The increased oil prices developed a sudden interest towards alternative energy sources to substitute part of the conventional energy production. As a consequence, the utilization of renewable energy sources, such as wind and solar, started to increase [2],[3]. Today, the oil price is just one motivating factor to seek new alternatives or develop further the existing renewable energy technologies. The green politics and the awareness of human impact on Earth have opened new perspectives in the energy business and formidable increase in the utilization of renewable energy sources; the concern about climate change, CO_2 emissions as well as the pollution are strong driving forces to develop environmentally friendly and sustainable solutions for the energy generation [1]-[3].

The solar or PV energy is recognized as one of the promising ways to secure the availability of energy and also to decrease the observed emissions and pollution [4]. The sun is an immense energy resource but only a fraction of its capacity is utilized: the

energy it provides during one hour would cover the yearly energy consumption of the whole world [5]. The idea of large-scale harvesting of solar energy is reasonable but it also needs efforts in other fields of technologies such as interfacing techniques. Power electronic devices possess the feature of high efficiency and they are already widely used in the conventional power conditioning and grid interfacing units. Thus, power electronics plays a key role also in the successful utilization of renewable energy sources [1].

Photovoltaics is a branch of solar energy technology in which the light is converted directly into electricity. Its history dates back to the mid-1800s when the relation between the light and electric potential was observed for the first time. The first PV cells were based on e.g. selenium providing impractically low conversion efficiency. As the silicon technology developed fast after the mid-1900s, it was eventually observed that the silicon-based pn-junction could provide much higher conversion efficiency than any material earlier [6],[7]. Efficiencies more than 20 % have been achieved with silicon cells (theoretical maximum for silicon is approximately 30 % [8]) and even up to 40 % with new multi-junction techniques utilizing elements such as gallium and indium [9]. Nevertheless, most of the commonly used PV cells are based on silicon because modern microelectronics is highly silicon orientated and the manufacturing processes are well known. Since the efficiency of the PV cell itself is rather low, the interfacing and energy storing techniques must be as efficient as possible to maximize the amount of harvested solar energy.

A single PV cell is basically a direct current (dc) source, where the current is determined by the area of the cell and the amount of exposed solar irradiation. The voltage of an individual silicon cell is in the order of 0.5 V. Thereby, the cells have to be connected in series to constitute modules (also known as panels) with reasonable voltage levels. The resulting modules have basically the same characteristics as the single cell [10]. The modules are usually grouped into larger entities of series connections (i.e. strings) in order to constitute, for example, a PV generator of several kilowatts. An efficient PV power generation also requires that a certain maximum-power point (MPP) of the PV generator is located. The maximum power is delivered at the operation point, where the magnitudes of the PV generator and load circuit resistances are equal [11]. This is usually performed by an interfacing dc-dc power converter employing certain MPP-tracking techniques and algorithms [12]-[15]. The operation point is held at the MPP by regulating either the current or voltage of the MPP-tracking converter. Smaller and inexpensive PV systems may not include the power maximizing facilities at all but just a simple regulator, where the power flow is adjusted e.g. according to the state of battery charge [10].

The basic elements of the PV power conditioning system are the dc-dc converter, single-stage dc-ac converter (inverter) and double-stage inverter shown in Fig. 1.1a-c [16]-[20]. If the purpose is to charge a battery or regulate a dc-bus as in space and telecom applications [19],[20], the system can be implemented by using only the dc-dc converters as depicted in Fig. 1.1a. The battery or bus voltage can be further regulated by other point-of-load converters. If the PV system is to be connected to the ac-grid (alternating current), the power conditioning unit requires a dc-ac conversion [16]-[18]. This can be implemented by using either single or double-stage inverter as depicted in Figs. 1.1b-c. In the single-stage inverter (Fig. 1.1b), a single dc-ac converter regulates the PV voltage/current and takes care of the grid connection. In the double-stage inverter (Fig. 1.1c), the dc-dc converter regulates the PV voltage/current and the second-stage dc-ac converter only performs the grid connection.

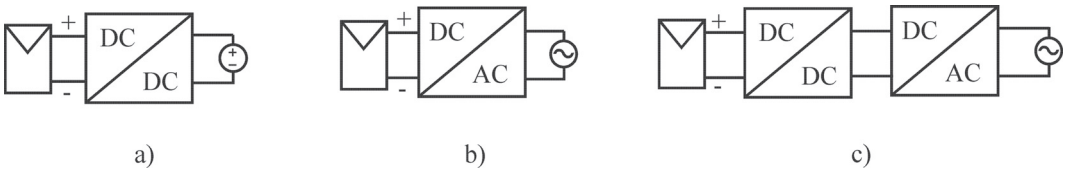

Fig. 1.1 Basic elements of a power conditioning system: a) dc-dc converter, b) single-stage inverter and c) double-stage inverter.

Conventionally, the PV energy systems have been based on centralized MPP-tracking as depicted in Fig. 1.2. The configuration in Fig. 1.2a is based on one MPP-tracking central inverter connected to a very large array of strings. This configuration is typical for large PV power plants and was frequently used in the past. The expanding of this kind of PV power plant may be problematic because the dimensioning of the existing central inverter may not comply with the expanded array. Thereby, these systems are being substituted by string inverter configurations as depicted in Fig. 1.2b [16]. This configuration is based on MPP-tracking string inverter that can be paralleled in order to expand the PV power plant.

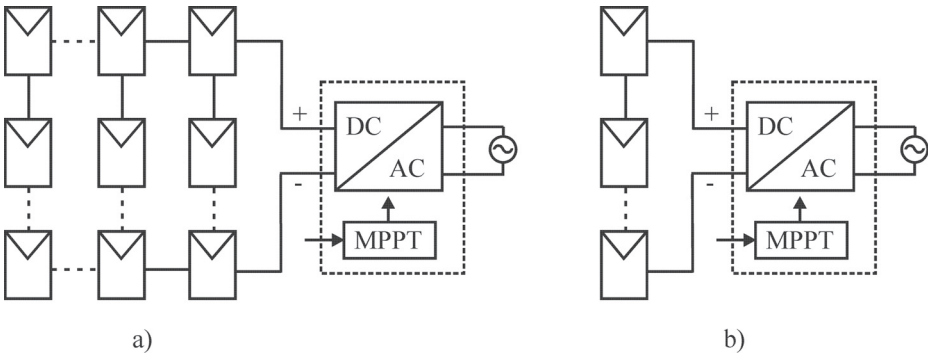

Fig. 1.2 Centralized MPP-tracking: a) array central inverter and b) string inverter.

It is well known, however, that centralized MPP-tracking does not always optimize energy production. The current and hence the energy production of the string may be significantly decreased even if just one of the PV modules is shaded in the string [21]-[23]. This kind of partial shading is typically handled by adding one or several bypass diodes in each module. However, the shaded and bypassed modules result in multiple local MPPs that complicate the MPP-tracking process and the operation point may drift far from the global MPP.

The energy losses caused by partial shading can be minimized by utilizing distributed MPP-tracking techniques based on modular structures as shown in Fig. 1.3 [24]-[30]. The main idea is to keep the operation point of each module at its own MPP regardless of the other components in the system. Thereby, the overall energy production is maximized. The configurations in Figs. 1.3a-b are based on parallel and series connections of module-integrated dc-dc converters that trace the MPPs of the individual modules [24]-[27] of which grid connection is carried out by a common inverter without the MPP-tracking facilities. The micro-inverter system shown in Fig. 1.3c represents even higher modularity [28]-[30]; the direct grid-connection is possible because the dc-ac converter is integrated into each PV module.

Regardless of the benefits distributed MPP-tracking provides, it increases the amount of power electronics in the system. Consequently, there may be complex interconnected structures resulting in stability problems. The interface between the dc-dc and dc-ac converters in Figs. 1.3a-b, for example, is crucial from the stability point of view due to the interacting input and output impedances of the converters.

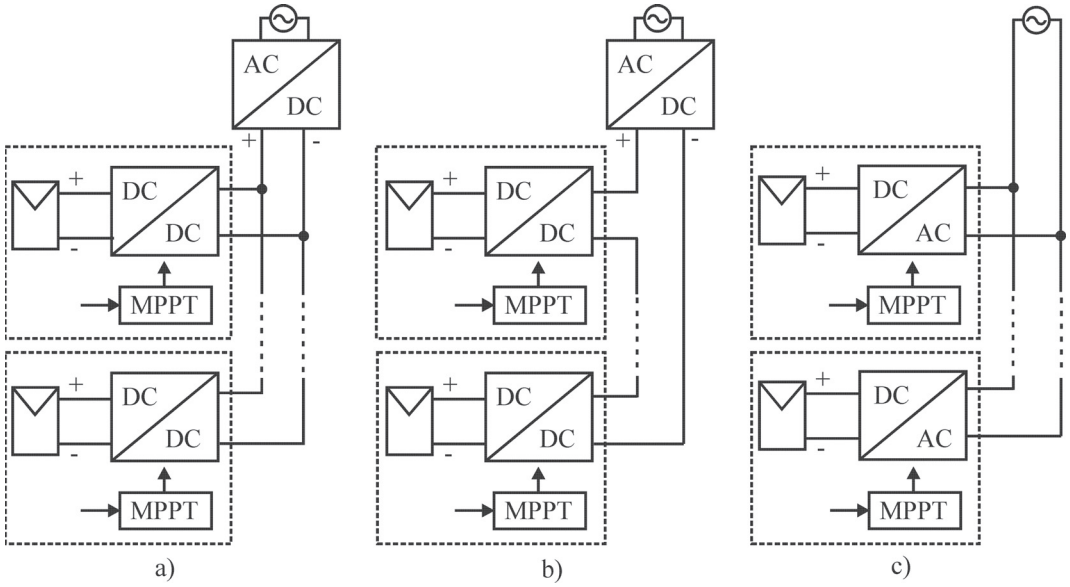

Fig. 1.3 Distributed MPP-tracking: a) parallel MPP-tracking dc-dc converters, b) series MPP-tracking dc-dc converters and c) MPP-tracking micro-inverter configuration.

1.2 Issues Regarding Photovoltaic DC-DC Interfacing

The existing energy delivery system was built to support centralized power generation in large power plants connected to high voltage transmission network. The electricity is then delivered into a distribution network and further to domestic consumers. PV energy can be generated in the conventional units but it also supports a decentralized or distributed power generation as well as many other renewable technologies [31]-[33]. As a consequence, the small-scale PV systems connected to the distribution network or even domestic electrical micro-grids have become common. The support mechanisms, such as green certificates and feed-in tariffs, further encourage new investments towards such development [34],[35]. Stand-alone or off-grid PV systems have become more common as well because of their ability to provide a solution for remote and rural areas without the main delivery of electrical energy [36],[37]. In some locations or applications, such as orbital space satellites, stand-alone power generation may be the only way to electrify the system. As a matter of fact, space industry provided the first applications which actually utilized PV energy [6]. The increased distributed and off-grid power generation has its drawbacks as well. Such power generation schemes may result in complex grid structures and cause unexpected problems regarding safety and protection as well as regulatory matters [33],[38]. The requirements for the off-grid systems are naturally high and supporting energy storages and generation are usually needed [10].

A fault in a small domestic PV system may not be crucial but the consequences of a malfunction in more critical PV systems, such as large-scale grid-connected power plant or space craft power conditioner, can be catastrophic. In addition, some of the problems may even be unobservable and cause undesired degradation in the energy production. Indeed, the reliability matters have become a broader problem. The PV modules themselves, however, are rather reliable elements and may have life expectancies from 20 to 30 years as discussed in [39] and [40]. The main concern is usually the interfacing power electronic devices, such as MPP-tracking converter and grid-connected inverter, which are recognized to be the most unreliable units of such systems [41]. Therefore it is extremely important to have consistent information regarding the nature of the energy source, interfacing devices as well as the load connected to the system to avoid the problems already in the design phase.

Electrical loads are usually considered to be current sinks requiring to be fed by voltage sources such as the electrical grid. Consequently, the power supply design is rather voltage orientated and the prevailing power processing systems are based mainly on voltage conversions. There are, however, energy sources which cannot be categorized strictly as voltage sources. A superconductive magnetic energy storage (SMES) [42], for example, is an explicit current source and some other energy sources, such as a fuel cell

and PV cell, may possess highly non-linear characteristics that limit their maximum power and complicate their interfacing [10], [43]-[45].

The PV cell can be considered to be a highly non-linear current source, which has limited output voltage and power as well as distinct constant-current (CC) and constant-voltage (CV) regions. MPP-tracking facilities are required for maximizing the energy at the output as discussed in the previous subsection. The non-linear and non-ideal properties of the PV cell are caused by its physical pn-junction structure. A simplified circuit model can be composed of a current source in parallel with a diode, capacitor and shunt and series resistances as shown in Fig. 1.4a [46]. If the parasitic elements are neglected, the output current can be given according to (1.1) [10],[47].

$$i_{\mathrm{pv}} = i_{\mathrm{sc}} - I_s\left(e^{\frac{u_{\mathrm{pv}}}{\eta U_{\mathrm{T}}}} - 1\right) \tag{1.1}$$

where i_{sc} is the short-circuit (SC) current, I_{s} saturation current of the diode, η diode ideality factor and U_{T} thermal voltage. The short-circuit current is directly proportional to the irradiation and slightly proportional to the level of the cell temperature. The PV terminal capacitance c_{pv}, dynamic resistance r_{pv} and current i_{pv} as well as the power p_{pv} depend significantly on the operation point as shown in Fig. 1.4b [46]-[48]. Static resistance R_{pv}, not shown in Fig. 1.4b, is simply $U_{\mathrm{pv}} / I_{\mathrm{pv}}$ and therefore, dependent on the operating point (in [P1] and [P2] $R_{\mathrm{pv}} = r_{\mathrm{con}}$). The terminal current i_{pv} remains at a somewhat constant level ($i_{\mathrm{pv}} \approx i_{\mathrm{sc}}$) in the CC region up to MPP voltage ($u_{\mathrm{pv}} \approx u_{\mathrm{mpp}}$). The current decreases if the voltage is further increased in the CV region eventually diminishing to zero when the open-circuit (OC) condition is reached.

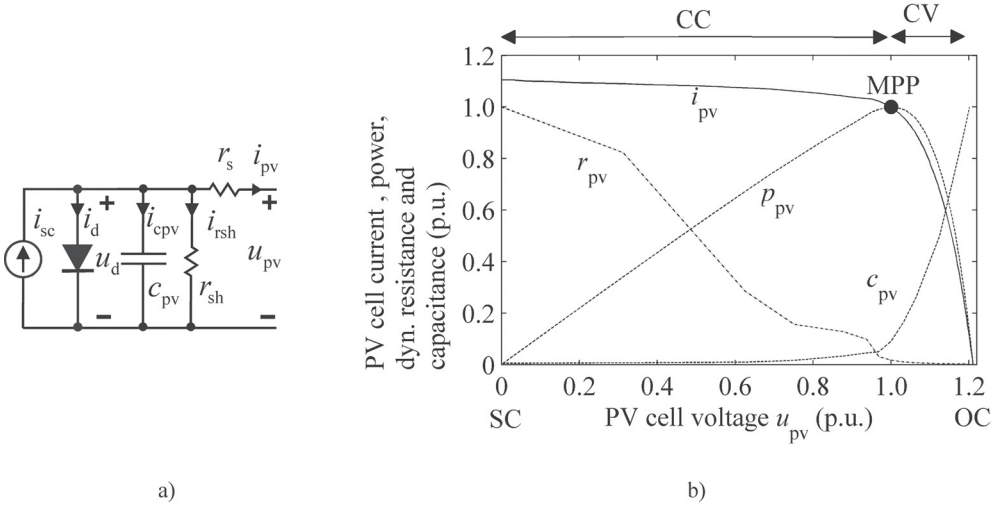

Fig. 1.4 a) Simplified circuit model of a PV cell and b) PV cell output current, power, dynamic resistance and dynamic capacitance as a function of PV cell output voltage (p.u.)

Dc-dc converters are essential elements in the MPP-tracking process. They are usually based either on switched-mode shunt, as in [49] and [50], or series regulation, as in [51]-[68]. The converters can be further classified into two main classes: voltage-fed (VF) and current-fed (CF) converters as discussed in [51]. The naming of the main classes is based on the type of the input energy source, i.e. the VF converter is fed by a voltage source and the CF converter by a current source, respectively. The structure of the VF power stage is based on switching cells which provide current sink at the input [69] and correspondingly, the CF power stage is based on switching structures providing voltage-type input [70]. Naturally, the input energy source and applied input-control methods have to comply with the nature of the input port of converter. The main classes can be further divided into sub-classes based on the applied load (current-sink or voltage-type load) and output-control method (voltage-output or current-output mode). The above mentioned categorizing yields four different conversion types, such as voltage-to-voltage, voltage-to-current, current-to-current and current-to-voltage depicted in Fig. 1.5, which can be dynamically represented by means of the two-port-network parameters known as G, Y, H and Z [71].

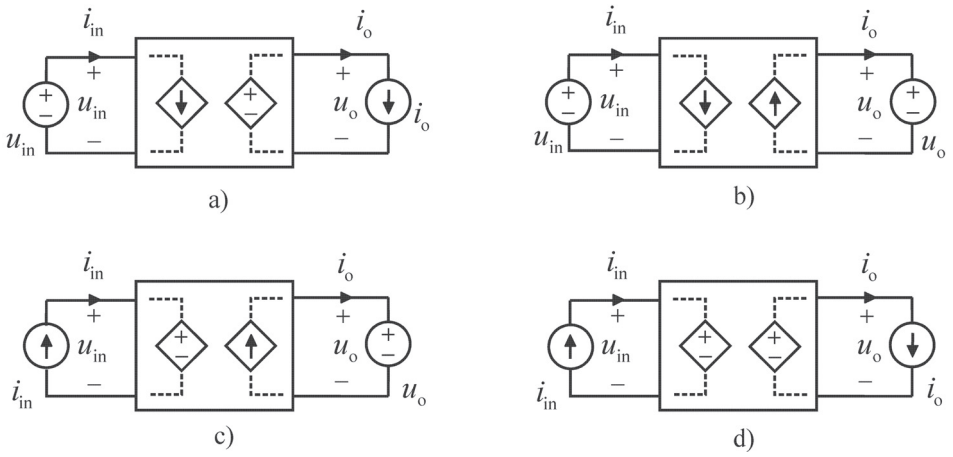

Fig. 1.5 a) Voltage-to-voltage, b) voltage-to-current, c) current-to-current and d) current-to-voltage conversion scheme

The MPP-tracking process of the PV generator can be performed either by controlling the input current or voltage of the interfacing converter because of its dual nature (i.e. current and voltage source [P1],[P2]). It is observed that the current control is prone to saturation, i.e. Kirchhoff's current law is to be violated when the operating point is moved to voltages less than the MPP voltage either by the MPP tracker or by changing environmental conditions. Therefore, the input voltage is recommended to be controlled in order to avoid saturation [52],[53]. The two-port networks in Figs. 1.5a-b imply that the application of input-voltage control in a conventional VF converter would not be feasible because the input voltage is considered a constant variable. The CF converters in

Figs. 1.5c-d, instead, support the input-voltage control because the input voltage is an output variable. This means also that the Kirchhoff's laws are automatically satisfied and the CF converter faces only the topological constraints in respect to the level of input and output voltages [P1],[P2]. The above discussion means also that the PV generator cannot be modeled as a voltage source with its whole range of operation points but only in the CV region applying Thévenin equivalent transformation.

Nevertheless, it seems that the existence of the four conversion schemes, which also define the possible control variables, is not commonly recognized in the PV converter design. The authors in [57] and [58] provide a comprehensive study of MPP-tracking PV systems. The power stages are based on conventional VF converters and, therefore, supporting only input-current control. The constraints related to the input-current control are not covered but instead, the input-voltage control is recommended to be used although it is obviously incompatible with the VF scheme. The current-source nature of PV generator and beneficial properties of the input-voltage control have been recognized in [63] and [64] suggesting the usage of the current-to-current converter. The small-signal modeling in [64] is, however, based on the model fed by a constant-voltage source. Basically, the converter is a voltage-to-current converter and operates in VF domain. The authors in [59] provide a comparative study of basic MPP-tracking dc-dc converters but only the conventional VF converters are covered. The control problem of the MPP-tracking converter is recognized in [68]. The suitability of both input-voltage and input-current control is investigated in conventional VF topologies. It was concluded that the direct control of input current is suitable for all the investigated converters. This is in accordance with the above presented four conversion schemes which state that the input-current control is naturally suitable for VF interfacing. These studies suggest that the VF interfacing is the prevailing technique among PV interfacing applications but also that the differences between the VF and CF domains are not clear.

There are several problems and peculiarities observed to appear in the existing MPP-tracking converters. A limit cycle oscillation discussed in [60] and observable e.g. in [72] is a common problem in the MPP-tracking devices leading e.g. to distorted grid currents discussed [73]. These may become even more serious problems as the distributed PV generation increases further. The PV converter systems are also recognized to be prone to certain types of instabilities as discussed in [54] and [55]. The sudden changes in the irradiation and partial shading of the PV modules are also challenging for the interfacing converters and may lead to problems regarding the system dynamics [21]-[23]. The validation methods of the MPP-tracking converters vary in the public literature as well. In some studies, the actual PV generator is replaced with a power-electronics-based solar array simulator (SAS) [29] or with a pure voltage source [62],[73]. The static IV curve of the SAS may resemble a real PV module but the dynamical behavior may differ from the actual PV module (i.e. incremental resistance and/or capacitance values). The use of a

voltage source as an input energy supply neglects entirely the current-source nature of a real PV module and may give inconsistent information on the behavior of the converter in real application.

The low-frequency small-signal or incremental impedance of a PV module is known to be a positive resistance in both CC and CV regions [23],[46]. However, some authors treat it as a negative resistance in some circumstances [55],[65]. This may cause problems in the stability assessment of the interconnected systems since the input terminal of the interfacing device may resemble negative resistance as well. From the stability assessment point of view, the resistance of the PV module is always positive but the system requires the minus sign in front of the module output resistance because the direction of the current is outwards from the source. In some publications, as e.g. in [58] and [59], a pure resistor is used as a converter load instead of a large capacitor bank or battery. This may be convenient and ease the practical measurements but it may also hide internal dynamics of the converter and lead to misinterpretations regarding the stability issues as discussed in [P2].

PV interfacing is challenging task and there is a need for clarification of the existing dc-dc converter topologies used in the PV applications. The problem seems to be the duality transformation which is applied to electric circuits already in the late 1960s [74]. The duality suggests that any electrical circuit can be transformed to its dual circuit, and the switched-mode power converters are no exceptions. In fact, the duality-based converters have been introduced since the 1970s [75]-[81] and proposed to be used e.g. in SMES and PV interfacing or in other current-source applications. Most often the duality concept is utilized to produce just another type of conventional converter from the original conventional converter as in [79]. The famous Ćuk converter, for example, is a dual of the conventional buck-boost converter [75], but considered to be a voltage converter, because the power stage also includes an additional input inductor and output capacitor recovering the VF properties.

It is worth noticing that the definition ‘current-sourced’ used in the literature very seldom corresponds to ‘current-fed’ converters discussed in this thesis. It is common to name a dc-dc converter ‘current-sourced’ if it has an input inductor but is still fed by a voltage source [82]. This structure is considered a current source [83],[84]. Basically, those converters are still conventional VF converters and, to avoid any confusion, the prefixes ‘voltage-fed’ and ‘voltage-sourced’ or ‘current-fed’ and ‘current-sourced’ should be used according to the actual input energy source of the converter. The duality also divides the conduction modes and control principles into VF and CF domains. The conventional continuous and discontinuous conduction modes (CCM and DCM) refer to inductor currents but in CF domain they refer to capacitor voltages [79]. The basic feedback control of a switched-mode converter is implemented by controlling the

switching duty ratio directly. Conventionally, this is called either direct-duty-ratio (DDR) or voltage-mode (VM) control. The possible inner-loop control is usually implemented from the current of the inductor, i.e. current-mode (CM) control. The CM control is not a property of CF domain where the inner-loop control should be implemented from the voltage of the capacitor. According to this context, the 'voltage-mode' or 'VM' control should refer only to inner-loop control of the capacitor voltage and 'DDR' universally to direct-duty-ratio control.

Fig. 1.6 introduces the dual pairs of certain circuit structures and elements used commonly in the converter circuits [78]. The conducting switch transforms to non-conducting switch, voltage sources to current sources, inductive elements to capacitive elements, open circuits to short circuits and *vice versa*. Consequently, the duality transformation changes the VF converter explicitly to its dual, a CF converter. The terminology for the duality-derived CF topologies can be consistently adopted from the original VF scheme. A conventional VF buck converter, for example, steps down the voltage, i.e. an input voltage provided by a constant voltage source is converted according to the duty ratio. Similarly, a CF buck steps down the current, i.e. an input current provided by a constant current source is converted according to the duty ratio as discussed in [P4].

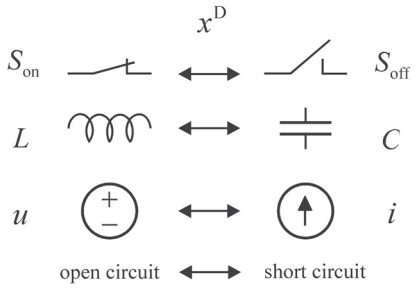

Fig. 1.6 Duality transformation of certain circuit structures and elements

The duality-derived CF converters have not become common although the PV or any current-based interfacing could benefit from them. This is partly understandable seeing as voltage-orientated systems dominate the electronics and power generation. The need of CF properties in PV interfacing is, however, recognized but they are usually achieved implicitly by modifying the conventional VF converter as in [52]-[67]. An additional capacitor at the input and application of input-voltage control with inverted control scheme (i.e., the polarity of the feedback and reference signal has to be changed for proper operation) provide the voltage-type input terminal and the VF converter is actually transformed into a CF converter. This kind of transformation is not commonly noticed to take place and, consequently, the change of dynamics of the converter is usually neglected. The right-half-plane (RHP) zero, for example, appears in the control-to-output

transfer function if a conventional VF buck converter is modified according to the above mentioned scheme. The resulting converter is actually a CF boost-type converter, which incorporates the RHP zero as discussed in [P7]. The existence of the RHP zero in buck-derived PV converter is recognized already in the 1970s in [62] and later e.g. in [54] and [68] but the connections to the dual CF domain have not been made.

PV interfacing may become even more complicated if the control of the interfacing converter is based on the control scheme such as peak-current-mode (PCM) control [65]-[67], which utilizes feedback signals from the inductive components. It is not recognized, however, that the PCM control tries to maintain the converter as a VF converter, which can reliably operate only in the CV region of the PV generator without substantial overcompensation in the current loop. In principle, the input-voltage control forces the converter to be a CF current-output converter although the inner current loop has VF properties. This incompatibility causes instability problems, which can be analyzed only by applying both the CF and VF converter models (i.e. H and Y parameter models) for one physical converter as discussed in [P8].

The stability of the conventional interconnected VF systems is assessed by means of the impedance ratio known as *minor-loop gain* [85],[86] by applying the Nyquist stability criterion. The minor-loop gain, introduced by R. D. Middlebrook in the 1970s, is composed of the output impedance of the source system and the input impedance of the load system, respectively [85]. The stability of the cascaded CF system can be assessed by using the *inverse* minor-loop gain as discussed in [P2] and [P3] and concluded also in [87]-[89]. Both of the minor-loop gains are excellent tools for analyzing the stability of the interconnected PV systems providing consistent explanations for the observed stability problems.

The static and dynamic properties of the VF converters are well known within the power electronics society, but a deep understanding of some basic control engineering principles seems to be at a rather low level. As a consequence of this, it is not recognized that the changing of input source and using input voltage as feedback control signal have also changed the dynamic properties of the converter from the original properties even if the power stages resemble each other. This has led to a situation where the analyses of the converters are deficient and many of the vital consequences may be unnoticed.

1.3 Structure of the Thesis

In addition to the introduction in Chapter 1, the thesis contains four chapters which are summarized as follows:

Chapter 2 provides a basic formalism to model converters at open and closed loop. The study introduces a generalized representation to cover all four conversion schemes known as G, Y, H and Z parameters. The effects of non-ideal source and load are analyzed as well and a general stability assessment is introduced and applied to PV interfacing.

Chapter 3 introduces methods to implement CF converters. The intuitive, explicit and implicit methods are discussed and illustrated by examples. It is shown how the intuitive method, and explicit method, based on duality principles have benefits over the third, implicit method, which is based on modification of existing VF converters.

Chapter 4 provides the experimental evidence for the arguments presented in this thesis. Different converter topologies and their experimental measurements are analyzed. Constraints related to VF converters as well as the performance of explicitly and implicitly implemented CF converters are illustrated. The performance of a PCM-controlled PV converter is evaluated.

Chapter 5 provides the summaries of the publications [P1]-[P8], final conclusions and discussion on future topics.

1.4 Objectives and the Main Scientific Contributions

The thesis discusses the true nature of the existing MPP-tracking dc-dc converters in PV energy systems. It is shown that the CF converters are real and already widely utilized among these systems but not recognized to exist nor treated accordingly. The reason may be that the CF converters can be implemented in three ways: 1) by intuition, 2) explicitly by transforming the circuit from the existing VF circuit by means of duality transformation methods and 3) implicitly by adding an input capacitor at the input of an existing VF power stage and modifying the feedback control scheme. The latter method is commonly used and may lead to inconsistent representations if the domain change from VF to CF is not recognized.

Misinterpretations can be avoided only if the true nature of the converter is recognized and the analyses are performed accordingly based on proper network representation (i.e. G, Y, H and Z parameters). The thesis will provide all possible dynamic representations for the dc-dc converters in terms of different conversion schemes, basic feedback control methods and effects of non-ideal source and load. The study also reveals new special parameters of which some are extremely useful in the practical dynamic analyses of the converters.

The main scientific contributions of the thesis can be summarized as follows:

- It is shown that the converters used in the PV energy systems are mostly CF converters but not commonly recognized due to their implicit implementation
- A generalized dynamic representation of a switched-mode converter is established including new dynamically significant special parameters. The representation is applied to cover all the basic conversion schemes.
- A generalized impedance-based stability-assessment method is introduced. An inverse of the conventional minor-loop gain is shown to be valid in analyzing the stability of interconnected CF systems.
- It is shown that there are three different ways to derive CF converters: intuitive approach and explicit and implicit duality transformation.
- Dynamics of fourth-order step-down current converter or CF superbuck is introduced for the first time.
- It is shown that the application of PCM control is not well suited for the internal control of CF converters.

2 Generalized Dynamic Representation of DC-DC Converter

2.1 Introduction

The dynamic analysis of a switched-mode converter can be performed by using certain network parameter models [71]. The parameters, i.e. transfer functions representing the dynamics of a converter under DDR control, can be obtained analytically by applying well-known state-space averaging method [90]. This chapter introduces a generalized representation that can be applied to describe the dynamic behavior of all possible conversion schemes at open and closed loop including the effect of non-ideal source and load. The generalized stability assessment of interconnected electrical systems is presented and applied to the PV interfacing. The information provided in this chapter completes the work carried out in [92], [94] and [95].

2.2 Characterization of Arbitrary Switched-Mode Converter

The operation of a switched-mode converter is non-linear due to its variable-structure nature. The modeling of such a system can be performed by averaging its operation over one switching period and linearizing the averaged model at certain operation point. The resulting small-signal model describes the mappings between the input and output variables (i.e., voltages and currents at input and output terminals) and state variables (i.e., currents and voltages of the capacitor and inductor).

The linear model can be expressed in matrix form as given in (2.1), where $\mathbf{u}(t)$ is an input variable vector, $\mathbf{y}(t)$ output variable vector and $\mathbf{x}(t)$ state variable vector. Matrices **A, B**, **C** and **D** are coefficient matrices consisting of constant elements such as resistances, inductances and capacitances.

$$\begin{aligned} \frac{\mathrm{d}\mathbf{x}(t)}{\mathrm{d}t} &= \mathbf{A}\cdot\mathbf{x}(t)+\mathbf{B}\cdot\mathbf{u}(t) \\ \mathbf{y}(t) &= \mathbf{C}\cdot\mathbf{x}(t)+\mathbf{D}\cdot\mathbf{u}(t) \end{aligned} \tag{2.1}$$

Dynamic modeling represents the behavior of the converter in a frequency domain. Therefore, the time-domain equations in (2.1) are expressed in frequency-domain by utilizing Laplace transformation which yields

$$\begin{aligned} s\mathbf{X}(s) &= \mathbf{A}\cdot\mathbf{X}(s)+\mathbf{B}\cdot\mathbf{U}(s) \\ \mathbf{Y}(s) &= \mathbf{C}\cdot\mathbf{X}(s)+\mathbf{D}\cdot\mathbf{U}(s) \end{aligned} \tag{2.2}$$

$$\begin{aligned} \mathbf{X}(s) &= (s\mathbf{I}-\mathbf{A})^{-1}\mathbf{B}\cdot\mathbf{U}(s) \\ \mathbf{Y}(s) &= (\mathbf{C}\cdot(s\mathbf{I}-\mathbf{A})^{-1}\mathbf{B}+\mathbf{D})\cdot\mathbf{U}(s) \\ \Rightarrow \mathbf{Y}(s) &= \mathbf{G}\cdot\mathbf{U}(s) \end{aligned} \tag{2.3}$$

Matrix $\mathbf{G}$ is known as the system transfer function matrix consisting of the transfer functions from the input variables to the output variables. (Note that the input variables are denoted by $\hat{x}$, not $\hat{u}$, in further analyses although the input variable vector is denoted by $\mathbf{U}(s)$. This is because the small-signal voltages are denoted generally by $\hat{u}$).

Generally, the dynamics of a switched-mode converter can be analyzed by utilizing a representation given in (2.4) and Fig. 2.1. The system typically has three input variables $\left[\hat{x}_{\mathrm{in}} \quad \hat{x}_{\mathrm{out}} \quad \hat{x}_{\mathrm{c}}\right]^{\mathrm{T}}$ and two output variables $\left[\hat{y}_{\mathrm{in}} \quad \hat{y}_{\mathrm{out}}\right]^{\mathrm{T}}$, where the subscript 'in' denotes the variables at the input terminal (either input voltage or current) and 'out' the variables at the output terminal (output current or voltage) and 'c' the general control variable. This yields six transfer functions to describe the dynamics between input and output variables: the ohmic characteristics of the input terminal $G_{11}=\hat{y}_{\mathrm{in}}/\hat{x}_{\mathrm{in}}$, output-to-input transfer function $G_{12}=\hat{y}_{\mathrm{in}}/\hat{x}_{\mathrm{out}}$, control-to-input transfer function $G_{13}=\hat{y}_{\mathrm{in}}/\hat{x}_{\mathrm{c}}$, input-to-output transfer function $G_{21}=\hat{y}_{\mathrm{out}}/\hat{x}_{\mathrm{in}}$, ohmic characteristics of the output terminal $G_{22}=\hat{y}_{\mathrm{out}}/\hat{x}_{\mathrm{out}}$ and control-to-output transfer function $G_{23}=\hat{y}_{\mathrm{out}}/\hat{x}_{\mathrm{c}}$.

$$\begin{bmatrix} \hat{y}_{\mathrm{in}} \\ \hat{y}_{\mathrm{o}} \end{bmatrix} = \begin{bmatrix} G_{11} & G_{12} & G_{13} \\ G_{21} & -G_{22} & G_{23} \end{bmatrix} \begin{bmatrix} \hat{x}_{\mathrm{in}} \\ \hat{x}_{\mathrm{out}} \\ \hat{x}_{\mathrm{c}} \end{bmatrix} \tag{2.4}$$

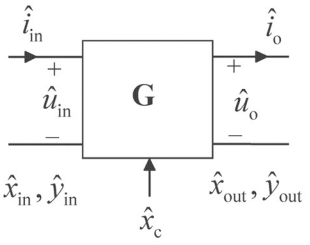

Fig. 2.1 Arbitrary chosen electrical converter system **G**

The minus sign in front of the transfer function G_{22} is justified since the general network presentation in [71] assumes that the current is always flowing into the port but the direction of the current is, in practice, opposite at the output port. This has been taken into account in the further analyses of this thesis.

2.2.1 Converter under Feedback Control

Negative-feedback control is commonly utilized to maintain the desired variable constant at the predefined value. As a consequence, the converter operates at closed loop. The feedback can be taken only from the output variables $\hat{y}_{in}$ and $\hat{y}_{out}$ yielding two different sets of closed-loop transfer functions. The closed-loop transfer functions under input control can be derived from Fig. 2.2 yielding (2.5) where subscripts '-o' denote the open-loop transfer functions, $L_{in} = G_{s\text{-}in}G_{c\text{-}in}G_aG_{13}$ input-feedback loop gain, $G_{s\text{-}in}$ input sensor gain, $G_{c\text{-}in}$ input-side controller transfer function and G_a modulator gain. Input variable $\hat{x}_{r\text{-}in}$ is the reference for the controlled variable and special transfer functions $G_{21\text{-}\infty}$ and $G_{22\text{-}\infty}$ are known as certain ideal output-side transfer functions.

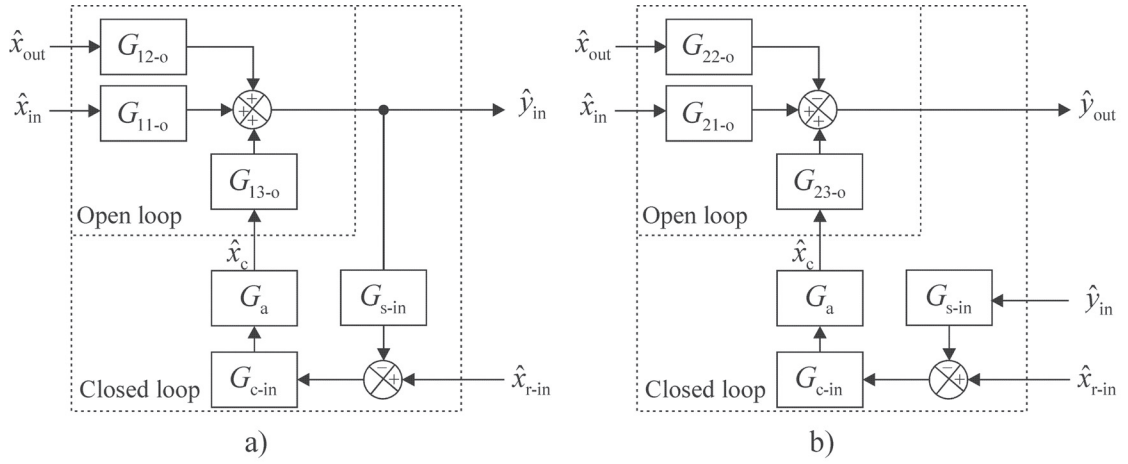

Fig. 2.2 a) Input and b) output dynamics when the feedback is from input

$$\begin{bmatrix} \hat{y}_{\text{in}} \\ \hat{y}_{\text{out}} \end{bmatrix} = \begin{bmatrix} \dfrac{G_{11\text{-o}}}{1+L_{\text{in}}} & \dfrac{G_{12\text{-o}}}{1+L_{\text{in}}} & \dfrac{1}{G_{\text{s-in}}}\dfrac{L_{\text{in}}}{1+L_{\text{in}}} \\ \left(\dfrac{G_{21\text{-o}}}{1+L_{\text{in}}}+\dfrac{L_{\text{in}}G_{21\text{-}\infty}}{1+L_{\text{in}}}\right) & -\left(\dfrac{G_{22\text{-o}}}{1+L_{\text{in}}}+\dfrac{L_{\text{in}}G_{22\text{-}\infty}}{1+L_{\text{in}}}\right) & \dfrac{G_{23\text{-o}}}{G_{\text{s-in}}G_{13\text{-o}}}\dfrac{L_{\text{in}}}{1+L_{\text{in}}} \end{bmatrix} \begin{bmatrix} \hat{x}_{\text{in}} \\ \hat{x}_{\text{out}} \\ \hat{x}_{\text{r-in}} \end{bmatrix} \tag{2.5}$$

$$G_{21\text{-}\infty} = G_{21\text{-o}} - \frac{G_{11\text{-o}}G_{23\text{-o}}}{G_{13\text{-o}}} \qquad G_{22\text{-}\infty} = G_{22\text{-o}} + \frac{G_{12\text{-o}}G_{23\text{-o}}}{G_{13\text{-o}}} \tag{2.6}$$

The closed-loop transfer functions under output control can be derived from Fig. 2.3 yielding (2.7) where subscripts '-o' denote the open-loop transfer functions, $L_{\text{out}} = G_{\text{s-out}}G_{\text{c-out}}G_{\text{a}}G_{23}$ output-feedback loop gain, $G_{\text{s-out}}$ output sensing gain and $G_{\text{c-out}}$ output-side controller transfer function. Input variable $\hat{x}_{\text{r-out}}$ is the reference for the controlled variable and special transfer functions $G_{11\text{-}\infty}$ and $G_{12\text{-}\infty}$ are known as certain ideal input-side transfer functions.

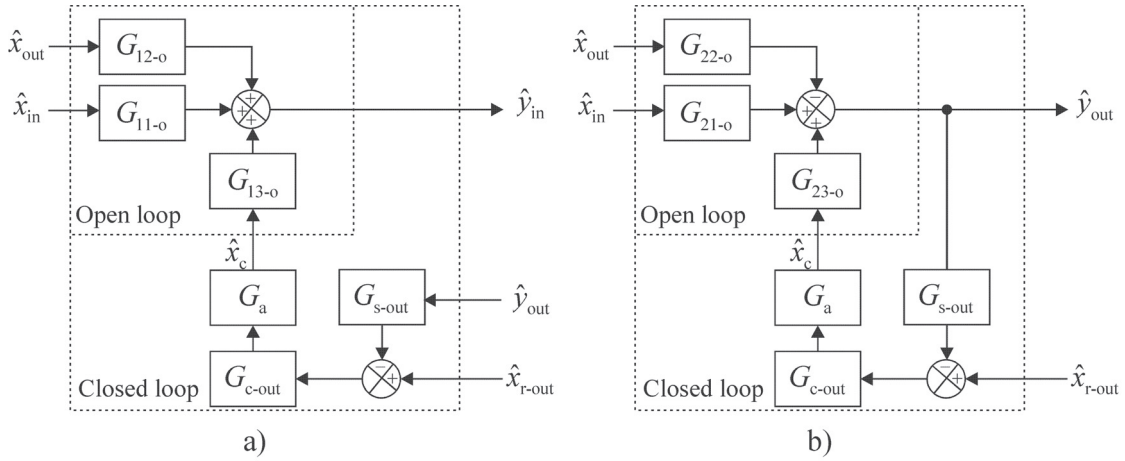

Fig. 2.3 a) Input and b) output dynamics when the feedback is from output

$$\begin{bmatrix} \hat{y}_{\text{in}} \\ \hat{y}_{\text{out}} \end{bmatrix} = \begin{bmatrix} \left(\dfrac{G_{11\text{-o}}}{1+L_{\text{out}}}+\dfrac{L_{\text{out}}G_{11\text{-}\infty}}{1+L_{\text{out}}}\right) & \left(\dfrac{G_{12\text{-o}}}{1+L_{\text{out}}}+\dfrac{L_{\text{out}}G_{12\text{-}\infty}}{1+L_{\text{out}}}\right) & \dfrac{G_{13\text{-o}}}{G_{\text{s-out}}G_{23\text{-o}}}\dfrac{L_{\text{out}}}{1+L_{\text{out}}} \\ \dfrac{G_{21\text{-o}}}{1+L_{\text{out}}} & -\dfrac{G_{22\text{-o}}}{1+L_{\text{out}}} & \dfrac{1}{G_{\text{s-out}}}\dfrac{L_{\text{out}}}{1+L_{\text{out}}} \end{bmatrix} \begin{bmatrix} \hat{x}_{\text{in}} \\ \hat{x}_{\text{out}} \\ \hat{x}_{\text{r-out}} \end{bmatrix} \tag{2.7}$$

$$G_{11\text{-}\infty} = G_{11\text{-o}} - \frac{G_{21\text{-o}}G_{13\text{-o}}}{G_{23\text{-o}}} \qquad G_{12\text{-}\infty} = G_{12\text{-o}} + \frac{G_{22\text{-o}}G_{13\text{-o}}}{G_{23\text{-o}}} \tag{2.8}$$

The above presented formulations are given for the four different converter schemes explicitly in Appendix A-F. The mathematical formulations for specific converter models can be found from [P4]-[P8].

2.2.2 Effect of Non-Ideal Source and Load

The input source and output load are non-ideal in practice and they may have significant effects on the converter performance. Fig. 2.4 represents an interconnected system consisting of the source subsystem **S** and converter subsystem **G**. The source system is assumed to be either voltage or current source possessing ohmic characteristics (either source impedance or admittance). The input variables of the system are denoted by $(\hat{x}_{\text{in1}}, \hat{x}_{\text{out2}}, \hat{x}_{\text{c}})$, output variables by $(\hat{y}_{\text{in1}}, \hat{y}_{\text{out2}})$ and intermediate variables by $(\hat{x}_{\text{s}}, \hat{y}_{\text{s}})$.

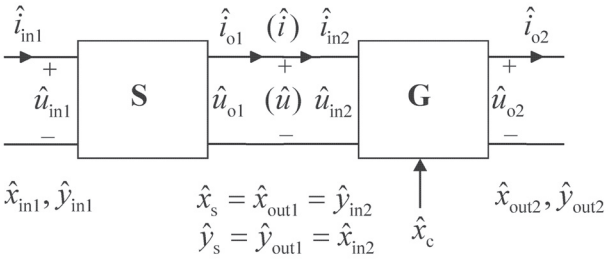

Fig. 2.4 Converter **G** fed by a non-ideal source system **S**

The subsystems in Fig. 2.4 can be presented by transfer function matrices given in (2.9). By utilizing the intermediate variables, the source-affected transfer functions between the system input and output variables can be derived as given in (2.10) where $G_{\text{11-xo}}$ denote the ohmic characteristics of the input port when the output port is either short-circuited (in case current-sink load) or open-circuited (in case of voltage-type load).

$$\begin{bmatrix} \hat{y}_{\text{in1}} \\ \hat{y}_{\text{s}} \end{bmatrix} = \begin{bmatrix} 0 & 1 \\ 1 & -S_{22} \end{bmatrix} \begin{bmatrix} \hat{x}_{\text{in1}} \\ \hat{x}_{\text{s}} \end{bmatrix} \qquad \begin{bmatrix} \hat{x}_{\text{s}} \\ \hat{y}_{\text{out2}} \end{bmatrix} = \begin{bmatrix} G_{11} & G_{12} & G_{13} \\ G_{21} & -G_{22} & G_{23} \end{bmatrix} \begin{bmatrix} \hat{y}_{\text{s}} \\ \hat{x}_{\text{out2}} \\ \hat{x}_{\text{c}} \end{bmatrix} \tag{2.9}$$

$$\begin{bmatrix} \hat{y}_{\text{in2}} \\ \hat{y}_{\text{out2}} \end{bmatrix} = \begin{bmatrix} \dfrac{G_{11}}{1+S_{22}G_{11}} & \dfrac{G_{12}}{1+S_{22}G_{11}} & \dfrac{G_{13}}{1+S_{22}G_{11}} \\ \dfrac{G_{21}}{1+S_{22}G_{11}} & -\dfrac{1+S_{22}G_{11\text{-xo}}}{1+S_{22}G_{11}}G_{22} & \dfrac{1+S_{22}G_{11\text{-}\infty}}{1+S_{22}G_{11}}G_{23} \end{bmatrix} \begin{bmatrix} \hat{x}_{\text{in1}} \\ \hat{x}_{\text{out2}} \\ \hat{x}_{\text{c}} \end{bmatrix} \tag{2.10}$$

$$G_{\text{11-xo}} = G_{\text{11-sco}} = G_{\text{11-oco}} = G_{11} + \frac{G_{12}G_{21}}{G_{22}} \tag{2.11}$$

The effect of the non-ideal load can be derived similarly. Fig. 2.5 presents an interconnected system consisting of the converter subsystem **G** connected to load subsystem **L**. The load subsystem is assumed to be either voltage-type load or current sink possessing ohmic characteristics (either load impedance or admittance).

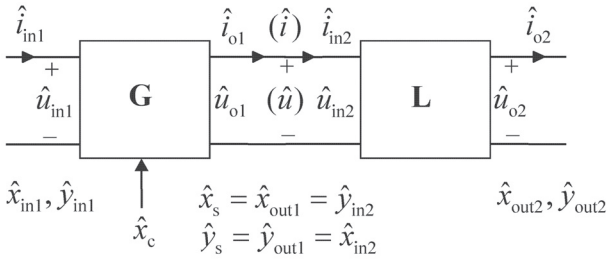

Fig. 2.5 Converter system **G** connected to a non-ideal load **L**

The sub-systems in Fig. 2.5 can be presented by transfer function matrices given in (2.12). By utilizing the intermediate variables, the load-affected transfer functions between the input and output variables can be derived as given in (2.13) where $G_{22\text{-xi}}$ denote the ohmic characteristics of the output port when the input port is either short-circuited (in case of input current source) or open-circuited (in case of input voltage source).

$$\begin{bmatrix} \hat{y}_{in1} \\ \hat{y}_s \end{bmatrix} = \begin{bmatrix} G_{11} & G_{12} & G_{13} \\ G_{21} & -G_{22} & G_{23} \end{bmatrix} \begin{bmatrix} \hat{x}_{in1} \\ \hat{x}_s \\ \hat{x}_c \end{bmatrix} \qquad \begin{bmatrix} \hat{x}_s \\ \hat{y}_{out2} \end{bmatrix} = \begin{bmatrix} L_{11} & 1 \\ 1 & 0 \end{bmatrix} \begin{bmatrix} \hat{y}_s \\ \hat{x}_{out2} \end{bmatrix} \tag{2.12}$$

$$\begin{bmatrix} \hat{y}_{in1} \\ \hat{y}_{out1} \end{bmatrix} = \begin{bmatrix} \dfrac{1+L_{11}G_{22\text{-xi}}}{1+L_{11}G_{22}} G_{11} & \dfrac{G_{12}}{1+L_{11}G_{22}} & \dfrac{1+L_{11}G_{22\text{-}\infty}}{1+L_{11}G_{22}} G_{13} \\ \dfrac{G_{21}}{1+L_{11}G_{22}} & -\dfrac{G_{22}}{1+L_{11}G_{22}} & \dfrac{G_{23}}{1+L_{11}G_{22}} \end{bmatrix} \begin{bmatrix} \hat{x}_{in1} \\ \hat{x}_{out2} \\ \hat{x}_c \end{bmatrix} \tag{2.13}$$

$$G_{22\text{-xi}} = G_{22\text{-sci}} = G_{22\text{-oci}} = G_{22} + \frac{G_{12}G_{21}}{G_{11}} \tag{2.14}$$

The source and load-affected transfer functions presented in (2.10) and (2.13) are naturally valid at closed loop as well. The above presented dynamic formulations are given for the four different conversion schemes explicitly in Appendices A-F. The mathematical formulations for specific converter models can be found from [P4]-[P8].

2.3 Generalized Stability Assessment of the Interconnected Electrical Systems

It is well known that the stability of a VF interconnected electrical system consisting of source and load subsystems can be determined by means of certain impedance ratio known as minor-loop gain by applying the Nyquist stability criterion [85],[86]. The impedance-based stability assessment method can be generalized as follows [P3]: Fig. 2.6

presents an interconnected system consisting of the source subsystem **S** and load subsystem **L**. The systems can be arbitrary electrical systems but the output port of **S** and input port of **L** have to be duals of each other; a current-type output connected to a voltage-type input or vice versa. The input variables of the system are denoted by $(\hat{x}_{\text{in1}}, \hat{x}_{\text{out2}})$, the output variables by $(\hat{y}_{\text{in1}}, \hat{y}_{\text{out2}})$ and intermediate variables by $(\hat{x}_{\text{s}}, \hat{y}_{\text{s}})$. Control variable $\hat{x}_{\text{c}}$ is assumed to be zero and the generalized stability assessment is derived for single-input-single-output system.

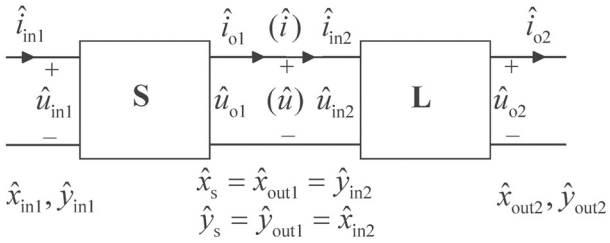

Fig. 2.6 An interconnected system

According to the selected variables, the dynamics of the subsystems can be presented as given in (2.15) and (2.16).

$$\begin{bmatrix} \hat{y}_{\text{in1}} \\ \hat{y}_{s} \end{bmatrix} = \begin{bmatrix} S_{11} & S_{12} \\ S_{21} & -S_{22} \end{bmatrix} \begin{bmatrix} \hat{x}_{\text{in1}} \\ \hat{x}_{\text{s}} \end{bmatrix} \tag{2.15}$$

$$\begin{bmatrix} \hat{x}_{\text{s}} \\ \hat{y}_{\text{out2}} \end{bmatrix} = \begin{bmatrix} L_{11} & L_{12} \\ L_{21} & -L_{22} \end{bmatrix} \begin{bmatrix} \hat{y}_{s} \\ \hat{x}_{\text{out2}} \end{bmatrix} \tag{2.16}$$

The stability of the interconnected system can be studied by constructing the mappings from the system input variables to the intermediate variables and to the output variables yielding (2.17) and (2.18). For stability to exist, all the transfer functions have to be stable, i.e. their poles have to be located at the closed left half of s-plane. If the original subsystems **S** and **L** are assumed to be stable as stand-alone systems, the stability of the interconnected system is dependent on term $1/(1+S_{22}L_{11})$. The boundary for the instability is $S_{22}L_{11} = -1$, where the poles are located at the imaginary axis and the system may oscillate at the frequency in which the condition is valid.

$$\begin{bmatrix} \hat{x}_{\text{s}} \\ \hat{y}_{\text{s}} \end{bmatrix} = \begin{bmatrix} \dfrac{S_{21}L_{11}}{1+S_{22}L_{11}} & \dfrac{L_{12}}{1+S_{22}L_{11}} \\ \dfrac{S_{21}}{1+S_{22}L_{11}} & -\dfrac{S_{22}L_{12}}{1+S_{22}L_{11}} \end{bmatrix} \begin{bmatrix} \hat{x}_{\text{in1}} \\ \hat{x}_{\text{out2}} \end{bmatrix} \tag{2.17}$$

$$\begin{bmatrix} \hat{y}_{\text{in1}} \\ \hat{y}_{\text{out2}} \end{bmatrix} = \begin{bmatrix} S_{11} + \dfrac{S_{12}S_{21}L_{11}}{1+S_{22}L_{11}} & \dfrac{S_{12}L_{12}}{1+S_{22}L_{11}} \\ \dfrac{S_{21}L_{21}}{1+S_{22}L_{11}} & -\left(L_{22} + \dfrac{S_{22}L_{12}L_{21}}{1+S_{22}L_{11}} \right) \end{bmatrix} \begin{bmatrix} \hat{x}_{\text{in1}} \\ \hat{x}_{\text{out2}} \end{bmatrix} \tag{2.18}$$

In the case of interconnected VF systems, $S_{22}L_{11}$ corresponds to product $Z_{\text{o-S}}Y_{\text{in-L}}$ which is known as minor-loop gain [85], where $Z_{\text{o-S}}$ is the output impedance of the source system and $Y_{\text{in-L}}$ input admittance of the load system. In the case of interconnected CF system, $S_{22}L_{11}$ corresponds to product $Y_{\text{o-S}}Z_{\text{in-L}}$, where $Y_{\text{o-S}}$ is the output admittance of the source circuit and $Z_{\text{in-L}}$ input impedance of the load circuit. The product $Y_{\text{o-S}}Z_{\text{in-L}}$ is clearly the inverse of the minor-loop gain of the VF system. [87], [P3]

The DC resistance of the PV generator (source impedance Z_{s}) is known to be positive resistance r_{pv} that equals the static terminal resistance $R_{\text{pv}} = U_{\text{pv}} / I_{\text{pv}}$ at the MPP [P1],[P2],[23]. Therefore, instability occurs in the Nyquist sense at the MPP if the input impedance of the MPP-tracking converter has the property of negative incremental resistance, i.e. $Z_{\text{o-S}}Y_{\text{in-L}} = -1$ in case VF converter and $Y_{\text{o-S}}Z_{\text{in-L}} = -1$ in case of CF converter.

2.4 Conclusion

The generalized dynamic formulations including source and load interactions as well as impedance-based stability assessment method were given in the chapter. They form the basis for the thesis and the dynamic analysis of the switched-mode converters and the systems composing of them. Similar formulations have not been publicly reported.

3 Implementation of Current-Fed Converters

3.1 Introduction

The implementation of CF converters can be divided into three categories. Firstly, the CF converters can be implemented intuitively as discussed e.g. in [70]. Basically, the practical power stage is constructed based on the circuit theory to comply with a current-type source. Secondly, the CF converters can be implemented by an explicit duality transformation method from the corresponding VF converter. The third method to implement CF converters is to add a capacitor at the input of a VF converter and to provide feedback control from the input voltage.

3.2 Intuitive Implementation

An arbitrarily chosen interfacing device or load does not automatically comply with an input current source as illustrated in Fig. 3.1. The system in Fig. 3.1a consists of current source (subsystem **S**) and current-sink load (subsystem **L**) requiring that the input current i_S and load current i_L are equal in all circumstances. In practice, the input current is considered as constant but the current-sink load may be based on a controllable switching device causing a situation where $i_S \neq i_L$. Consequently, Kirchhoff's current law is violated. The connection in Fig. 3.1b satisfies Kirchhoff's current law since it consists of a dual pair of circuit elements, i.e. a current source connected to a voltage-type load. It can be concluded that a current source requires an interfacing device that resembles a voltage-type load.

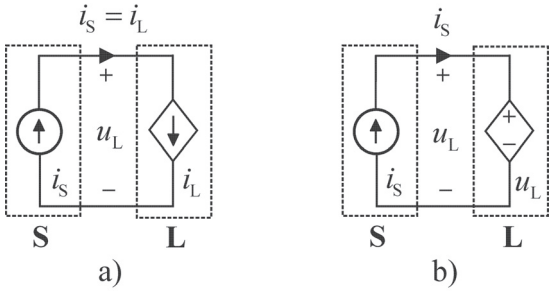

Fig. 3.1 a) Invalid and b) valid interfacing of a current source

Consider an implementation of a switched-mode battery charger fed by a constant current source. The input variables of the system are obviously the input current and output (battery) voltage and the output variables output (charge) current and input voltage. First, the physical power stage has to comply with the equivalent model shown in Fig. 3.2a; the input port must be a voltage-type load to satisfy Kirchhoff's current law and the output port a current source to satisfy Kirchhoff's voltage law. The capacitor is known to resist changes in the voltage, i.e. it resembles constant-voltage load when it is charged and voltage source when discharged. Similarly, the inductor is known to resist the changes in the current, i.e. it resembles current sink when it is charged and current source when discharged. Therefore, the power stage is based on the usage of an input capacitor *C* and output inductor *L* as shown in Fig. 3.2b.

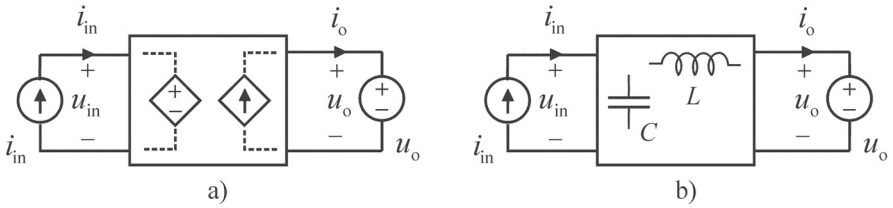

Fig. 3.2 a) Equivalent model of a CF battery charger and b) the principle of an actual CF power stage

The basic current converters or regulators are based on stepping the current either up or down. If the input current is higher than the allowed charging current, the current must be stepped down naturally. Respectively, if the current source provides a rather low current, the step-up function is desired. The output voltage can be also seen to be reversely stepped up/down to the input terminal. This is possible because the input source is assumed to be constant current source of which voltage can be controlled and regulated.

3.2.1 Step-Down Current Regulator

In order to step down the charge current, the current regulation has to be arranged in such way that it chops the input current. This can be implemented by the switching structure shown in Fig. 3.3a. Basically, the switch *S* is chopping the input current and the

current ripple is filtered by the CL-filter. In position 1 (Fig. 3.3b), the switch provides a current path from input to output. When the switch is changed to position 2 (Fig. 3.3c), the input current source is short-circuited and the charge current is maintained by the CL structure.

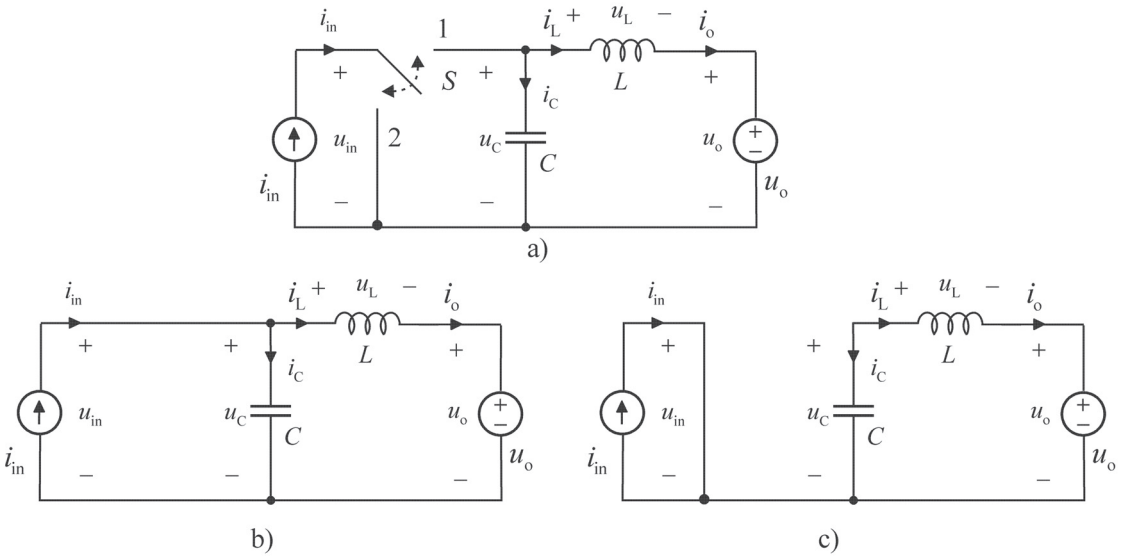

Fig. 3.3 a) Step-down current regulator, b) sub-circuit when the switch is in position 1 and b) position 2

The small-ripple approximated currents and voltages at different switch positions are as follows:

$$u_{\text{in-1}} = U_{\text{C}} \qquad u_{\text{in-2}} = 0$$
$$i_{\text{o-1}} = I_{\text{L}} \qquad i_{\text{o-2}} = I_{\text{L}}$$
$$u_{\text{L-1}} = U_{\text{C}} - U_{\text{o}} = U_{\text{in}} - U_{\text{o}} \qquad u_{\text{L-2}} = U_{\text{C}} - U_{\text{o}}$$
$$i_{\text{C-1}} = I_{\text{in}} - I_{\text{L}} = I_{\text{in}} - I_{\text{o}} \qquad i_{\text{C-2}} = -I_{\text{L}} = -I_{\text{o}}$$

where switch position 1 is denoted by subscript '-1' and position 2 by subscript '-2'. The relations between the input variables and output variables can be solved by applying ampere-second balance for the capacitor over one switching period [91]:

$$\int_0^{T_S} i_C(t)dt = \int_0^{t_1} i_{\text{C-1}}dt + \int_{t_1}^{T_S} i_{\text{C-2}}dt = \int_0^{t_1} (I_{\text{in}} - I_{\text{o}})dt + \int_{t_1}^{T_S} -I_{\text{o}}dt = 0 \tag{3.1}$$

where T_S is the switching period and t_1 the time the switch is in position 1. This time interval can be expressed by using certain duty ratio D yielding $t_1 = DT_S$. Consequently, the output current can be solved from (3.1) as a function of the input current and duty ratio yielding

$$I_o = DI_{in}, \tag{3.2}$$

If the losses are neglected, the input power equals the output power (i.e. $P_{in} = U_{in}I_{in} = P_o = U_oI_o$) and the input voltage can be given as follows:

$$U_{in} = DU_o. \tag{3.3}$$

Since the duty ratio D is always equal to or less than one, the step-down function of the current is obvious according to (3.2) and analogous to conventional VF buck converter which steps down the voltage instead. Therefore, the converter under study is known as dual buck or CF buck converter [78],[P4].

3.2.2 Step-Up Current Regulator

In order to step up the current, the current regulation has to be arranged in such a way that it accumulates the charge current. This can be implemented by the switching structure shown in Fig. 3.4a. When switch S is in position 1 (Fig. 3.4b) the capacitor is charged by the input current source and charge current is maintained by the output inductor. When the switch is changed into position 2 (Fig. 3.4c) the charge current is accumulated because it is a sum of input current and capacitor discharge current.

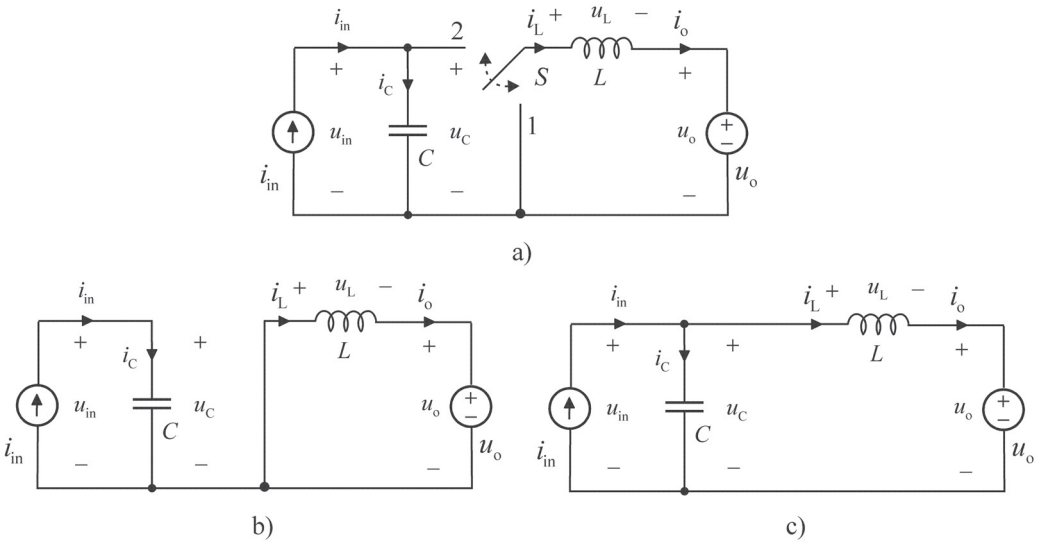

Fig. 3.4 a) Step-up current regulator, b) sub-circuit when the switch is in position 1 and b) position 2

The small-signal approximated currents and voltages at different switch positions are as follows:

$u_{\text{in-1}} = U_{\text{C}}$ $u_{\text{in-2}} = U_{\text{C}}$

$i_{\text{o-1}} = I_{\text{L}}$ $i_{\text{o-2}} = I_{\text{L}}$

$u_{\text{L-1}} = -U_{\text{o}}$ $u_{\text{L-2}} = U_{\text{C}} - U_{\text{o}} = U_{\text{in}} - U_{\text{o}}$

$i_{\text{C-1}} = I_{\text{in}}$ $i_{\text{C-2}} = I_{\text{in}} - I_{\text{L}} = I_{\text{in}} - I_{\text{o}}$

where switch position 1 is denoted by subscript '-1' and position 2 by subscript '-2'. The ampere-second balance for the capacitor is as follows [91]:

$$\int_0^{T_S} i_C(t)dt = \int_0^{t_1} i_{\text{C-1}}dt + \int_{t_1}^{T_S} i_{\text{C-2}}dt = \int_0^{t_1} I_{\text{in}}dt + \int_{t_1}^{T_S} (I_{\text{in}} - I_{\text{o}})dt = 0 \tag{3.4}$$

where T_S is the switching period and t_1 the time switch is in position 1. This time interval can be expressed by using duty ratio D yielding $t_1 = DT_S$. Consequently, the output current can be solved from (3.4) as a function of the input current and duty ratio yielding

$$I_{\text{o}} = \frac{I_{\text{in}}}{D'}, \tag{3.5}$$

where $D' = 1 - D$, i.e. the complement of the duty ratio. If the losses are neglected, the input voltage can be given as follows:

$$U_{\text{in}} = \frac{U_{\text{o}}}{D'}. \tag{3.6}$$

Since term $(1/D')$ is always equal to or more than one, the current-boosting nature of the converter is obvious according to (3.5) and is analogous to conventional VF boost converter, which steps up voltage instead. Therefore, the converter is known in literature as the dual boost or CF boost converter [78],[P7].

3.3 Explicit Duality Transformation

Duality is a well-known concept in electrical engineering [74] and applied in power electronics since the 1970s [75]-[81]. Duality transformation changes all the circuit elements and structures into their dual pairs, i.e. voltage sources to current sources, capacitors to inductors, short circuits to open circuits, parallel connections to series connections and vice versa. Consequently, VF converters can be transformed into their dual CF converters. The idea behind the transformation is first to convert the power stage of the VF converter into equivalent graphs. The transformation procedure can be illustrated by a simple LC-filter example as shown in Fig. 3.5. First, an ordinary LC-filter circuit fed by a voltage source (Fig. 3.5a) is redrawn as a graph shown in Fig. 3.5b. The graph presentation is then converted into its dual graph by means of duality

transformation methods yielding the dual graph shown in Fig. 3.5c. The final dual CL-filter circuit in Fig. 3.5d is derived by changing all the branches of the graph in Fig. 3.5c into their dual components.

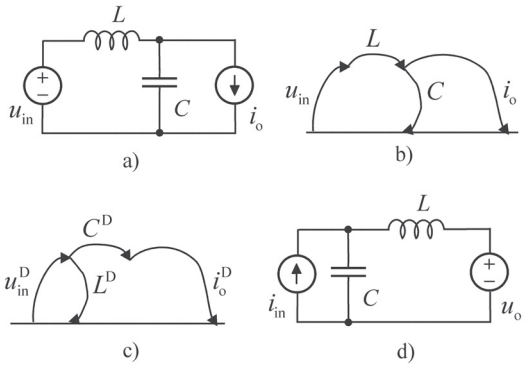

Fig. 3.5 a) Ordinary LC filter, b) its graph, c) dual graph and d) dual CL filter

If the circuit is more complicated and includes e.g. switching elements, the above mentioned graph method does not always lead directly to the desired result. The transformation can be then performed conveniently by placing a dot inside each loop in the power stage and one dot outside the circuitry and connecting the dots with the dual of the branches lying between the corresponding dots. Following these procedures a conventional synchronous VF boost converter shown in Fig. 3.6a, for example, can be transformed into its dual, a CF boost converter. Fig. 3.6b shows the original power stage of a VF converter with the corresponding dual branches drawn by dashed lines. Fig. 3.6c shows the resulting power stage of the CF boost converter.

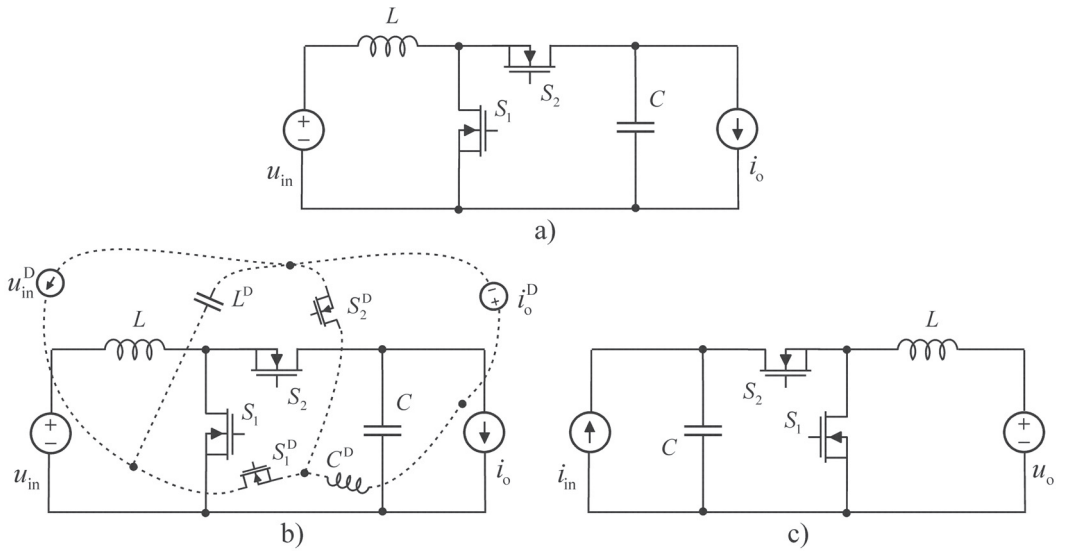

Fig. 3.6 a) Conventional VF boost converter, b) VF boost converter with its dual graph (dashed line) and c) CF boost converter

The switching principle of the conventional VF boost power stage is known to result in the following relations between its input variables (input voltage and output current) and output variables (output voltage and input current) [91],[92]:

$$U_{\mathrm{o}} = \frac{U_{\mathrm{in}}}{D'} \tag{3.7}$$

$$I_{\mathrm{in}} = \frac{I_{\mathrm{o}}}{D'} \tag{3.8}$$

where the duty ratio D determines the time interval when the transistor S_1 conducts. The corresponding relations for the CF boost converter can be concluded by applying the duality principles as follows:

$$U_{\mathrm{o}}^{\mathrm{D}} = \frac{U_{\mathrm{in}}^{\mathrm{D}}}{D'} \rightarrow \text{duality} \rightarrow I_{\mathrm{o}} = \frac{I_{\mathrm{in}}}{D'} \tag{3.9}$$

$$I_{\mathrm{in}}^{\mathrm{D}} = \frac{I_{\mathrm{o}}^{\mathrm{D}}}{D'} \rightarrow \text{duality} \rightarrow U_{\mathrm{in}} = \frac{U_{\mathrm{o}}}{D'} \tag{3.10}$$

The CF boost converter shown in Fig. 3.6c and the equations in (3.9) and (3.10) correspond to the step-up current regulator analyzed in the previous subsection, but the generic switch S is now substituted with a practical switching structure consisting of MOSFETs S_1 and S_2.

3.4 Implicit Duality Transformation

It is recognized that a conventional VF converter does not comply with energy sources that possess current-source characteristics. Thereby, the power stages that incorporate current sources, such as PV modules, are usually modified by inserting a capacitor between the input current source and the VF converter. This is understandable according to Fig. 3.7a-b. It is common to consider voltage source in series with inductor as a current source [84] and the same idea can be applied to the parallel connection of current source and capacitor yielding voltage source as shown in Fig. 3.7b. This kind of modification suggests that the interfacing of a PV module and VF converter could be implemented just by adding a capacitor between the module and converter. The above mentioned generalization may, however, lead to misinterpretations in the analysis of the PV power system because the adding of the capacitor does not practically remove the effects of the current source or the PV module. The capacitor can be added to ease the PV interfacing, but then it should be considered as a part of the converter power stage instead of energy source.

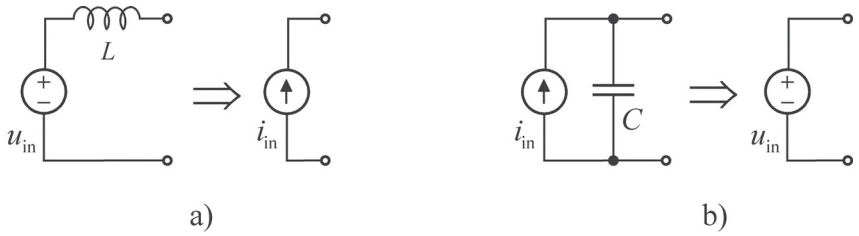

Fig. 3.7 Common generalizations: a) a voltage source in series with an inductor becomes a current source and b) a current source in parallel with a capacitor becomes a voltage source.

Consider a battery charger that is based on a conventional VF buck power stage shown in Fig. 3.8a. If an ideal battery is connected to the output terminal as shown in Fig. 3.8b, the output capacitor will be neglected because the battery is a short circuit from the dynamic point of view. Eventually, when the current source and capacitor are connected to the input terminal as shown in Fig. 3.8c, the power stage actually resembles the CF boost converter analyzed in the previous subsection instead of the conventional VF buck converter that was originally planned to be used.

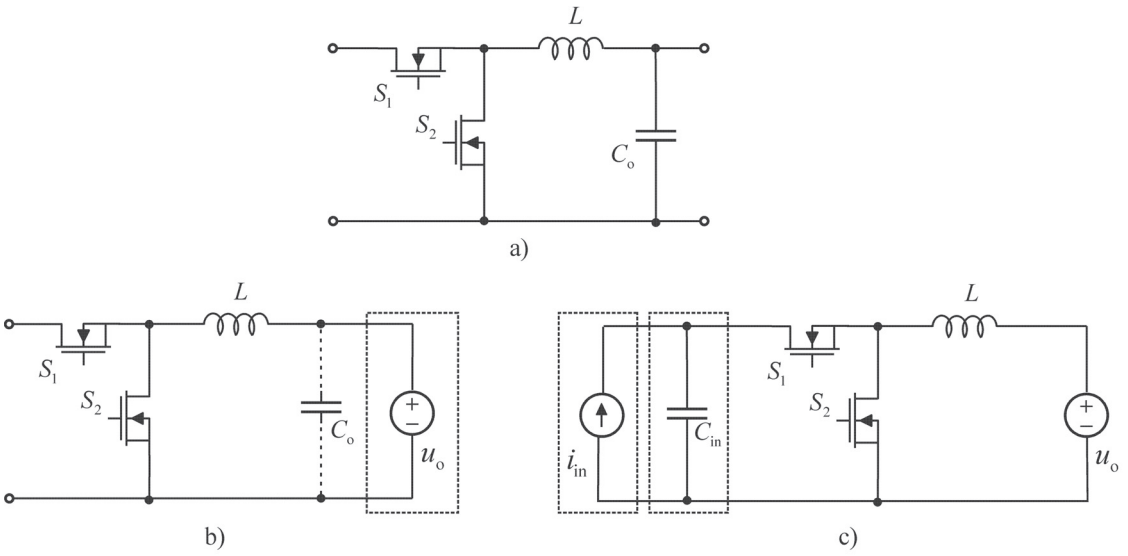

Fig. 3.8 a) Conventional VF buck power stage, b) battery connected to the output terminal and c) current source and capacitor connected to input terminal

If the switching scheme of the converter is maintained original, i.e. duty ratio D determines the conduction time of the high-side switch (S_1 in Fig. 3.8), the relations between input and output variables are as follows:

$$U_{in} = \frac{U_o}{D} \tag{3.11}$$

$$I_{\mathrm{o}} = \frac{I_{\mathrm{in}}}{D} \tag{3.12}$$

The equations (3.11) and (3.12) suggest that a decrease in the duty ratio would increase the input voltage and output current. Therefore, the application of a conventional negative feedback control does not work desirable but resembles positive feedback leading to instability. This can be avoided by modifying the switching scheme in such a way that the conduction time of the low-side transistor is determined by the duty ratio *D*. This can be carried out by inverting the gate signals of the transistors S_1 and S_2, yielding

$$U_{\mathrm{in}} = \frac{U_{\mathrm{o}}}{D} \rightarrow \text{inverted control scheme} \rightarrow U_{\mathrm{in}} = \frac{U_{\mathrm{o}}}{D'} \tag{3.13}$$

$$I_{\mathrm{o}} = \frac{I_{\mathrm{in}}}{D} \rightarrow \text{inverted control scheme} \rightarrow I_{\mathrm{o}} = \frac{I_{\mathrm{in}}}{D'}. \tag{3.14}$$

The same effect can be also obtained by changing the polarity of the feedback and reference signals in the control system or using a descending PWM ramp signal instead of the conventional ramp signal.

Now the converter assumed to be a VF buck converter is actually a CF boost converter. Due to the implicitness of the duality transformation it is not commonly recognized to have taken place. The confusion is partly understandable because the basic physical relations of the currents and voltages in the VF buck and CF boost converters are the same: the input voltage is higher than the output voltage and output current higher than the input current in both cases. The essence of the power-stage design is, however, to recognize the correct input variables, which are constant by nature, and the output variables, which can be controlled. The open-loop analysis does not determine the class of the converter by itself but the class can change if the controllable variable is not selected correctly. Basically, any converter topology can be transformed into a CF converter if the input voltage is controlled and into a VF converter if the input current is controlled, respectively.

3.5 Conclusion

The chapter introduced briefly the methods to implement CF converters either by intuition or from the existing VF converters applying duality transformation methods. It was also demonstrated how an implicit duality transformation may change conventional VF converters into CF converters but which are still considered to be the original VF converters even if the steady-state and dynamic analysis yield contradictory results.

4 Experimental Verification

4.1 Introduction

This chapter provides the experimental evidence to verify the arguments presented in the thesis. The main objective is to prove that the distinction between conventional VF and CF converters in MPP-tracking PV applications actually exists. The important features of a real PV module are also illustrated by measurements. Constraints, such as impedance-based instability, related to VF and CF MPP-tracking converters as well as the performance of implicitly implemented CF converters are demonstrated by practical converter prototypes. The converters are introduced in the order which firstly illustrates the differences in the interfacing constraints between the VF and CF converters, secondly, the different methods to implement CF converters and finally the effect of application of PCM control in a CF converter. The mathematical formulations for specific converter models are presented, in more detailed form, in [P1]-[P8].

4.2 Test Environment and Properties of Photovoltaic Generator

The experimental validating was carried out by measuring frequency responses of the converter prototypes and PV module by using Venable Industries' frequency-response analyzer Model 3120 with an impedance measurement kit. Time-domain measurements were used as well to complete the experimental validation.

Impedance measurement technique utilized in the experiments is demonstrated in Appendix G. The Appendices from H to K present examples of Matlab-based predictions for measured frequency responses of studied converters at certain operation points. Similarly, Appendix L presents an example of computing the transfer functions of CF converter with non-ideal source and load. More detailed validation of converter models is presented e.g. in [P5] and [P7].

The PV module supplying the converter prototypes is RALOSS SR30-36 and the artificial sun used in the experiments is a fluorescent lamp unit. An example of a

measurement setup, the lamp unit as well as the converter prototypes are shown in Appendices M and N. The lamp unit can produce an irradiation of 500 W/m^2 yielding an approximate short-circuit current of 1.0 A, open-circuit voltage of 19.4 V, MPP current of 0.9 A and MPP voltage of 15.8 V at the operational temperature of 44 °C. The constant-voltage load at the output of the converter was provided by valve-regulated lead-acid storage batteries or Chroma 6312A electronic load.

Fig. 4.1a shows the measured frequency responses of PV module (RALOSS SR30-36) impedance Z_s $(= Y_s^{-1})$ from the short-circuit (SC) to open-circuit condition (OC). The measuring technique is based on configuration shown in Fig. G.1b (see Appendix G); the input voltage of interfacing device is varied changing also the operation point of PV module. The impedance measurements are carried out in several points between the SC and OC (for PV module under study, range is approx. 0 V – 19.4 V at irradiation level of 500 W/m^2). Fig. 4.1b shows the dynamic and static resistances r_{pv} and R_{pv} captured from the corresponding measurements. The measurements indicate that the resistances coincide at the MPP as the power transfer theorem implies and the dynamic resistance is higher than the static resistance in the CC region (i.e. voltages lower than the MPP) and lower in the CV region (i.e. voltages higher than the MPP), respectively. The low-frequency phase is definitely zero, not 180 degrees, at all measured operation points. This may cause confusion, because the minus sign in front of the DC resistance is a property of the system in the stability assessment, not the PV module.

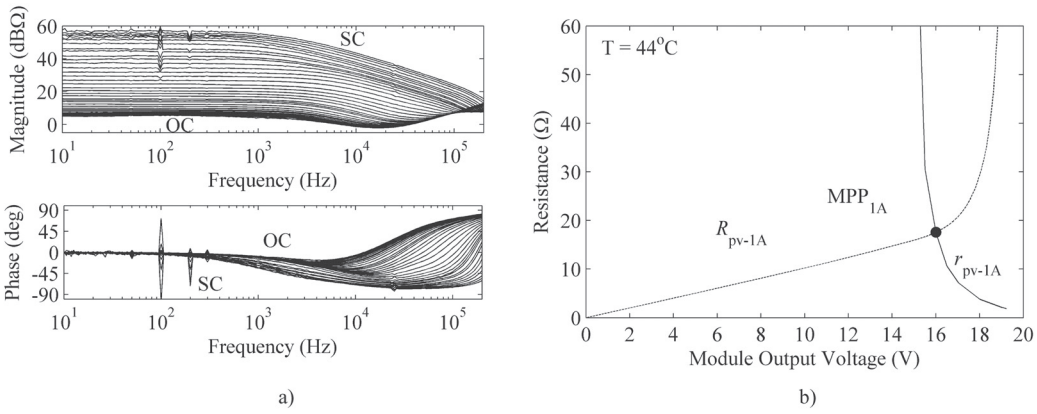

Fig. 4.1 a) Measured frequency responses of PV module impedance and b) comparison of dynamic and static resistances of PV module.

Basically, the magnitude of the static terminal resistance R_{pv} corresponds to the DC resistance of input impedance $|Z_{in}|$ of the output-controlled MPP-tracking converter but the phase of the impedance may have an initial phase shift of 180 degrees. Consequently, the input terminal of the converter possesses the nature of incremental negative resistance, which may lead to impedance-based instability as discussed in Chapter 2.

In practice, the impedance-based instability can be studied by applying source-affected transfer functions given in B.2, C.2, D.2 and E.2 (see Appendices B-E), where the effect of PV module appears either in form of source impedance Z_s (in case of VF converters) or source admittance Y_s (in case of CF converters). Because the magnitude of DC resistance is of interest, the most convenient way to include source effects in the converter model is to substitute Z_s (or Y_s) with predicted dynamic resistance r_{pv} (or r_{pv}^{-1}). However, the authentic source effects can be taken into account by measuring the frequency response of PV module impedance (or admittance), as illustrated in Fig. G.1b (see Appendix G), and substituting Z_s (or Y_s) with it. The measuring techniques presented in Appendix G also enable the separate measuring of source and input impedance/admittance. This actually makes the interaction analysis possible because it would not be reasonable to compare source impedance and already source-affected input impedance.

4.3 Fourth-Order Buck Converters in PV applications

A conventional DDR-controlled fourth-order buck converter shown in Fig. 4.2, known also as a VF superbuck, is a frequently used topology in the PV interfacing due to its continuous input and output currents and voltages [93]. Since the topology is VF by nature, the voltage-source properties of the PV module are enhanced by adding a large capacitor $C_{\mathbf{in}}$ (1 mF) in parallel with the module. An accurate operation at the MPP also requires that the input current ripple is small enough. Therefore, a coupling between inductors L_1 and L_2 was implemented to decrease the input current ripple as much as possible and to avoid the usage of additional input filters. The input-current of the converter is regulated and output voltage is monitored to avoid the damaging of the battery at the output. The cascaded controllers operate as follows. During normal operation, the input current is regulated according to the input-current reference $i_{r\text{-}in}$. In a practical control system, this appears as a reference voltage $u_{r\text{-}in}$ which can be manually adjusted or provided by a microprocessor-based MPP-tracking unit. As soon as the battery voltage exceeds the predefined voltage limit $u_{r\text{-}out}$, the output-voltage-limiting control is activated. This kind of control scheme can be analyzed through voltage-to-voltage and voltage-to-current conversion schemes (G and Y network models presented in Appendices B and C) shown in Figs. B.1 and C.1. The converter balances between these schemes depending on the active feedback loops. If the output loop is active, the closed-loop transfer functions are as given in (C.5) but if only the input loop is active the closed-loop transfer functions are as given in (B.4). The block diagram of the control system is presented in Fig. O.1a (Appendix O) and more detailed analysis of the converter can be found in [P1]. The following will briefly present the results of the practical experiments.

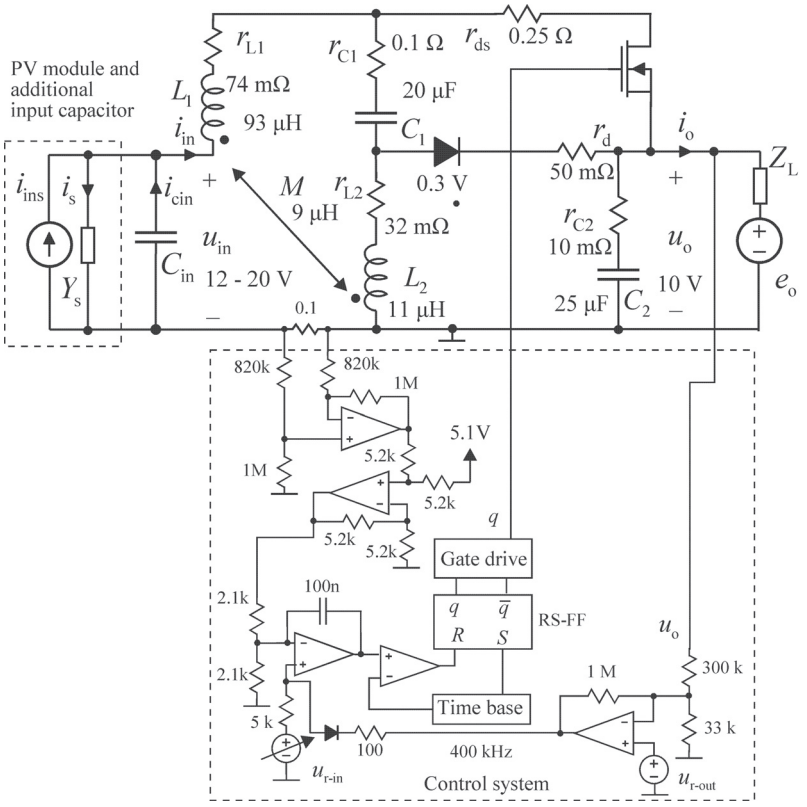

Fig. 4.2 Experimental coupled-inductor VF superbuck converter with a cascaded input-current and output-voltage control.

In order to point out the constraints related to PV interfacing, the source (i.e. PV module and capacitor in parallel) impedance and the input impedance of VF superbuck were measured under both input-current and output-voltage control at several operation points. MPP-tracking was not active during the frequency response measurements but the operation point was varied by changing reference signal $u_{\text{r-in}}$ (i.e., $i_{\text{r-in}}$ reference for input current) or $u_{\text{r-out}}$ manually.

Under input control, the input impedance is as given in (4.1) implying that there are no problems to regulate the input current if the input-current loop $(L_{\text{in}}^{\text{y}})$ itself is designed properly. Fig. 4.3a shows the comparison of measured source and converter input impedances Z_{s} and $Z_{\text{in-c}}^{\text{y}}$ at the vicinity of MPP in both CC and CV regions, confirming that a minor-loop based instability does not occur since the phase shift between the impedances does not reach 180 degrees at any operation point. From this point of view, the operation will be stable in all regions. The sudden changes in the input current may, however, saturate the input-current controller. This means, in practice, that the input-current reference attempts to exceed the sum of PV module and input capacitor currents, i.e. $i_{\text{in}} > i_{\text{ins}} - i_{\text{s}} + i_{\text{cin}}$ (Kirchhoff's current law is to be violated). Fig. 4.3b demonstrates this kind of phenomenon; when the operation point is moved from the CV region to the

vicinity of MPP, the input current reaches the short-circuit current of the PV module and the voltage collapses. This validates also that the PV generator cannot be modeled as a voltage source within its whole range of operation points.

$$Z_{\text{in-c}}^{\text{y}} = \left(Y_{\text{in-c}}^{\text{y}}\right)^{-1} = \left(\frac{Y_{\text{in-o}}^{\text{y}}}{1+L_{\text{in}}^{\text{y}}}\right)^{-1} \tag{4.1}$$

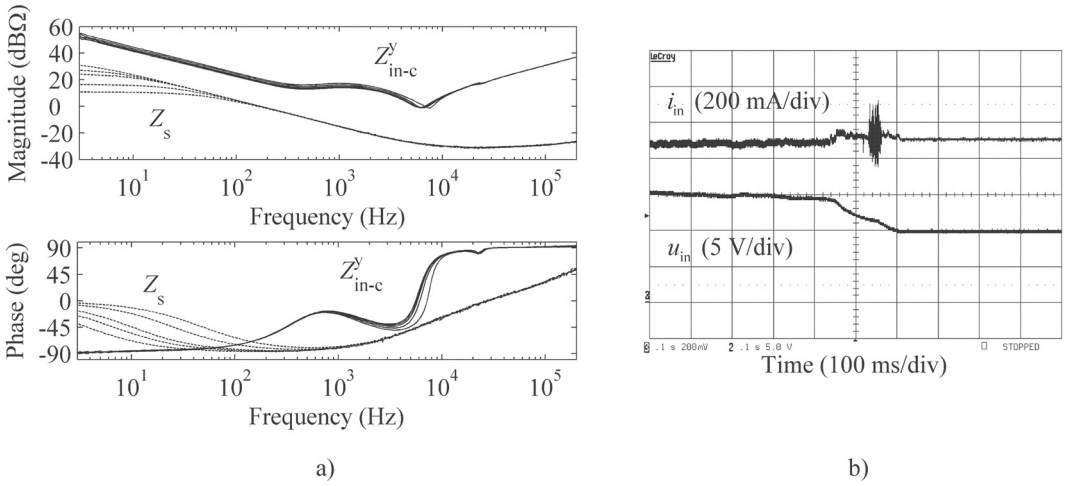

Fig. 4.3 VF superbuck converter under input-current control: a) source impedance Z_{s} (dashed line) vs. converter input impedance $Z_{\text{in-c}}^{\text{y}}$ (solid line) and b) the saturation of the converter input current in the vicinity of the MPP.

Under output-voltage control the input impedance is as given in (4.2) indicating that there are parameters that may cause problems. The loop gain $L_{\text{out}}^{\text{g}}$ is usually high at the low frequencies. Consequently, the ideal input impedance $Z_{\text{in-}\infty}^{\text{g}} = \left(Y_{\text{in-}\infty}^{\text{g}}\right)^{-1}$ which is known to behave as negative resistance, dominates at the DC according to (4.3). Fig. 4.4a shows the comparison of source impedance Z_{s} and converter input impedance $Z_{\text{in-c}}^{\text{g}}$ under output-voltage control at different operation points. The closed-loop input impedance is clearly negative incremental resistance. At the MPP, the magnitudes of the source and converter impedances are equal with opposite phases. As a consequence, minor-loop-based instability takes place. The condition where stability can exist is $\left|Z_{\text{s}}\right| < \left|Z_{\text{in-c}}^{\text{g}}\right|$, and therefore the stable operation is possible only in the CV region of the PV module. The minor-loop-based instability can be demonstrated also by time-domain measurements. Fig. 4.4b shows a situation where the operation point of the output-voltage-controlled VF superbuck is moved from the CV region into the vicinity of the MPP. As soon as the MPP is reached, the instability takes place and the input voltage collapses and operation point moves into the CC region. The converter cannot automatically recover from the instability but is stuck in the CC region.

$$Z_{\text{in-c}}^{\text{g}} = \left(Y_{\text{in-c}}^{\text{g}}\right)^{-1} = \left(\frac{Y_{\text{in-o}}^{\text{g}}}{1+L_{\text{out}}^{\text{g}}} + \frac{L_{\text{out}}^{\text{g}} Y_{\text{in-}\infty}^{\text{g}}}{1+L_{\text{out}}^{\text{g}}}\right)^{-1} \tag{4.2}$$

$$Z_{\text{in-c}}^{\text{g}} \approx \left(Y_{\text{in-}\infty}^{\text{g}}\right)^{-1} \approx -\frac{U_{\text{in}}}{I_{\text{in}}} \tag{4.3}$$

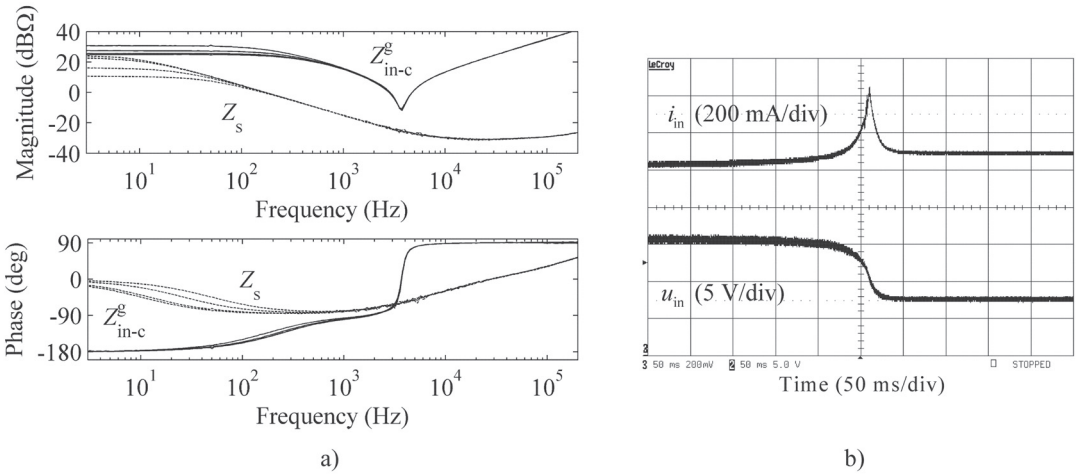

Fig. 4.4 VF superbuck converter under output-voltage control: a) source impedance Z_{s} (dashed lines) vs. converter input impedance $Z_{\text{in-c}}^{\text{g}}$ (solid lines) and b) the behavior of the converter input current i_{in} and voltage u_{in} (PV module voltage) as minor-loop based instability takes place at the MPP.

The investigations show that the VF superbuck converter can operate reliably only in the CV region of the PV module due to the possibility of saturation of current-loop controller under input-current control and impedance-based instability under output-voltage control. The additional capacitor in parallel with the module does not change the source to voltage source and does not have a significant effect on the stability of the interconnection either because the instability takes place at DC.

The fourth-order buck converter shown in Fig. 4.5, known as CF superbuck is a recently developed from the conventional VF superbuck converter [69] also by utilizing duality transformation methods [P5],[P6]. This topology has benefits over the conventional superbuck converter in PV interfacing in terms of operational constraints. The input and output currents and voltages are continuous as in the original superbuck but the CF topology supports the input-voltage control, which is known to be well suited for PV interfacing. The control system is basically the same as in the VF superbuck converter (DDR), but now the input regulation is implemented by controlling the input voltage instead of input current. The block diagram of the control system is presented in Fig. O.1b (Appendix O). Consequently, the dynamics of such a converter can be analyzed by means of current-to-current and current-to-voltage schemes (H and Z parameter

models presented in Appendices D and E) shown in Figs. D.1 and E.1. If only the input loop is active, the closed-loop transfer functions are as given in (D.4) but as soon as the output-voltage limiting control is activated, the closed-loop transfer functions are as given in (E.5). More detailed information on this converter can be found in [P5] and [P6]. The following will briefly present the results of the practical experiments.

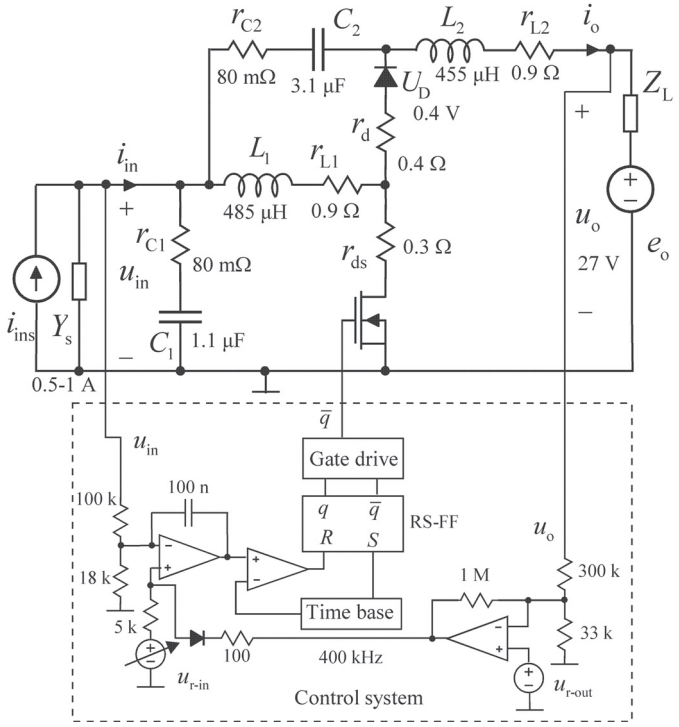

Fig. 4.5 Experimental prototype of the CF superbuck converter with a cascaded input-output voltage control.

The compliance of CF superbuck to interface PV generator was investigated similarly to the VF superbuck in the previous subsection. The output impedances of the PV module and input impedances of the converter were measured at different operation points under both input and output-voltage control and the implications of the frequency-domain measurements were verified with the time-domain measurements. MPP-tracking was not active during the frequency-response measurements but the operation point was varied by changing reference signal $u_{\text{r-in}}$ or $u_{\text{r-out}}$ manually.

The input impedance of CF superbuck under input-voltage control is as given in (4.4). Again, it can be concluded that if the input-voltage loop $(L_{\text{in}}^{\text{h}})$ is properly designed and the peaking is small enough at the resonant frequency, the impedance-based instability should not take place. Frequency responses in Fig. 4.6a confirm that the instability is avoided because the magnitudes of the PV module impedance $Z_{\text{s}} = (Y_{\text{s}})^{-1}$ and converter input impedance $Z_{\text{in-c}}^{\text{h}}$ do not coincide with opposite phases. It was observed that the

input controller of the conventional VF superbuck may saturate in the vicinity of the MPP as demonstrated in Fig. 4.3b. This is not the case with the corresponding CF converter. Fig. 4.6b shows how the microcontroller-based MPP-tracker sweeps the input-voltage reference in such way that the operation point of the PV module moves from deep CC region (5 V) to deep CV region (18 V) and back. The converter operates in a stable manner in all operation points including the MPP. This validates also that the PV generator can be modeled as a current source within its whole range of operation points.

$$Z_{\text{in-c}}^{\text{h}} = \frac{Z_{\text{in-o}}^{\text{h}}}{1 + L_{\text{in}}^{\text{h}}} \tag{4.4}$$

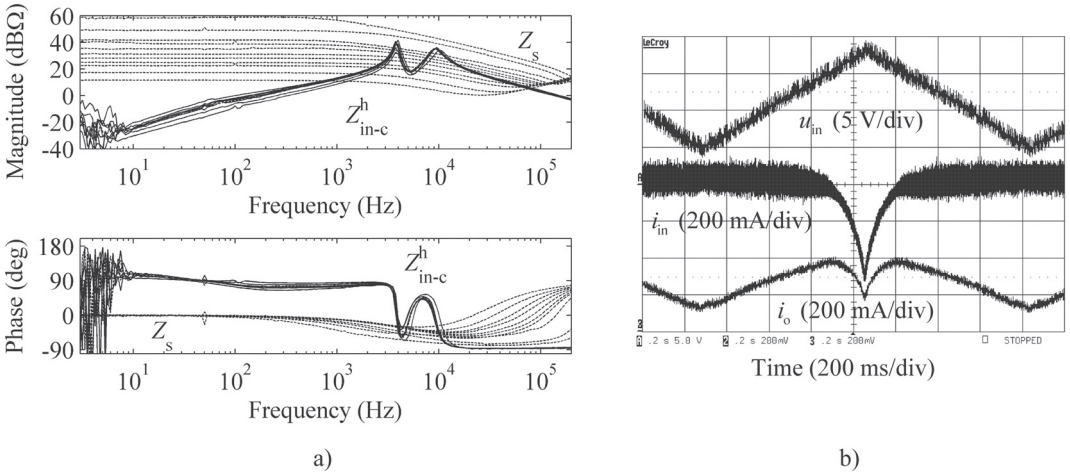

Fig. 4.6 CF superbuck under input-voltage control: a) PV module impedance Z_s (dashed lines) vs. converter input impedance $Z_{\text{in-c}}^{\text{h}}$ (solid lines) and b) time domain behavior of input current i_{in} (PV module current) and output current i_o when the input voltage u_{in} (PV module voltage) is swept by the MPP-tracker from CC region to CV region and back.

The application of output-voltage control makes the CF superbuck prone to the minor-loop-gain-based instability similarly to the case of VF superbuck. Under the output-voltage control, the input impedance of the CF superbuck is as given in (4.5) with the DC characteristics given in (4.6). Fig. 4.7a shows that the DC magnitudes of converter input impedance and PV module impedance coincide at the MPP with opposite phases and instability takes place. The behavior is dual to the VF converter since the condition for the stability is $\left|Z_s\right| > \left|Z_{\text{in-c}}^{\text{z}}\right|$, and therefore the stable operation is possible only in the CC region. The instability can be demonstrated by the time-domain measurements as shown in Fig. 4.7b: The converter operates first under pure input-voltage control in the CV region. As soon as the output voltage limit is reached, the output voltage control activates. Consequently, the instability occurs and the operation point moves quickly into the CC region, where the converter can operate in a stable manner again.

$$Z_{\text{in-c}}^{\text{z}} = \left(\frac{Z_{\text{in-o}}^{\text{z}}}{1 + L_{\text{out}}^{\text{z}}} + \frac{L_{\text{out}}^{\text{z}} Z_{\text{in-}\infty}^{\text{z}}}{1 + L_{\text{out}}^{\text{z}}} \right) \tag{4.5}$$

$$Z_{\text{in-c}}^{\text{z}} \approx Z_{\text{in-}\infty}^{\text{z}} \approx -\frac{U_{\text{in}}}{I_{\text{in}}} \tag{4.6}$$

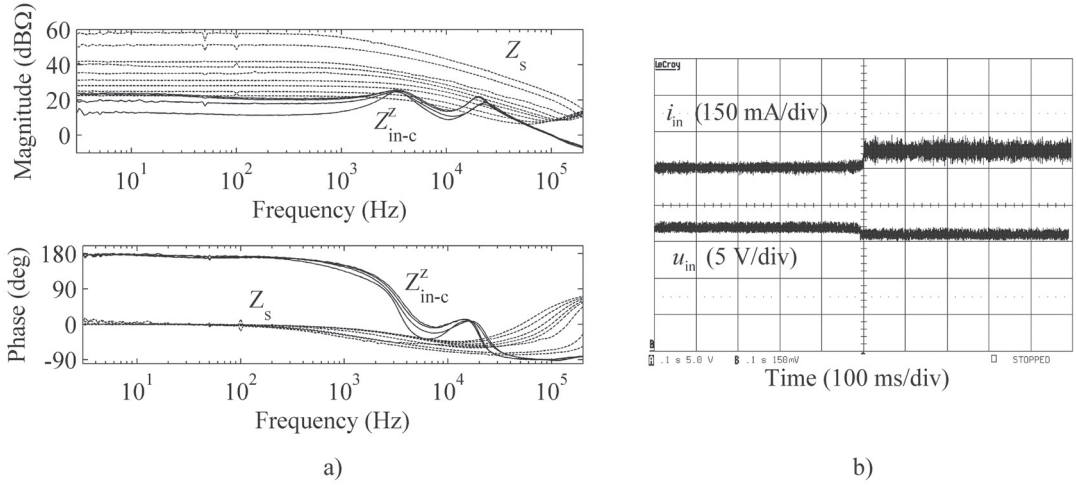

Fig. 4.7 CF superbuck converter under output-voltage control: a) PV module impedance Z_s vs. converter input impedance $Z_{\text{in-c}}^{\text{z}}$ and b) the behavior of the converter input current i_{in} (PV module current) and voltage u_{in} (PV module voltage) when the minor-loop based instability takes place.

The operational constraints of the VF and CF topologies are clearly duals of each other as one could expect. The conclusion is that the current-source properties of the PV module cannot be hidden by an input capacitor if the input current is regulated. It was experimentally proven that the CF superbuck is more suitable for PV interfacing under both input and output control. The VF converter was constrained to operate only in the CV region due to the possibility of the saturation of the current-loop controller or impedance-based instability (minor-loop gain). The saturation of the input-voltage controller does not take place in a CF converter enabling the wide operating range. It was also demonstrated that it can recover from the impedance-based instability automatically.

4.4 Buck-Derived PV Converters

A conventional buck power stage is commonly used as a MPP-tracking converter due to its simple structure and implementation. The input current of a VF buck is not, however, continuous and it is not as such suitable for the PV interfacing. Therefore, a capacitor is usually added at the input of the converter and the input voltage is regulated by means of inverted control scheme as discussed in the previous chapter. As a consequence, the converter actually resembles a dual or CF boost converter. The power stage is not, however, derived by explicit duality transformation method as the CF

superbuck in the previous subsection but implicitly by modifying the existing VF power stage. The transformation is then indirect from the buck-type converter to the boost-type converter. Therefore, the converter can be also called "buck-derived" PV converter. The properties of the corresponding converter are analyzed in detail in [P7] and the following will briefly present the results of the experiments.

Fig. 4.8 shows the experimental DDR-controlled buck-derived power stage connected to a PV module. The output capacitor is basically neglected due to the battery at the output terminal and the input capacitor and input voltage control enables the CF interfacing.

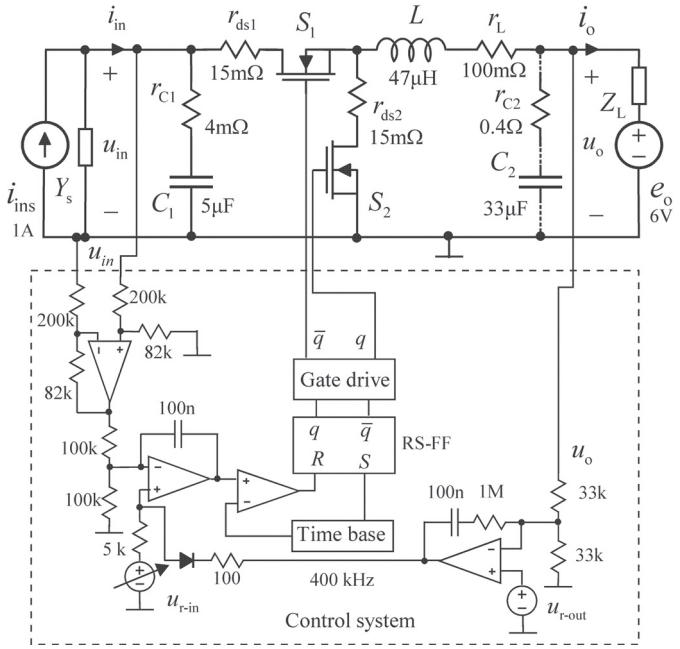

Fig. 4.8 Experimental buck-derived PV converter with a cascaded input-output voltage control

The principle of the cascaded input-output-voltage control system is similar to the CF superbuck converter introduced in the previous subsection: during the normal battery-charging mode, the input voltage is regulated according to the reference voltage which is adjusted manually or provided by the MPP-tracking unit. The output voltage limiting is activated when the predefined output voltage limit is exceeded. Consequently, the dynamics of the converter can be analyzed by utilizing the H and Z parameter models introduced in Appendices D and E. The block diagram of the control system can be found from Appendix O.

As in the previous frequency-response measurements, MPP-tracking was not active but the operation point was varied by changing reference signal $u_{\text{r-in}}$ or $u_{\text{r-out}}$ manually. The measured open-loop responses in Fig. 4.9a show the control-to-input-voltage transfer

function $G_{\text{ci-o}}^{\text{h}}$ in CC and CV region implying that the input-voltage control can be implemented without problems. The responses in Fig. 4.9b show that the open-loop control-to-output-current transfer function $G_{\text{co-o}}^{\text{h}}$ has a low-frequency phase shift of 180 degrees at the CV region, which is challenging for the control design. As a consequence, the output-controlled converter is constrained to operate reliably only in the CC region similarly as the CF superbuck converter. It can also be observed that the RHP zero exists approximately at $I_{\text{in}} / (2\pi\, U_{\text{in}} C_{\text{in}}) \approx 2$ kHz in the CC region as analyses predicted in [P7].

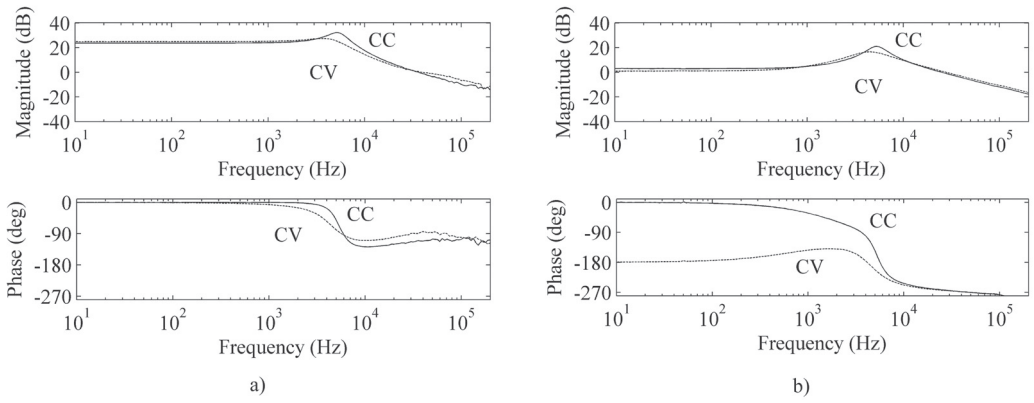

Fig. 4.9 Measured open-loop responses of a) control-to-input-voltage transfer function $G_{\text{ci-o}}^{\text{h}}$ and b) control-to-output-current transfer function $G_{\text{co-o}}^{\text{h}}$ in CC region (solid lines) and CV region (dashed lines) of PV module.

The time-domain measurements in Fig. 4.10 verify that the converter operates in a stable manner under input-voltage control. The theoretical input-voltage range of the converter is from 6 V to 19 V due to the buck nature and the level of output voltage (i.e., 6-V battery) and the open-circuit voltage of the PV module of 19 V. The location of the MPP ($U_{\text{mpp}} \approx 16$ V, $I_{\text{mpp}} \approx 0.9$ A) is observable where the output current i_{o} reaches its maximum value. Fig. 4.10a shows that the operation is stable within this range: the operation point is swept from 8 V to 18 V and back to 8 V without problems. The MPP-tracking with perturb-and-observe algorithm and input-voltage regulation is demonstrated in Fig. 4.10b. The tracking is initiated from the CC region and moves step-by-step towards the MPP and finally reaches it.

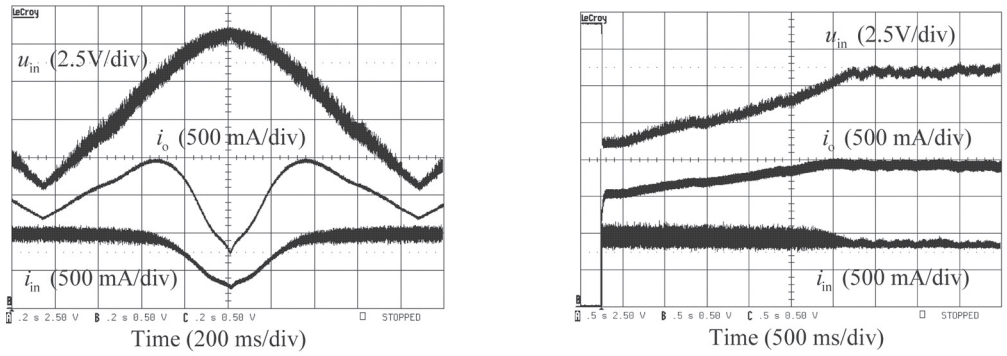

Fig. 4.10 Buck-derived PV converter under input-voltage control: the behavior of the converter input voltage u_{in} (PV module voltage), input current i_{in} (PV module current) and output current i_o during a) the input-voltage reference sweep and b) the MPP-tracking process based and perturb-and-observe algorithm.

If the output control is activated, the stable operation is possible only in the CC region as the measured frequency responses predict in Fig. 4.9b. The situation can be studied by the inverse minor-loop gain similarly to the CF superbuck converter. Fig. 4.11a shows how the PV module impedance Z_s and converter input impedance $Z^z_{in\text{-}c}$ coincide with the opposite phases at the MPP. Consequently, the inverse minor-loop gain equals -1 and the instability occurs. Fig. 4.11b shows the time-domain behavior of the input voltage u_{in}, input current i_{in} and output current i_o when the minor-loop-based instability takes place. The converter first charges the battery in the CV region ($U_{in} \approx 18$ V) until the output-voltage control activates and instability occurs. Operation is stabilized when the operation point enters into the CC region ($U_{in} < 16$ V).

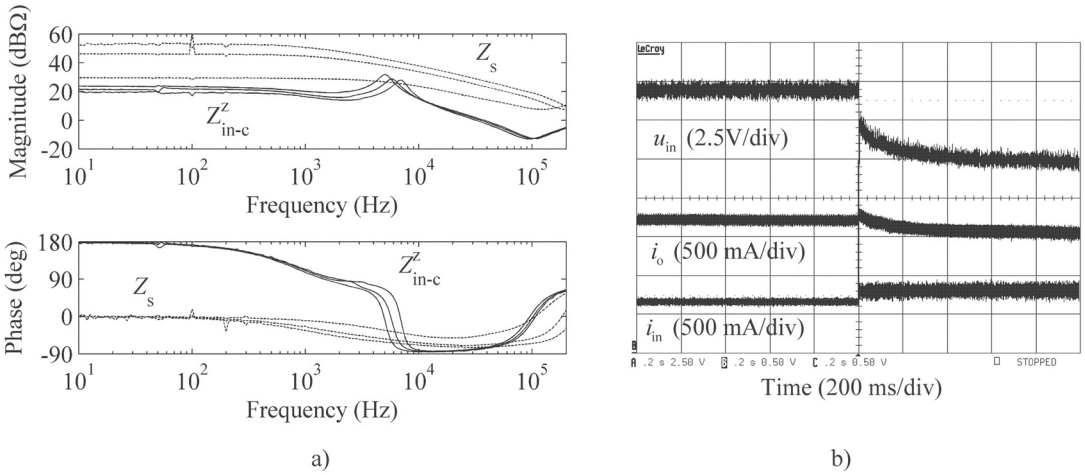

Fig. 4.11 Buck-derived PV converter under output-voltage control: a) PV module impedance Z_s (dashed lines) vs. converter input impedance $Z^z_{in\text{-}c}$ (solid lines) and b) the behavior of the converter input voltage u_{in} (PV module voltage), input current i_{in} (PV module current) and output current i_o when the minor-loop based instability takes place in CV region.

The experiments verify that the converter is actually a CF boost converter, not the VF buck, which was the basis of the converter power stage. The VF-buck properties emerge in the CV region under open loop because the PV module impedance is small neglecting the input capacitor. However, the CF properties dominate in both CC and CV regions if the converter operates under input-voltage control.

The controlling of the buck-based PV converter becomes even more complicated if multiple control loops are involved. The PCM-control is used in the conventional VF converters due to the many benefits it provides [92]. It is also applied in the PV converters but it is recognized that the same benefits cannot be achieved. In fact, the conventional PCM-controlled buck converter is observed to have certain operational constraints (such as RHP pole) in PV interfacing under different regulation modes [65]-[67]. It is not, however, recognized that the problems of such a multi-loop interfacing originate from the relations of incompatible control loops, i.e. loops from both VF and CF domains. The incompatibilities can be pointed out by introducing both voltage-to-current and current-to-current converter models (i.e. Y and H parameter models represented in Appendices C and D) for one physical PV converter. A detailed analysis of such a converter can be found in [P8] and the following will briefly present the practical experiments that support the theoretical findings.

It is well-known that the input impedance of the PCM-controlled buck converter resembles negative resistance at the wide frequency range and that the power stage has a property of a voltage-to-current converter at the open loop [92]. If the converter is used in a PV application as such and its input voltage is controlled, the converter is 'enforced' to operate in the current-to-current conversion mode. Fig. 4.12 shows an experimental PCM-controlled buck converter with input-voltage control. The PCM-control is implemented as with a conventional synchronous VF buck converter and the input-voltage regulation is based on an inverse control scheme (i.e., changing the polarity of the feedback and reference signals). The block diagram of the control system can be found from Appendix O.

The frequency responses under pure PCM control (i.e., MPP-tracking and input-voltage feedback control are not active) in Fig. 4.13a verify that the converter is constrained to operate only in the CV region. The minor-loop-gain-based instability takes place if the CC region is entered because the DC magnitude of PV module impedance Z_{s} (dashed line) and $Z^{\mathrm{y}}_{\mathrm{in\text{-}pcm}}$ coincide at the MPP with opposite phases. Fig. 4.13b shows the time-domain behavior of the instability: input voltage u_{in} and output current i_{o} collapse and the operation point moves quickly into the CC region as a consequence of current-loop-controller saturation.

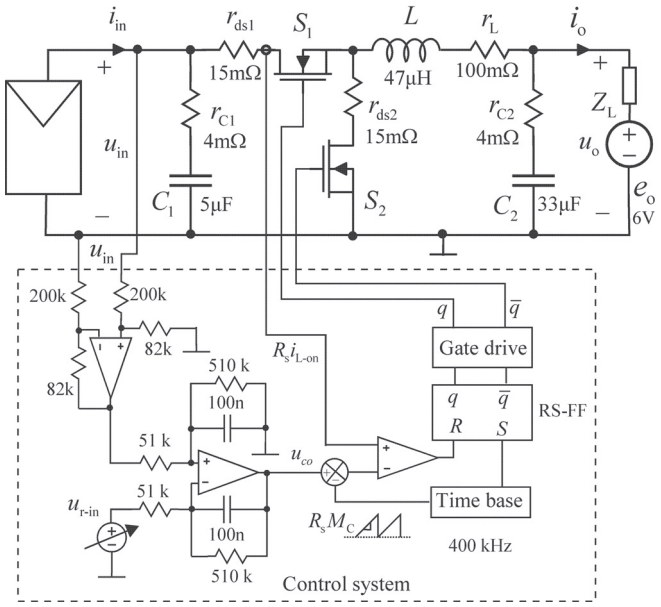

Fig. 4.12 Experimental PCM-controlled buck-based converter under outer-loop input-voltage control

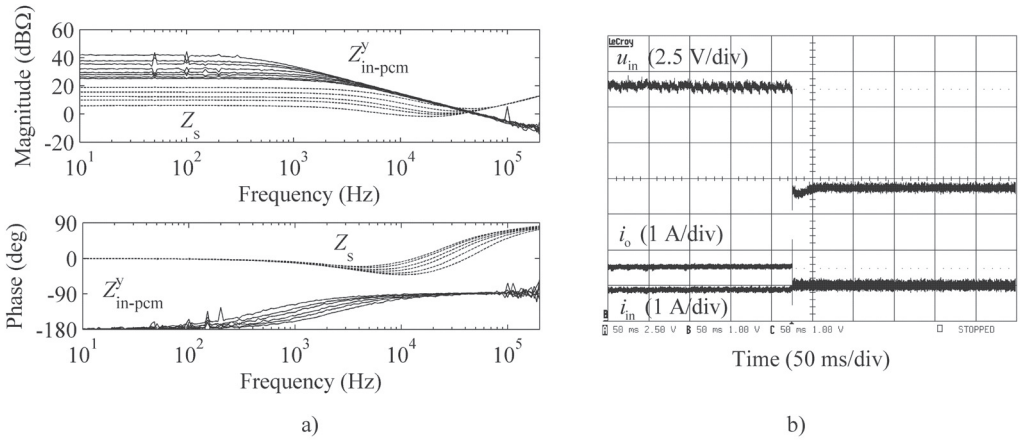

Fig. 4.13 Buck-derived PV converter under pure PCM-control: a) PV module impedance Z_s (dashed lines) vs. converter input impedance $Z^y_{in\text{-}pcm}$ (solid lines) and b) the behavior of the input voltage u_{in} (PV module voltage), input current i_{in} (PV module current) and output current i_o when minor-loop based instability takes place in the MPP region.

The above mentioned behavior is problematic if the input-voltage regulation is applied. The input-voltage control forces the converter operating as a CF converter but the internal PCM control tries to maintain the VF properties at the same time. In practice, an RHP pole appears in the converter transfer functions due to the input-voltage control that is based on inversed conversion scheme ($D \rightarrow D'$) and the converter ceases to operate in a stable manner [P8]. The RHP pole can be removed by heavily overcompensating the inductor-current loop as discussed in [66] but the benefits of the PCM control will naturally be lost as well. The condition for the stable operation is given by

$$M_c > \frac{U_o}{2L} + \frac{I_{in}}{T_s D^2}, \tag{4.7}$$

where M_c is the inductor-current slope compensation, U_o output voltage, L inductance of the power stage inductor, I_{in} input current, T_s switching period and D duty ratio. Fig. 4.14a illustrates the movement of the pole from the RHP to LHP when the inductor-current compensation is increased. Consequently, the input-voltage loop L_{in}^h is stabilized as shown in Fig. 4.14b. Since the stable operation is possible only at a rather high compensation level, the behavior of the converter basically resembles the input-voltage controlled CF boost converter, not the PCM-controlled buck converter.

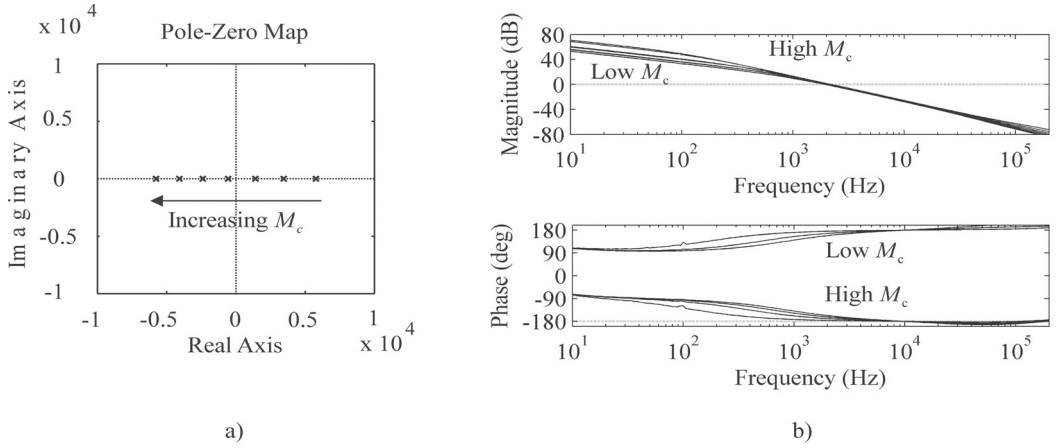

Fig. 4.14 a) Locations of a certain pole (denoted by x) at different inductor-current slope compensation values (M_c) and b) input-voltage loop gain L_{in}^h at corresponding compensation values

The experiments clearly show that the application of a conventional buck converter may yield undesired surprises in PV interfacing. Indeed, the dual nature of a PV module complicates the converter design. Therefore, one should pay attention to the true nature of the converter power stages and control methods used in the PV interfacing. The feedback from the current(s) of power stage inductor(s) is actually the control method of the VF converters which is not suitable for controlling the CF converters, where the internal feedback controls shall be from the voltage(s) of power stage capacitor(s).

4.5 Conclusion

The chapter introduced briefly the experimental frequency and time-domain measurements carried out during the thesis work. The main focus was in the impedance-based stability issues of PV interfacing especially at the DC level signals. The measurements clearly confirm that the theoretical findings reported in the thesis overview and the attached publications are valid.

5 Conclusion

This chapter provides the summaries of the papers [P1]-[P8], the final conclusions and the scientific contributions of the thesis as well as discussion of future topics.

5.1 Summary of the Publications

[P1]

This paper investigates PV interfacing in terms of stability and operational constraints when the MPP-tracking device is based on a VF switched-mode converter. The investigations clearly show that the PV generator is basically a current source with a property of positive incremental resistance at DC. As a consequence, there are two main reasons for the interfacing problems. Firstly, Kirchhoff's current law must be satisfied by ensuring that the input current of the VF converter is always less than the photocurrent. If this condition is not satisfied, the current controller will saturate and the operation point of the PV generator shifts to voltages lower than the MPP voltage. Secondly, the converter is prone to instability if the output voltage or current is controlled due to the negative incremental resistance appearing at the input of the converter. This can be studied by means of well-known minor-loop gain and applying the Nyquist stability criterion. The main conclusion is that the converter can operate reliably only at the voltages higher than the MPP voltage, i.e. in the constant-voltage region.

[P2]

The main contribution of the paper is to make a distinction between the conventional VF and CF interfacing and their stability assessments. The paper investigates the stability and operational constraints of the MPP-tracking CF converter in PV applications. The investigations show that the CF interfacing does not have the same constraints as the VF interfacing. Kirchhoff's current law is satisfied naturally but the input terminal will resemble incremental negative resistance if the output is controlled. The behavior of the converter is dual compared to the VF converters and therefore, the stability of the system can be assessed by means of an *inverse* minor-loop gain. The conclusion is that the operating range of the output controlled CF converter is constrained only at voltages lower than the maximum power point, i.e. constant-current region. However, the CF

converter is shown to be more suitable in PV interfacing than the VF converter under pure input control, because it is not prone to the saturation of the input-voltage controller. It will also recover automatically from the impedance-based instability.

[P3]

This paper investigates the general dynamic properties of CF converters used as MPP-tracking devices in PV applications. A general stability assessment of interconnected CF systems is provided in terms of an impedance-based method. The investigations also reveal new special parameters that govern either the DC behavior of the closed-loop converter or affect the source or load interactions. It is pointed out that the CF converters can be implemented explicitly by duality transformation methods or by adding a capacitor at the input of the converter and controlling their input voltage. The first method is straightforward retaining the original dynamic properties of the converter, e.g. a VF buck converter becomes a CF buck converter. The second method implicitly transforms the converter into the CF domain with significant changes in its steady state and dynamic properties, e.g. a VF buck converter becomes a CF boost converter with its characteristic features such as the existence of RHP zero in its output control dynamics.

[P4]

The implementation of CF converters by using explicit duality transformation methods is investigated in this paper. It is suggested that the energy sources possessing a current-source nature may benefit from the use of such converters. The dynamic characterization of a CF buck converter (called current-sourced buck in the paper) is presented for the first time by also presenting correctly the controlling of the associated MOSFET (i.e., conduction during off time).

[P5], [P6]

These papers investigate the dynamic properties of the fourth-order step-down current converter or CF superbuck converter and its suitability for PV interfacing. The power stage of the converter is developed from the corresponding VF converter by applying explicit duality transformation methods. Its dynamic characterization is presented for the first time in these papers. The investigations show that the state-space-averaging can be applied similarly to conventional VF converters. The analytically obtained dynamic model is verified by an experimental CF superbuck prototype. The main findings of the investigations are that the converter operates without constraints under input-voltage control and MPP tracking but the application of output control (in order to avoid battery overcharge) makes the system prone to instability. It is also observed that the control design should be carried out in the constant-current region of the PV module because it represents the worst-case scenario in terms of resonant behavior and damping.

[P7]

The true steady state and dynamic properties of a conventional buck-based converter in PV applications are investigated in this paper. It is shown that the commonly used buck-based converter is transformed implicitly into a CF boost converter due to the input capacitor and input-voltage control. The steady-state relations of input and output variables as well as the appearance of a RHP zero are clear evidences that the converter possesses boost-type characteristics. The properties of the original VF buck power stage are valid only at open loop and at the constant-voltage region of the PV module, because the output impedance of the module is rather low. This is not, however, true under input voltage control, which transforms the converter definitively into the CF domain. Input-voltage control provides the voltage-type input port, which only supports the CF interfacing. The MPP tracking capability and the existence of a wide operating range are demonstrated by a practical CF boost power stage. It was also remarked that the damping in loop gain may vary significantly due to the operation-point-dependent impedance of the PV generator. However, this actually eases the control design, because the increase in the loop gain is compensated automatically by the corresponding increase in the circuit damping.

[P8]

This paper investigates the suitability of conventional PCM control in PV interfacing converters. The dynamic characterization of a buck-based PCM-controlled converter in PV applications is presented. The main contribution of this paper is that the PCM control is not suitable as an internal control method in the CF converters, because the control of inductor current forces the converter to maintain the properties of VF domain. The PCM-controlled converter works only with extensively compensated inductor-current loop, which actually removes the effect of PCM control.

5.2 Final Conclusions

Generally, electrical engineering is based on voltage-orientated thinking. Power electronics is not an exception, because the VF converters also dominate in power supply applications. This is understandable because most of the energy sources are voltage sources by nature. This way of thinking seems to be, however, very persistent and applied without considering the real nature of the application environment and the theoretical basis of the controlling, etc. This thesis revealed for the first time in practice that there are four different main types of converters. The study concentrated on analyzing the MPP-tracking switched-mode PV converters. One of the main objectives was to emphasize the distinction between the VF and CF domains in this context.

It is known that the PV interfacing is challenging due to the highly varying terminal characteristics of the energy harvesting unit, i.e., the PV generator constructed from individual PV cells, which basically possesses a current-source nature. The environmental conditions and load determine its characteristics and therefore, the generator needs a proper interfacing device to regulate the power flow and trace a certain MPP. The tracing is often performed by a dc-dc switched-mode converter employing some MPP-tracking algorithm. This should bring up a question of what kind of conversion scheme and control methods can be used. Conventionally, this problem is solved by applying the existing VF converter technologies. The VF converters are dedicated to interface energy sources possessing constant-voltage properties such as batteries or voltage buses. This technology is mature and familiar to the design engineers and therefore the same converters are commonly used as a basis for MPP tracking devices. It is observed, however, that an optimal PV interfacing with such converters requires certain modifications. An additional input capacitor is usually added between the source and converter to enhance the constant-voltage properties of the source. This is a logical action since the PV generator is basically a current source and the VF converter does not support it as such. Nevertheless, the regulation of PV voltage is preferred instead of the current, because the latter one is known to be prone to cause saturation of the corresponding feedback controller. This means that the input voltage of the interfacing converter is most often controlled, which is not a property of VF domain. The investigations in this thesis show that the abovementioned modifications change the properties of a converter drastically. As a consequence of this, the VF converter actually transforms into a CF converter and the dynamics and operational constraints change accordingly.

The study also concluded that the problem in the design of PV converters is that the duality of electrical circuits is not recognized or treated properly. The duality principles were first applied in the late 1960s and the duality-derived CF converters were already introduced in the 1970s. Nevertheless, the CF converters implemented by the explicit duality transformation have not become common in the PV interfacing although they support current-type energy supplies by definition. Obviously, the implementation of a PV converter relies strongly on its voltage-orientated past.

The implementation of CF converters in this thesis was divided into three categories. Firstly, the converters can be implemented based on intuition. This method is analogous to the design of conventional VF converters but it is performed under CF domain. The intuitive approach can be compared to natural problem solving where the conversion structure is forced to comply with the circuit theory, input energy supply and output load. This was demonstrated by developing the basic CF buck and boost topologies. The second method is the explicit duality transformation. It transforms the VF converter into a CF converter in such a way that the dynamic characteristics are retained, e.g. the VF

buck transforms into a CF buck. This was demonstrated by comparing experimental VF and CF superbuck converters. It was also noticed also that the CF superbuck topology, not characterized earlier, is well suited for PV interfacing due to its continuous input voltage and output current. The third method is the implicit implementation as discussed already above. This method is based on the duality as well but it is not commonly recognized to produce such converters. It was demonstrated both theoretically and experimentally that a conventional VF buck converter transforms indirectly into a CF boost converter, which incorporates a RHP zero and duty-ratio dependent resonant behavior. This kind of transformation may yield undesired surprises in the behavior of the converter if it is not recognized. The RHP zero, for example, limits the achievable control bandwidth.

Due to the observed discrepancies in the design of the PV converter, a generalized dynamic model of a switched-mode converter was developed in this thesis. The generalized model can be applied to derive all the possible conversion schemes, i.e. voltage-to-voltage, voltage-to-current, current-to-current and current-to-voltage, which can be dynamically represented by means of parameters known as G, Y, H and Z. The first two belong to the familiar VF domain and the latter two belong to the CF domain. The study included the interaction analyses and operation under closed loop for all the possible conversion schemes revealing new special parameters. The special parameters are useful because they govern the DC behavior of the closed-loop of the operation or affect the source and load interactions. The significance of ideal input impedance and admittance was pointed out theoretically as well as demonstrated by practical experiments.

The stability of interconnected VF systems can be studied by means of a certain impedance ratio known as minor-loop gain by applying the Nyquist stability criterion. The concept of the minor-loop gain was originally related to the input-filter design of a conventional voltage regulator and established by R. D. Middlebrook in the 1970s. The impedance-based stability assessment method was now generalized and the inverse of the minor-loop gain was shown to be applicable in the CF domain. The practical frequency and time-domain experiments confirm that the theoretical findings are valid.

5.3 Future Topics

The thesis provided a comprehensive study of converters that were basically forgotten to exist. It can be said that the dynamic profile of a CF switched-mode converter was established in this study completing the previous works related to the dynamics of the conventional VF converters [92],[94],[95]. However, this work was just the beginning and there are still a multitude of questions left. It is also obvious that the terminology

used in power electronics has to be modified to correspond to the new situation in order to avoid confusion.

The thesis analyzed converters operating only in CCM, because it is usually preferred in PV interfacing. Some applications may, however, benefit from operation in DCM. The DCM analysis in the CF domain is analogous to the VF domain but the capacitor voltage is treated as a discontinuous variable, not the inductor current.

Only the basic feedback control methods were covered in this thesis. A control method that is based on capacitor voltage (analogous to the control of inductor current) is an interesting CF concept that may yield beneficial properties regarding converter dynamics. More advanced CF converters may also employ feedforward techniques in order to create new desired dynamic features.

One challenge is, of course, how the ideas and concepts provided in this thesis will be adopted into practical usage. Theoretical formulations can often be seen just as academic trivia that cannot be conveniently applied in practical engineering. This study proves, however, that there can be a powerful relation between theory and practice if only the basic concepts related to the nature of energy source, interfacing converter and load are clear. After that, any difficult and theoretical formulations can be simplified into practical rules of thumb.

References

[1] B. K. Bose, “Global warming: Energy, environmental pollution, and the impact of power electronics ,” *IEEE Industrial Electronics Magazine*, vol. 4, no. 1, pp. 6-17, March 2010.

[2] S. R. Bull, “Renewable energy today and tomorrow,” *Proceedings of the IEEE*, vol. 89, no. 8, pp. 1216-1226, August 2001.

[3] S. Rahman, ”Green power: what is it and where can we find it?,” *IEEE Power and Energy Magazine*, vol. 1, no. 1, pp. 30-37, January-February 2003.

[4] A. Jäger-Waldau, “Photovoltaics and renewable energies in Europe,” *Renewable and Sustainable Energy Reviews*, vol. 11, no. 7, pp. 1414-1437, September 2007.

[5] B. Kroposki, R. Margolis, and D. Ton, “Harnessing the sun – An overview of solar technologies,” *IEEE Power and Energy Magazine*, vol. 7, no. 3, pp. 22-33, May-June 2009.

[6] S. R. Wenham and M. A. Green, “Silicon solar cells,” *Progress in Photovoltaics: Research and Application*, vol. 4, no. 1, January-February 1996.

[7] D. M. Chapin, C. S. Fuller, and G. L. Pearson, “A new p-n junction photocell for converting solar radiation into electrical power,” Bell Telephone Laboratories Inc., Murray Hill, New Jersey, 1954.

[8] A. Luque, and S. Hegedus, *Handbook of Photovoltaic Science and Engineering*, John Wiley & Sons, Ltd, 2003.

[9] M. A. Green, K. Emery, Y. Hishikawa and W. Warta, “Solar cell efficiency tables (version 37)”, *Progress in Photovoltaics: Research and Application*, vol. 19, no. 1, pp. 84-92, January 2011.

[10] S. R. Wenham, M. A. Green, M. E. Watt, and R. Corkish, *Applied Photovoltaics*, 2nd ed., Earthscan, 2007.

[11] J. C. McLaughlin, and K. L. Kaiser, “Deglorifying the maximum power transfer theorem and factors in impedance selection,” *IEEE Trans. on Education*, vol. 50, no. 3, pp. 251-255, August 2007.

[12] T. Esram, and P. L. Chapman, “Comparison of photovoltaic array maximum power point tracking techniques,” *IEEE Trans. on Energy Conversion*, vol. 22, no. 2, pp. 439-449, June 2007.

[13] V. Salas, E. Olias, A. Barrado, and A. Lazaro, "Review of the maximum power point tracking algorithms for stand-alone photovoltaic systems," *Solar Energy Materials and Solar Cells*, vol. 90, no. 11, pp. 1555-1578, July 2006.

[14] S. Jain, and V. Agarwal, "Comparison of the performance of maximum power point tracking schemes applied to single-stage grid connected photovoltaic systems," *IET Electric Power Applications*, vol. 1, no. 5, pp. 753-762, September 2007.

[15] D. P. Hohm, and M. E. Ropp, "Comparative study of maximum power point tracking algorithms," *Progress in Photovoltaics: Research and Applications*, vol. 11, no. 1, pp. 47-62, January 2003.

[16] S. B. Kjaer, J. K. Pedersen, and F. Blaabjerg, "A review of single-phase grid-connected inverters for photovoltaic modules," *IEEE Trans. on Industry Applications*, vol. 41, no. 5, pp. 1292-1306, September/October 2005.

[17] M. Calais, J. Myrzik, T. Spoonet, and V. G. Agelidis, "Inverters for single-phase connected photovoltaic systems – an overview," in *Proc. IEEE Power Electronics Specialist Conference*, pp. 1995-2000, 2002.

[18] J. M. Carrasco, L. G. Franquelo, J. T. Bialasiewicz, E. Galvan, R. C. P. Guisado, Ma. A. M. Prats, J. I. Leon, and N. Moreno-Alfonso, "Power-electronic systems for the grid integration of renewable energy sources: a survey," *IEEE Trans. on Industrial Electronics*, vol. 53, no. 4, pp. 1002-1016, August 2006.

[19] A. Capel, D. O'Sullivan, and J.C. Marpinard, "High-power condition for space applications," *Proceedings of the IEEE*, vol. 76, no. 4, pp. 391-408, April 1988.

[20] M. Mack, "Solar power for telecommunications – the last decade," in *Proc. IEEE International Telecommunication Energy Conference*, pp. 274-281, 1984.

[21] Y. J. Wang, and P. C. Hsu, "Analytical modelling of partial shading and different orientation of photovoltaic modules," *IET Renewable Power Generation*, vol. 4, no. 3, pp. 272-282, May 2010.

[22] H. Patel, and V. Agarwal, "Maximum power point tracking scheme for PV systems operating under partially shaded conditions," *IEEE Trans. on Industrial Electronics*, vol. 55, no. 4, pp. 1689-1698, April 2008.

[23] A. Mäki, S. Valkealahti, and T. Suntio, "Dynamic terminal characteristics of a photovoltaic generator," *Power Electronics and Motion Control Conference*, pp. T12-76 – T12-80, 2010.

[24] N. Femia, G. Lisi, G. Petrone, and G. Spagnuolo, M. Vitelli, "Distributed maximum power point tracking of photovoltaic arrays," *IEEE Trans. on Industrial Electronics*, vol. 55, no. 7, pp. 2610-2621, July 2008.

[25] A. I. Bratcu, I. Munteanu, S. Bacha, D. Picault, and B. Raison, "Cascaded DC-DC converter photovoltaic systems: power optimization issues," *IEEE Trans. on Industrial Electronics*, vol. 58, no. 2, pp. 403-411, February 2011.

[26] J. Imhoff, J. R. Pinheiro, J. L. Russi, D. Brum, R. Gules, and H.L Hey. "DC-DC converters in a multistring configuration for stand-alone photovoltaic systems," in *Proc. IEEE Power Electronics Specialists Conference*, pp. 2806-2812, 2008.

[27] G. R. Walker, and J. C. Pierce, "Photovoltaic DC-DC module integrated converter for novel cascaded and bypass grid connection topologies – design and optimisation," in *Proc. IEEE Power Electronics Specialists Conference*, pp. 1-7, 2006.

[28] M. Meinhardt, T. O'Donnell, H. Schneider, J. Flannery, C. O. Mathuna, P. Zacharias, and T. Krieger, "Miniaturised 'low profile' module integrated converter for photovoltaic applications with integrated magnetic components," *in Proc. IEEE Applied Power Electronics Conference and Exposition*, pp. 305-311, 1999.

[29] B. Sahan, A. N. Vergara, N. Henze, A. Engler, and P. Zacharias, "A single-stage PV module integrated converter based on a low-power current-source inverter," *IEEE Trans. on Industrial Electronics*, vol. 55, no. 7, July 2008.

[30] J. J. Bzura, "The AC module: an overview and update on self-contained modular PV systems – summary of a panel session presentation," *IEEE Power and Energy Society General Meeting*, pp. 1-3, 2010.

[31] H. B., Puttgen, P. R. MacGregor and F. C. Lambert, "Distributed generation: semantic hype or the dawn of new era," *IEEE Power & Energy Magazine*, vol. 1, no. 1, pp. 22-29, January-February 2003.

[32] J. M. Guerrero, F. Blaabjerg, T. Zhelev, K. Hemmes, E. Monmasson, S. Jemeï, M. P. Comech, R. Granadino, and J. I. Frau, "Distributed generation: toward a new energy paradigm," *IEEE Industrial Electronics Magazine*, vol. 4, no. 1, pp. 52-64, March 2010.

[33] E. Caamaño-Martín, H. Laukamp, M. Jantsch, T. Erge, J. Thornycroft, H. De Moor, S. Cobben, D. Suna and B. Gaiddon, "Interaction between photovoltaic distributed generation and electricity networks," *Progress in Photovoltaics: Research and Application*, vol. 16, no. 7, pp. 629-643, August 2008.

[34] D. Fouquet, and T. B. Johansson, "European renewable energy policies at crossroads – focus on electricity support mechanisms," *Energy Policies*, vol. 36, no. 11, pp. 4079-4092, August 2008.

[35] S. Ropenus, H. K. Jacobsen, and S. T. Schrörer, "Network regulation and support schemes – how policy interactions affect the integration of distributed generation," *Renewable Energy*, vol. 36, no. 7, pp. 1949-1956, July 2011.

[36] E. Lorenzo, "Photovoltaic rural electrification", *Progress in Photovoltaics: Research and Application*, vol. 5, no.1, pp. 3-27, 1997.

[37] A. Doing, "Off-grid electricity for developing countries," *IEE Review*, vol. 45, no. 1, pp. 25-28, January 1999.

[38] E. J. Coster, J. M. A. Myrzik, B. Kruimer, and W. L. Kling, "Integration issues of distributed generation in distribution grids," *Proceedings of the IEEE*, vol. 99, no. 1, January 2011.

[39] N. G. Dhere, "Reliability of PV modules and balance-of-system components," in *Proc. IEEE Photovoltaic Specialists Conference*, pp. 1570-1576, 2005.

[40] M. A. Quintana, D. L. King, F. M. Hosking, J. A. Kratochvil, R. W. Johnson, B. R. Hansen, N. G. Dhere, and M. B. Pandit, "Diagnostic analysis of silicon photovoltaic modules after 20-year field exposure," in *Proc. IEEE Photovoltaic Specialists Conference*, pp. 1420 -1423, 2000.

[41] G. Petrone, G. Spagnuolo, R. Teodorescu, M. Veerachary, and M. Vitelli, "Reliability issues in photovoltaic power processing systems," *IEEE Trans. on Industrial Electronics*, vol. 55, no. 7, pp. 2569-2580, July 2008.

[42] R. W. Boom and H. A. Peterson, "Superconductive energy storage for power systems," *IEEE Trans. on Magnetics*, vol. 8, no. 3, pp. 701-703, September 1972.

[43] P. Thounthong, B. Davat, S. Raël, and P. Sethakul, "Fuel cell high-power applications", *IEEE Industrial Electronics Magazine*, vol. 3, no. 1, pp. 32-46, March 2009.

[44] C. Wang, M. H. Nehrir, and S. Shaw, "Dynamic models and model validation for PEM fuel cells using electrical circuits," *IEEE Trans. on Energy Conversion*, vol. 20, no. 2, pp. 442-451, June 2005.

[45] A. Guistiniani, G. Petrone, G. Spagnuolo, and M. Vitelli, "Low-frequency current oscillations and maximum power point tracking in grid-connected fuel-cell-based systems," *IEEE Trans. on Industrial Electronics*, vol. 57, no. 6, pp. 2042-2053, June 2010.

[46] J. Thongpron, K. Kirtikara, and C. Jivicate, "A method for determination of dynamic resistance of photovoltaic modules under illumination", *Solar Energy Materials and Solar Cells*, vol. 90, nos. 18-19, pp. 3078-3084, November 2006.

[47] S. Lyi, and R. A. Dougal, "Dynamic multiphysics model for solar array," *IEEE Trans. on Energy Conversion*, vol. 17, no. 2, pp. 285-294, June 2002.

[48] R. A. Kumar, M. S. Suresh, and J. Nagaraju, "Effect of solar array capacitance on the performance of switching shunt voltage regulator," *IEEE Trans. on Power Electronics*, vol. 21, no. 2, pp. 543-548, March 2006.

[49] R. D. Middlebrook and S. G. Kimble, "Design of the HEAO main bus shunt regulator," *IEEE Trans. on Aerospace and Electronics Systems*, vol. AES-12, no. 2, pp. 162–172, Mar. 1976.

[50] A. Garrigos, J. M. Blanes, J. A. Carrasco, A. H. Weinberg, E. Maset, E. Sanchis-Kilders, J. B. Ejea, and A. Ferreres, "The sequential switching shunt maximum power regulator and its application in the electric propulsion system of spacecraft," in *Proc. IEEE Power Electronics Specialists Conference*, pp. 1374–1379, 2007.

[51] A. Capel, J. C. Marpinard, J. Jalade and M. Valentin, "Current fed and voltage fed switching DC/DC converters – Steady state and dynamic models, their applications in space technology," in *Proc. IEEE International Telecommunications Energy Conference*, pp. 421-430, 1983.

[52] W. Xiao, W. G. Dunford, P. R. Palmer, and A. Capel, "Regulation of photovoltaic voltage," *IEEE Trans. on Industrial Electronics*, vol. 54, no. 3, pp. 1365-1374, June 2007.

[53] W. Xiao, N. Ozog, and W. G. Dunford, "Topology study of photovoltaic interface for maximum power point tracking," *IEEE Trans. on Industrial Electronics*, vol. 54, no. 3, pp. 1696-1704, June 2007.

[54] K. Siri, "Study of system instability in solar-array-based power systems," *IEEE Trans. on Aerospace and Electronic Systems*, vol. 36, no. 3, pp. 957-964, July 2000.

[55] H. Bae, J. Lee, S. Park, and B. H. Cho, "Large-signal stability analysis of solar array power system," *IEEE Trans. on Aerospace and Electronic Systems*, vol. 44, no. 2, pp. 538-546, April 2008.

[56] A. M. Pernia, J. Arias, M. J. Prieto, and J. A. Martinez, "A modular strategy for isolated photovoltaic systems based on microcontroller," *Renewable Energy*, vol. 34, no. 7, pp. 1825-1832, July 2009.

[57] H. Dehbonei, S. R. Lee, and H. Nehrir, "Direct energy transfer for high efficiency photovoltaic energy systems Part I: Concepts and hypothesis," *IEEE Trans. on Aerospace and Electronic Systems*, vol. 45, no. 1, pp. 31–45, January 2009.

[58] H. Dehbonei, S. R. Lee, and S. H. Ko, "Direct energy transfer for high efficiency photovoltaic energy systems Part II: Experimental evaluation," *IEEE Trans. on Aerospace Electronic Systems*, vol. 45, no. 1, pp. 46–57, January 2009.

[59] J. M. Enrique, E.Duran, M. Sidrach-de-Cardona, and J. M. Andujar, "Theoretical assessment of the maximum power point tracking efficiency of photovoltaic facilities with different converter topologies," *Solar Energy*, vol. 81, no. 1, pp. 31–38, January 2007.

[60] R. P. Venturini, V. V. R. Scarpa, G. Spiazzi, and S. Buso, "Analysis of limit cycle oscillations in maximum power point tracking algorithms," in *Proc. IEEE Power Electronics Specialists Conference*, pp. 378-384, 2008.

[61] J. H. Yang, H. S. Bae, J. H. Lee, and B. H. Cho, "A simplified series-parallel structure for the regulated peak power tracking (RPPT) system," in *Proc. IEEE Applied Power Electronics Conference and Exposition*, pp. 160-166, 2008.

[62] M. C. Glass, "Advancements in the design of solar-array to battery charge current regulations," in *Proc. IEEE Power Electronics Specialists Conference*, pp. 346-350, 1977.

[63] M. G. Villalva, and E. F. Ruppert, "Input-controlled buck converter for photovoltaic applications: modeling and design," *IET Power Electronics, Machines and Drives Conference*, pp. 505-509, 2008.

[64] M. G. Villalva, T. G. de Siqueira and E. Ruppert, "Voltage regulation of photovoltaic arrays: small-signal analysis and control design," *IET Power Electronics*, vol. 3, no. 6, pp. 869-880, 2010.

[65] P. T. Huynh, and B. H. Cho, "Design and analysis of a regulated peak-power tracking system," *IEEE Trans. on Aerospace and Electronic Systems*, vol. 35, no. 1, pp. 84-92, January 1999.

[66] S. H. Park, H. S. Bae, J. H. Lee, and B. H. Cho, "Design of peak and charge current-mode control for parallel module solar array regulator system," in *Proc. IEEE Power Electronics Specialists Conference*, p. 1-5, 2006.

[67] S. J. Park, F. S. Kang, S. E. Cho, C. J. Moon, H. K. Nam, and T. Ise, "New parallel driving strategy based on modified converters and peak current mode control for photovoltaic power generation systems," *Solar Energy*, vol. 80, no. 5, pp. 524-534, May 2006.

[68] F. Tonicello, "The control problem of maximum point power tracking in power systems," in *Proc. European Space Power Conference*, p. 7, May 2005.

[69] R. Tymersky, and V. Vorpérian, "Generation and classification of PWM DC-to-DC converters," *IEEE Trans. on Aerospace and Electronic Systems*, vol. 24, no. 6, pp. 743-754, November 1988.

[70] D. Shmilovitz, "Gyrator realization based on a capacitive switched cell," *IEEE Trans. on Circuits and Systems I: Regular Papers*, vol. 53, no. 12, pp. 1418-1422, December 2006.

[71] C. K. Tse, *Linear Circuit Analysis*, Harlow, England, Addison Wesley Longman, 1998, pp. 226-240.

[72] G. M. S. Azevedo, M. C. Cavalcanti, K. C. Oliveira, F. A. S. Neves, and Z. D. Lins, "Evaluation of maximum power point tracking methods for grid connected photovoltaic systems," in *Proc. IEEE Power Electronics Specialists Conference*, pp. 1456-1462, 2008.

[73] G. Chicco, J. Schlabbach, and F. Spertino, "Experimental assessment of the waveform distortion in grid-connected photovoltaic installations," *Solar Energy*, vol. 83, no. 7, pp. 1026-1039, July 2009.

[74] C. A. Desoer and E. S. Kuh, *Basic Circuit Theory*, Tokyo, Japan, McGraw-Hill Kogausha, Ltd, 1969, pp. 444-449.

[75] S. Cuk, "General topological properties of switching structures," in *IEEE Proc. Power Electronics Specialists Conference*, pp. 109-130, 1979.

[76] R. Rabinovici and B. Z. Kaplan, "Novel DC-DC convertor schemes obtained through duality principle and topological considerations," *Electronics Letters*, vol. 27, no. 21, pp. 1948-1950, October 1991.

[77] P. J. Wolfs, "A current-sourced DC-DC converter derived via the duality principle from the half-bridge converter," *IEEE Trans. on Industrial Electronics*, vol. 40, no. 1, pp. 139-144, February 1993.

[78] D. Shmilovitz, "Application of duality for derivation of current converter topologies," *HAIT Journal of Science and Engineering B*, vol. 2, nos. 3-4, pp. 529-557, July 2005.

[79] C. K. Tse, Y. M. Lai, R. J. Xie, and M. H. L Chow, "Application of duality principle to synthesis of single-stage power-factor-correction voltage regulator," *International Journal of Circuit Theory and Applications*, vol. 31, no. 6, pp. 555-570, November/December 2003.

[80] D. Shmilovitz, and S. Singer, "Interfacing photovoltaic panels via a capacitive converter," in *Proc. IEEE Convention of Electrical and Electronics Engineers in Israel*, pp. 160–162, 2002.

[81] D. Shmilovitz, and S. Singer, "A switched mode converter suitable for superconductive magnetic energy storage (SMES) systems," in *Proc. IEEE Applied Power Electronics Conference and Exposition*, pp. 630–634, 2002.

[82] W. W. Weaver, and P. T. Krein, "Analysis and application of a current-sourced buck converter," In *Proc. IEEE Applied Power Electronics Conference*, pp. 1664-1670, 2007.

[83] T. F. Wu, and Y. K. Chen, "Modeling PWM DC/DC converters out of basic converter units," *IEEE Trans. on Power Electronics*, vol. 13, no. 5, pp. 870-881, September 1998.

[84] P. T. Krein, *Elements of Power Electronics*, New York, Oxford University Press, 1998.

[85] R. D. Middlebrook, "Input filter considerations in design and application of switching regulators," in *Proc. IEEE Industry Applications Society*, pp. 91-107, 1976.

[86] K. Zenger, A. Altowati and T. Suntio, "Dynamic properties of interconnected power systems – a system theoretic approach," in *Proc. IEEE Industrial Electronics and Applications*, pp. 1-6, 2006.

[87] J. Sun, "AC power electronic systems: Stability and power quality," in *IEEE Workshop on Control and Modeling for Power Electronics*, pp. 1-10, 2008.

[88] M. Céspedes, and J. Sun, "Renewable energy systems instability involving grid-parallel inverters," in *Proc. IEEE Applied Power Electronics Conference and Exposition*, pp. 1971-1977, 2009.

[89] J. Sun, "Impedance-based stability criterion for grid-connected inverters," *IEEE Trans. on Power Electronics*, DOI: 10.1109/TPEL.2011.2136439, 2011.

[90] R. D. Middlebrook and S. Cuk, "A general unified approach to modelling switching-converter power stages," *International Journal of Electronics*, vol. 42, no. 6, pp. 521-550, June 1977.

[91] R. W. Erickson, and D. Maksimovic, *Fundamentals of Power Electronics*, Kluwer Academic Publishers, 2nd edition, 2001.

[92] T. Suntio, *Dynamic Profile of Switched-Mode Converter – Modeling, Analysis and Control*, Weinham, Wiley-VCH, 2009.

[93] M. Veerachary, "Fourth-order buck converter for maximum power point tracking applications," *IEEE Trans. on Aerospace and Electronic Systems*, vol. 47, no. 2, pp. 896-911, April 2011.

[94] M. Hankaniemi, *Dynamical Profile of Switched-Mode Converter – Fact or fiction?*, Doctoral Thesis, Tampere University of Technology, TUT Publication 687, pp. 131, November 2007.

[95] M. Karppanen, *Issues in Dynamic Analysis and Design of Interconnected DC-DC Power Supply Systems*, Doctoral Thesis, Tampere University of Technology, TUT Publication 764 pp. 105, November 2008.

Appendices

Appendix A: Transformation table from general to specific representation

		Parameters			
		G	Y	H	Z
Input variables	$\hat{x}_{in}$	$\hat{u}_{in}$	$\hat{u}_{in}$	$\hat{i}_{in}$	$\hat{i}_{in}$
	$\hat{x}_{out}$	$\hat{i}_{o}$	$\hat{u}_{o}$	$\hat{u}_{o}$	$\hat{i}_{o}$
	$\hat{x}_{c}$	$\hat{c}$	$\hat{c}$	$\hat{c}$	$\hat{c}$
	$\hat{x}_{r\text{-}in}$	$\hat{i}_{r\text{-}in}$	$\hat{i}_{r\text{-}in}$	$\hat{u}_{r\text{-}in}$	$\hat{u}_{r\text{-}in}$
	$\hat{x}_{r\text{-}out}$	$\hat{u}_{r\text{-}out}$	$\hat{i}_{r\text{-}out}$	$\hat{i}_{r\text{-}out}$	$\hat{u}_{r\text{-}out}$
Output variables	$\hat{y}_{in}$	$\hat{i}_{in}$	$\hat{i}_{in}$	$\hat{u}_{in}$	$\hat{u}_{in}$
	$\hat{y}_{out}$	$\hat{u}_{o}$	$\hat{i}_{o}$	$\hat{i}_{o}$	$\hat{u}_{o}$
Transfer functions	G_{11}	Y_{in}^{g}	Y_{in}^{y}	Z_{in}^{h}	Z_{in}^{z}
	G_{12}	T_{oi}^{g}	T_{oi}^{y}	T_{oi}^{h}	T_{oi}^{z}
	G_{13}	G_{ci}^{g}	G_{ci}^{y}	G_{ci}^{h}	G_{ci}^{z}
	G_{21}	G_{io}^{g}	G_{io}^{y}	G_{io}^{h}	G_{io}^{z}
	G_{22}	Z_{o}^{g}	Y_{o}^{y}	Y_{o}^{h}	Z_{o}^{z}
	G_{23}	G_{co}^{g}	G_{co}^{y}	G_{co}^{h}	G_{co}^{z}
Special transfer functions	$G_{11\text{-}\infty}$	$Y_{in\text{-}\infty}^{g}$	$Y_{in\text{-}\infty}^{y}$	$Z_{in\text{-}\infty}^{h}$	$Z_{in\text{-}\infty}^{z}$
	$G_{12\text{-}\infty}$	$T_{oi\text{-}\infty}^{g}$	$T_{oi\text{-}\infty}^{y}$	$T_{oi\text{-}\infty}^{h}$	$T_{oi\text{-}\infty}^{z}$
	$G_{21\text{-}\infty}$	$G_{io\text{-}\infty}^{g}$	$G_{io\text{-}\infty}^{y}$	$G_{io\text{-}\infty}^{h}$	$G_{io\text{-}\infty}^{z}$
	$G_{22\text{-}\infty}$	$Z_{o\text{-}\infty}^{g}$	$Y_{o\text{-}\infty}^{y}$	$Y_{o\text{-}\infty}^{h}$	$Z_{o\text{-}\infty}^{z}$
	$G_{11\text{-}xo}$	$Y_{in\text{-}sco}^{g}$	$Y_{in\text{-}oco}^{y}$	$Z_{in\text{-}oco}^{h}$	$Z_{in\text{-}sco}^{z}$
	$G_{22\text{-}xi}$	$Z_{o\text{-}oci}^{g}$	$Y_{o\text{-}oci}^{y}$	$Y_{o\text{-}sci}^{h}$	$Z_{o\text{-}sci}^{z}$

Appendix B: Voltage-to-voltage conversion scheme (G parameters)

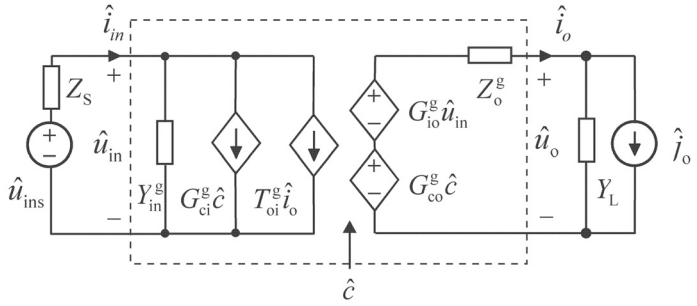

Fig. B.1 Equivalent model of voltage-to-voltage converter with non-ideal source and load

$$\begin{bmatrix}\hat{i}_{in}\\ \hat{u}_o\end{bmatrix}=\begin{bmatrix}Y_{in}^g & T_{oi}^g & G_{ci}^g\\ G_{io}^g & -Z_o^g & G_{co}^g\end{bmatrix}\begin{bmatrix}\hat{u}_{in}\\ \hat{i}_o\\ \hat{c}\end{bmatrix} \tag{B.1}$$

Effect of non-ideal source and load:

$$\begin{bmatrix}\hat{i}_{in}\\ \hat{u}_o\end{bmatrix}=\begin{bmatrix}\dfrac{Y_{in}^g}{1+Z_sY_{in}^g} & \dfrac{T_{oi}^g}{1+Z_sY_{in}^g} & \dfrac{G_{ci}^g}{1+Z_sY_{in}^g}\\ \dfrac{G_{io}^g}{1+Z_sY_{in}^g} & -\dfrac{1+Z_sY_{in\text{-}sco}^g}{1+Z_sY_{in}^g}Y_o^g & \dfrac{1+Z_sY_{in\text{-}\infty}^g}{1+Z_sY_{in}^g}G_{co}^g\end{bmatrix}\begin{bmatrix}\hat{u}_{ins}\\ \hat{i}_o\\ \hat{c}\end{bmatrix} \tag{B.2}$$

$$\begin{bmatrix}\hat{i}_{in}\\ \hat{u}_o\end{bmatrix}=\begin{bmatrix}\dfrac{1+Y_LZ_{o\text{-}oci}^g}{1+Y_LZ_o^g}Y_{in}^g & \dfrac{T_{oi}^g}{1+Y_LZ_o^g} & \dfrac{1+Y_LZ_{o\text{-}\infty}^g}{1+Y_LZ_o^g}G_{ci}^g\\ \dfrac{G_{io}^g}{1+Y_LZ_o^g} & -\dfrac{Y_o^g}{1+Y_LZ_o^g} & \dfrac{G_{co}^g}{1+Y_LZ_o^g}\end{bmatrix}\begin{bmatrix}\hat{u}_{in}\\ \hat{j}_o\\ \hat{c}\end{bmatrix} \tag{B.3}$$

Closed-loop transfer functions:

$$\begin{bmatrix}\hat{i}_{in}\\ \hat{u}_o\end{bmatrix}=\begin{bmatrix}\dfrac{Y_{in\text{-}o}^g}{1+L_{in}^g} & \dfrac{T_{oi\text{-}o}^g}{1+L_{in}^g} & \dfrac{1}{G_{s\text{-}in}}\dfrac{L_{in}^g}{1+L_{in}^g}\\ \left(\dfrac{G_{io\text{-}o}^g}{1+L_{in}^g}+\dfrac{L_{in}^gG_{io\text{-}\infty}^g}{1+L_{in}^g}\right) & -\left(\dfrac{Z_{o\text{-}o}^g}{1+L_{in}^g}+\dfrac{L_{in}^gZ_{o\text{-}\infty}^g}{1+L_{in}^g}\right) & \dfrac{G_{co\text{-}o}^g}{G_{s\text{-}in}G_{ci\text{-}o}^g}\dfrac{L_{in}^g}{1+L_{in}^g}\end{bmatrix}\begin{bmatrix}\hat{u}_{in}\\ \hat{i}_o\\ \hat{i}_{r\text{-}in}\end{bmatrix} \tag{B.4}$$

$$\begin{bmatrix}\hat{i}_{in}\\ \hat{u}_o\end{bmatrix}=\begin{bmatrix}\left(\dfrac{Y_{in\text{-}o}^g}{1+L_{out}^g}+\dfrac{L_{out}^gY_{in\text{-}\infty}^g}{1+L_{out}^g}\right) & \left(\dfrac{T_{oi\text{-}o}^g}{1+L_{out}^g}+\dfrac{L_{out}^gT_{oi\text{-}\infty}^g}{1+L_{out}^g}\right) & \dfrac{G_{ci\text{-}o}^g}{G_{s\text{-}out}G_{co\text{-}o}^g}\dfrac{L_{out}^g}{1+L_{out}^g}\\ \dfrac{G_{io\text{-}o}^g}{1+L_{out}^g} & -\dfrac{Z_{o\text{-}o}^g}{1+L_{out}^g} & \dfrac{1}{G_{s\text{-}out}}\dfrac{L_{out}^g}{1+L_{out}^g}\end{bmatrix}\begin{bmatrix}\hat{u}_{in}\\ \hat{i}_o\\ \hat{u}_{r\text{-}out}\end{bmatrix} \tag{B.5}$$

Appendix C: Voltage-to-current conversion scheme (Y parameters)

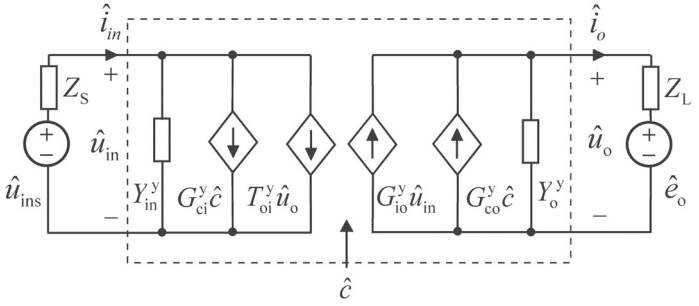

Fig. C.1 Equivalent model of voltage-to-current converter with non-ideal source and load

$$\begin{bmatrix}\hat{i}_{in}\\ \hat{i}_o\end{bmatrix}=\begin{bmatrix}Y_{in}^y & T_{oi}^y & G_{ci}^y\\ G_{io}^y & -Y_o^y & G_{co}^y\end{bmatrix}\begin{bmatrix}\hat{u}_{in}\\ \hat{u}_o\\ \hat{c}\end{bmatrix} \tag{C.1}$$

Effect of non-ideal source and load:

$$\begin{bmatrix}\hat{i}_{in}\\ \hat{i}_o\end{bmatrix}=\begin{bmatrix}\dfrac{Y_{in}^y}{1+Z_sY_{in}^y} & \dfrac{T_{oi}^y}{1+Z_sY_{in}^y} & \dfrac{G_{ci}^y}{1+Z_sY_{in}^y}\\ \dfrac{G_{io}^y}{1+Z_sY_{in}^y} & -\dfrac{1+Z_sY_{in\text{-}oco}^y}{1+Z_sY_{in}^y}Y_o^y & \dfrac{1+Z_sY_{in\text{-}\infty}^y}{1+Z_sY_{in}^y}G_{co}^y\end{bmatrix}\begin{bmatrix}\hat{u}_{ins}\\ \hat{u}_o\\ \hat{c}\end{bmatrix} \tag{C.2}$$

$$\begin{bmatrix}\hat{i}_{in}\\ \hat{i}_o\end{bmatrix}=\begin{bmatrix}\dfrac{1+Z_LY_{o\text{-}oci}^y}{1+Z_LY_o^y}Y_{in}^y & \dfrac{T_{oi}^y}{1+Z_LY_o^y} & \dfrac{1+Z_LY_{o\text{-}\infty}^y}{1+Z_LY_o^y}G_{ci}^y\\ \dfrac{G_{io}^y}{1+Z_LY_o^y} & -\dfrac{Y_o^y}{1+Z_LY_o^y} & \dfrac{G_{co}^y}{1+Z_LY_o^y}\end{bmatrix}\begin{bmatrix}\hat{u}_{in}\\ \hat{e}_o\\ \hat{c}\end{bmatrix} \tag{C.3}$$

Closed-loop transfer functions:

$$\begin{bmatrix}\hat{i}_{in}\\ \hat{i}_o\end{bmatrix}=\begin{bmatrix}\dfrac{Y_{in\text{-}o}^y}{1+L_{in}^y} & \dfrac{T_{oi\text{-}o}^y}{1+L_{in}^y} & \dfrac{1}{G_{s\text{-}in}}\dfrac{L_{in}^y}{1+L_{in}^y}\\ \left(\dfrac{G_{io\text{-}o}^y}{1+L_{in}^y}+\dfrac{L_{in}^yG_{io\text{-}\infty}^y}{1+L_{in}^y}\right) & -\left(\dfrac{Y_{o\text{-}o}^y}{1+L_{in}^y}+\dfrac{L_{in}^yY_{o\text{-}\infty}^y}{1+L_{in}^y}\right) & \dfrac{G_{co\text{-}o}^y}{G_{s\text{-}in}G_{ci\text{-}o}^y}\dfrac{L_{in}^y}{1+L_{in}^y}\end{bmatrix}\begin{bmatrix}\hat{u}_{in}\\ \hat{u}_o\\ \hat{i}_{r\text{-}in}\end{bmatrix} \tag{C.4}$$

$$\begin{bmatrix}\hat{i}_{in}\\ \hat{i}_o\end{bmatrix}=\begin{bmatrix}\left(\dfrac{Y_{in\text{-}o}^y}{1+L_{out}^y}+\dfrac{L_{out}^yY_{in\text{-}\infty}^y}{1+L_{out}^y}\right) & \left(\dfrac{T_{oi\text{-}o}^y}{1+L_{out}^y}+\dfrac{L_{out}^yT_{oi\text{-}\infty}^y}{1+L_{out}^y}\right) & \dfrac{G_{ci\text{-}o}^y}{G_{s\text{-}out}G_{co\text{-}o}^y}\dfrac{L_{out}^y}{1+L_{out}^y}\\ \dfrac{G_{io\text{-}o}^y}{1+L_{out}^g} & -\dfrac{Y_{o\text{-}o}^y}{1+L_{out}^y} & \dfrac{1}{G_{s\text{-}out}}\dfrac{L_{out}^y}{1+L_{out}^y}\end{bmatrix}\begin{bmatrix}\hat{u}_{in}\\ \hat{u}_o\\ \hat{i}_{r\text{-}out}\end{bmatrix} \tag{C.5}$$

Appendix D: Current-to-current conversion scheme (H parameters)

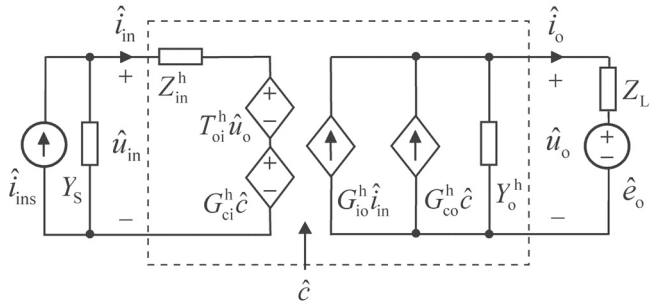

Fig. D.1 Equivalent model of current-to-current converter with non-ideal source and load

$$\begin{bmatrix}\hat{u}_{in}\\ \hat{i}_o\end{bmatrix}=\begin{bmatrix}Z^h_{in} & T^h_{oi} & G^h_{ci}\\ G^h_{io} & -Y^h_o & G^h_{co}\end{bmatrix}\begin{bmatrix}\hat{i}_{in}\\ \hat{u}_o\\ \hat{c}\end{bmatrix} \tag{D.1}$$

Effect of non-ideal source and load:

$$\begin{bmatrix}\hat{u}_{in}\\ \hat{i}_o\end{bmatrix}=\begin{bmatrix}\dfrac{Z^h_{in}}{1+Y_sZ^h_{in}} & \dfrac{T^h_{oi}}{1+Y_sZ^h_{in}} & \dfrac{G^h_{ci}}{1+Y_sZ^h_{in}}\\ \dfrac{G^h_{io}}{1+Y_sZ^h_{in}} & -\dfrac{1+Y_sZ^h_{in\text{-}oco}}{1+Y_sZ^h_{in}}Y^h_o & \dfrac{1+Y_sZ^h_{in\text{-}\infty}}{1+Y_sZ^h_{in}}G^h_{co}\end{bmatrix}\begin{bmatrix}\hat{i}_{ins}\\ \hat{u}_o\\ \hat{c}\end{bmatrix} \tag{D.2}$$

$$\begin{bmatrix}\hat{u}_{in}\\ \hat{i}_o\end{bmatrix}=\begin{bmatrix}\dfrac{1+Z_LY^h_{o\text{-}sci}}{1+Z_LY^h_o}Z^h_{in} & \dfrac{T^h_{oi}}{1+Z_LY^h_o} & \dfrac{1+Z_LY^h_{o\text{-}\infty}}{1+Z_LY^h_o}G^h_{ci}\\ \dfrac{G^h_{io}}{1+Z_LY^h_o} & -\dfrac{Y^h_o}{1+Z_LY^h_o} & \dfrac{G^h_{co}}{1+Z_LY^h_o}\end{bmatrix}\begin{bmatrix}\hat{i}_{in}\\ \hat{e}_o\\ \hat{c}\end{bmatrix} \tag{D.3}$$

Closed-loop transfer functions:

$$\begin{bmatrix}\hat{u}_{in}\\ \hat{i}_o\end{bmatrix}=\begin{bmatrix}\dfrac{Z^h_{in\text{-}o}}{1+L^y_{in}} & \dfrac{T^h_{oi\text{-}o}}{1+L^y_{in}} & \dfrac{1}{G_{s\text{-}in}}\dfrac{L^h_{in}}{1+L^h_{in}}\\ \left(\dfrac{G^h_{io\text{-}o}}{1+L^h_{in}}+\dfrac{L^h_{in}G^h_{io\text{-}\infty}}{1+L^h_{in}}\right) & -\left(\dfrac{Y^h_{o\text{-}o}}{1+L^h_{in}}+\dfrac{L^h_{in}Y^h_{o\text{-}\infty}}{1+L^h_{in}}\right) & \dfrac{G^h_{co\text{-}o}}{G_{s\text{-}in}G^h_{ci\text{-}o}}\dfrac{L^h_{in}}{1+L^h_{in}}\end{bmatrix}\begin{bmatrix}\hat{i}_{in}\\ \hat{u}_o\\ \hat{u}_{r\text{-}in}\end{bmatrix} \tag{D.4}$$

$$\begin{bmatrix}\hat{u}_{in}\\ \hat{i}_o\end{bmatrix}=\begin{bmatrix}\left(\dfrac{Z^h_{in\text{-}o}}{1+L^h_{out}}+\dfrac{L^h_{out}Z^h_{in\text{-}\infty}}{1+L^h_{out}}\right) & \left(\dfrac{T^h_{oi\text{-}o}}{1+L^h_{out}}+\dfrac{L^h_{out}T^h_{oi\text{-}\infty}}{1+L^h_{out}}\right) & \dfrac{G^h_{ci\text{-}o}}{G_{s\text{-}out}G^h_{co\text{-}o}}\dfrac{L^h_{out}}{1+L^h_{out}}\\ \dfrac{G^h_{io\text{-}o}}{1+L^h_{out}} & -\dfrac{Y^h_{o\text{-}o}}{1+L^h_{out}} & \dfrac{1}{G_{s\text{-}out}}\dfrac{L^h_{out}}{1+L^h_{out}}\end{bmatrix}\begin{bmatrix}\hat{i}_{in}\\ \hat{u}_o\\ \hat{i}_{r\text{-}out}\end{bmatrix} \tag{D.5}$$

Appendix E: Current-to-voltage conversion scheme (Z parameters)

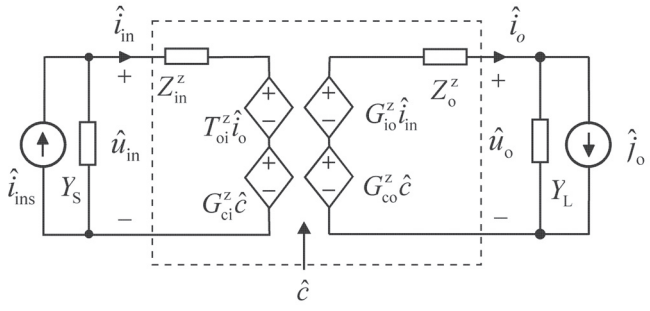

Fig. E.1 Equivalent model of current-to-voltage converter with non-ideal source and load

$$\begin{bmatrix}\hat{u}_{in}\\ \hat{u}_o\end{bmatrix}=\begin{bmatrix}Z^z_{in} & T^z_{oi} & G^z_{ci}\\ G^z_{io} & -Z^z_o & G^z_{co}\end{bmatrix}\begin{bmatrix}\hat{i}_{in}\\ \hat{i}_o\\ \hat{c}\end{bmatrix} \tag{E.1}$$

Effect of non-ideal source and load:

$$\begin{bmatrix}\hat{u}_{in}\\ \hat{u}_o\end{bmatrix}=\begin{bmatrix}\dfrac{Z^z_{in}}{1+Y_sZ^z_{in}} & \dfrac{T^z_{oi}}{1+Y_sZ^z_{in}} & \dfrac{G^z_{ci}}{1+Y_sZ^z_{in}}\\ \dfrac{G^z_{io}}{1+Y_sZ^z_{in}} & -\dfrac{1+Y_sZ^z_{in\text{-}sco}}{1+Y_sZ^z_{in}}Z^z_o & \dfrac{1+Y_sZ^z_{in\text{-}\infty}}{1+Y_sZ^z_{in}}G^z_{co}\end{bmatrix}\begin{bmatrix}\hat{i}_{ins}\\ \hat{i}_o\\ \hat{c}\end{bmatrix} \tag{E.2}$$

$$\begin{bmatrix}\hat{u}_{in}\\ \hat{u}_o\end{bmatrix}=\begin{bmatrix}\dfrac{1+Y_LZ^z_{o\text{-}sci}}{1+Y_LZ^z_o}Z^z_{in} & \dfrac{T^z_{oi}}{1+Y_LZ^z_o} & \dfrac{1+Y_LZ^z_{o\text{-}\infty}}{1+Y_LZ^z_o}G^g_{ci}\\ \dfrac{G^z_{io}}{1+Y_LZ^z_o} & -\dfrac{Z^z_o}{1+Y_LZ^z_o} & \dfrac{G^z_{co}}{1+Y_LZ^z_o}\end{bmatrix}\begin{bmatrix}\hat{i}_{in}\\ \hat{j}_o\\ \hat{c}\end{bmatrix} \tag{E.3}$$

Closed-loop transfer functions:

$$\begin{bmatrix}\hat{u}_{in}\\ \hat{u}_o\end{bmatrix}=\begin{bmatrix}\dfrac{Z^z_{in\text{-}o}}{1+L^z_{in}} & \dfrac{T^z_{oi\text{-}o}}{1+L^z_{in}} & \dfrac{1}{G_{s\text{-}in}}\dfrac{L^z_{in}}{1+L^z_{in}}\\ \left(\dfrac{G^z_{io\text{-}o}}{1+L^z_{in}}+\dfrac{L^z_{in}G^z_{io\text{-}\infty}}{1+L^z_{in}}\right) & -\left(\dfrac{Z^z_{o\text{-}o}}{1+L^z_{in}}+\dfrac{L^z_{in}Z^z_{o\text{-}\infty}}{1+L^z_{in}}\right) & \dfrac{G^z_{co\text{-}o}}{G_{s\text{-}in}G^z_{ci\text{-}o}}\dfrac{L^z_{in}}{1+L^z_{in}}\end{bmatrix}\begin{bmatrix}\hat{i}_{in}\\ \hat{i}_o\\ \hat{u}_{r\text{-}in}\end{bmatrix} \tag{E.4}$$

$$\begin{bmatrix}\hat{u}_{in}\\ \hat{u}_o\end{bmatrix}=\begin{bmatrix}\left(\dfrac{Z^z_{in\text{-}o}}{1+L^z_{out}}+\dfrac{L^z_{out}Z^z_{in\text{-}\infty}}{1+L^z_{out}}\right) & \left(\dfrac{T^z_{oi\text{-}o}}{1+L^z_{out}}+\dfrac{L^z_{out}T^z_{oi\text{-}\infty}}{1+L^z_{out}}\right) & \dfrac{G^z_{ci\text{-}o}}{G_{s\text{-}out}G^z_{co\text{-}o}}\dfrac{L^z_{out}}{1+L^z_{out}}\\ \dfrac{G^z_{io\text{-}o}}{1+L^z_{out}} & -\dfrac{Z^z_{o\text{-}o}}{1+L^z_{out}} & \dfrac{1}{G_{s\text{-}out}}\dfrac{L^z_{out}}{1+L^z_{out}}\end{bmatrix}\begin{bmatrix}\hat{i}_{in}\\ \hat{i}_o\\ \hat{u}_{r\text{-}out}\end{bmatrix} \tag{E.5}$$

Appendix F: Special parameters

Voltage-to-voltage scheme (G)

$$Y^{g}_{\text{in-sco}} = Y^{g}_{\text{in}} + \frac{G^{g}_{\text{io}} T^{g}_{\text{oi}}}{Z^{g}_{\text{o}}} \qquad Y^{g}_{\text{in-}\infty} = Y^{g}_{\text{in}} - \frac{G^{g}_{\text{io}} G^{g}_{\text{ci}}}{G^{g}_{\text{co}}} \qquad T^{g}_{\text{oi-}\infty} = T^{g}_{\text{oi}} + \frac{Z^{g}_{\text{o}} G^{g}_{\text{ci}}}{G^{g}_{\text{co}}}$$

$$Z^{g}_{\text{o-oci}} = Z^{g}_{\text{o}} + \frac{G^{g}_{\text{io}} T^{g}_{\text{oi}}}{Y^{g}_{\text{in}}} \qquad Z^{g}_{\text{o-}\infty} = Z^{g}_{\text{o}} + \frac{T^{g}_{\text{oi}} G^{g}_{\text{co}}}{G^{g}_{\text{ci}}} \qquad G^{g}_{\text{io-}\infty} = G^{g}_{\text{io}} - \frac{Y^{g}_{\text{in}} G^{g}_{\text{co}}}{G^{g}_{\text{ci}}}$$

Voltage-to-current scheme (Y)

$$Y^{y}_{\text{in-oco}} = Y^{y}_{\text{in}} + \frac{G^{y}_{\text{io}} T^{y}_{\text{oi}}}{Y^{y}_{\text{o}}} \qquad Y^{y}_{\text{in-}\infty} = Y^{y}_{\text{in}} - \frac{G^{y}_{\text{io}} G^{y}_{\text{ci}}}{G^{y}_{\text{co}}} \qquad T^{y}_{\text{oi-}\infty} = T^{y}_{\text{oi}} + \frac{Y^{y}_{\text{o}} G^{y}_{\text{ci}}}{G^{y}_{\text{co}}}$$

$$Y^{y}_{\text{o-oci}} = Y^{y}_{\text{o}} + \frac{G^{y}_{\text{io}} T^{y}_{\text{oi}}}{Y^{y}_{\text{in}}} \qquad Y^{y}_{\text{o-}\infty} = Y^{y}_{\text{o}} + \frac{T^{y}_{\text{oi}} G^{y}_{\text{co}}}{G^{y}_{\text{ci}}} \qquad G^{y}_{\text{io-}\infty} = G^{y}_{\text{io}} - \frac{Y^{y}_{\text{in}} G^{y}_{\text{co}}}{G^{y}_{\text{ci}}}$$

Current-to-current scheme (H)

$$Z^{h}_{\text{in-oco}} = Z^{h}_{\text{in}} + \frac{G^{h}_{\text{io}} T^{h}_{\text{oi}}}{Y^{h}_{\text{o}}} \qquad Z^{h}_{\text{in-}\infty} = Z^{h}_{\text{in}} - \frac{G^{h}_{\text{io}} G^{h}_{\text{ci}}}{G^{h}_{\text{co}}} \qquad T^{h}_{\text{oi-}\infty} = T^{h}_{\text{oi}} + \frac{Y^{h}_{\text{o}} G^{h}_{\text{ci}}}{G^{h}_{\text{co}}}$$

$$Y^{h}_{\text{o-sci}} = Y^{h}_{\text{o}} + \frac{G^{h}_{\text{io}} T^{h}_{\text{oi}}}{Z^{h}_{\text{in}}} \qquad Y^{h}_{\text{o-}\infty} = Y^{h}_{\text{o}} + \frac{T^{h}_{\text{oi}} G^{h}_{\text{co}}}{G^{h}_{\text{ci}}} \qquad G^{h}_{\text{io-}\infty} = G^{h}_{\text{io}} - \frac{Z^{h}_{\text{in}} G^{h}_{\text{co}}}{G^{h}_{\text{ci}}}$$

Current-to-voltage scheme (Z)

$$Z^{z}_{\text{in-sco}} = Z^{z}_{\text{in}} + \frac{G^{z}_{\text{io}} T^{z}_{\text{oi}}}{Z^{z}_{\text{o}}} \qquad Z^{z}_{\text{in-}\infty} = Z^{z}_{\text{in}} - \frac{G^{z}_{\text{io}} G^{z}_{\text{ci}}}{G^{z}_{\text{co}}} \qquad T^{z}_{\text{oi-}\infty} = T^{z}_{\text{oi}} + \frac{Z^{z}_{\text{o}} G^{z}_{\text{ci}}}{G^{z}_{\text{co}}}$$

$$Z^{z}_{\text{o-sci}} = Z^{z}_{\text{o}} + \frac{G^{z}_{\text{io}} T^{z}_{\text{oi}}}{Z^{z}_{\text{in}}} \qquad Z^{z}_{\text{o-}\infty} = Z^{z}_{\text{o}} + \frac{T^{z}_{\text{oi}} G^{z}_{\text{co}}}{G^{z}_{\text{ci}}} \qquad G^{z}_{\text{io-}\infty} = G^{z}_{\text{io}} - \frac{Z^{z}_{\text{in}} G^{z}_{\text{co}}}{G^{z}_{\text{ci}}}$$

Appendix G: Impedance measurement technique

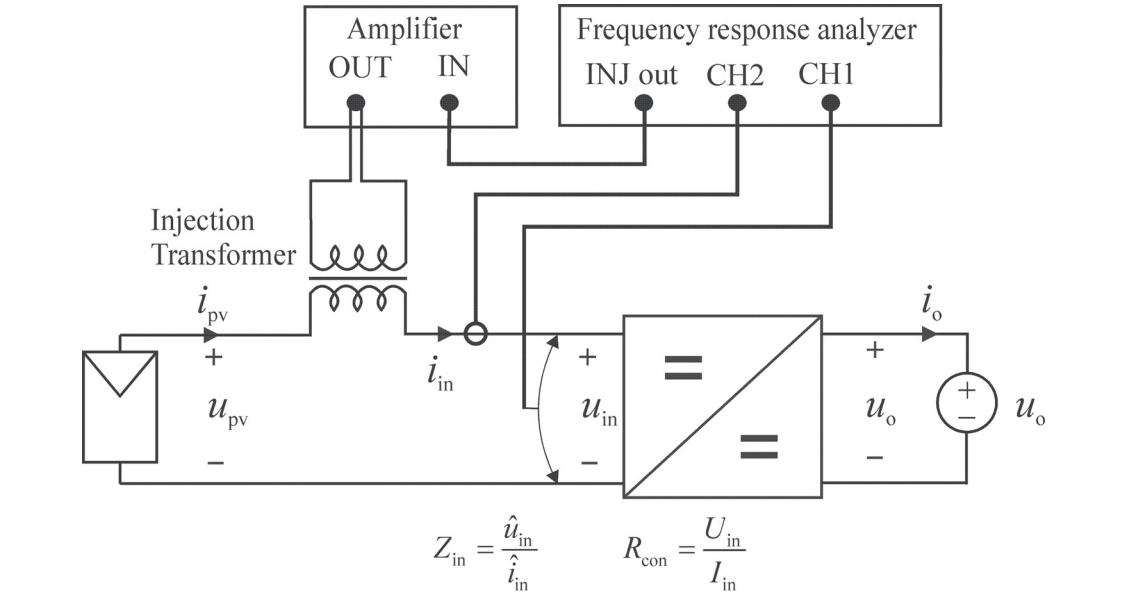

a)

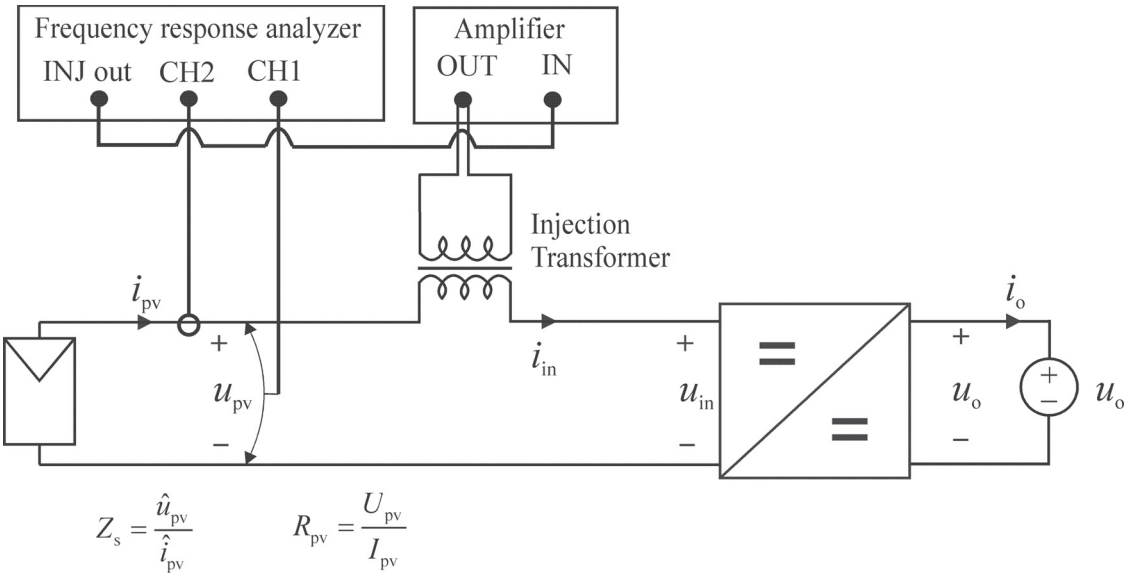

b)

Fig. G.1 Examples of frequency response measurements: a) measuring setup for ohmic characteristics of converter input and b) PV module output

Appendix H: Matlab code for VF superbuck converter

```
%%%%%%%%%%%%%%%%%%%%%%%%%%%%%%%%%%%%%%%%%%%%%%%%%%%%%%%%%%%%%%%%%%%%%%%%%%%%%%%
% Method to predict transfer functions of VF superbuck converter     %
% Tampere University of Technology                                   %
% Department of Electrical Energy Engineering                        %
% Jari Leppäaho / 2011                                               %
%%%%%%%%%%%%%%%%%%%%%%%%%%%%%%%%%%%%%%%%%%%%%%%%%%%%%%%%%%%%%%%%%%%%%%%%%%%%%%%

% Coupled inductor parameters
ne = 0.347; k = 0.260; L22 = 7.2138e-6; rL1 = 74e-3; rL2 = 32e-3;

% Operation point and component values
Uin = 17.3; Io = 1; fs = 400e3; Ts = 1/fs; Du = 0.625; Du_ = 1-Du;
C1 = 18.8e-6; C2 = 23.5e-6;

% Parasitics
rC1 = 100e-3; rC2 = 10e-3; rDS = 250e-3; rD  = 50e-3; UD  = 0.3;

% State-space model parameters
Lm = k*L22/(ne^2); Ll1 = L22*(1-k)/(ne^2); Ll2 = L22*(1-k);
L1 = Ll1+Lm; L2 = Ll2+Lm*ne^2; M = ne*Lm; X = L1*L2-M^2;
R1 = rL1+rC2+Du*rDS+Du_*(rD+rC1); R2 = rC2+Du*rDS+Du_*rD;
R3 = rL2+rC2+Du*(rDS+rC1)*Du_*rD;
U1 = Uin+UD+(rD-rDS+Du*rC1-Du*rL1+Du_*rL2)*Io; U2 = U1-rC1*Io;

s = tf('s')

% Coefficient matrices

Am = [-(L2*R1-M*R2)/X, -(L2*R2-M*R3)/X, -(L2*Du_+M*Du)/X, -(L2-M)/X;
     -(L1*R2-M*R1)/X, -(L1*R3-M*R2)/X,  (Du*L1+M*Du_)/X, -(L1-M)/X;
     Du_/C1, -Du/C1, 0, 0;
     1/C2, 1/C2, 0, 0];
Bm = [L2/X, (L2-M)*rC2/X, (L2*U1-M*U2)/X;
     -M/X, (L1-M)*rC2/X, (L1*U2-M*U1)/X;
     0, 0, -Io/C1;
     0, -1/C2, 0];
Cm = [1, 0, 0, 0;
     rC2, rC2, 0, 1];
Dm = [0, 0, 0;
     0, -rC2, 0];

% State-Space model (SSM) and system transfer function matrix (TFS)
SSM = ss(Am,Bm,Cm,Dm); TFS = tf(SSM);

% Transfer Functions
Yin = TFS(1,1);      % Input admittance
Gio = TFS(2,1);      % Input-to-output transfer function
Toi = TFS(1,2);      % Output-to-input transfer function
Zo = -TFS(2,2);      % Output impedance
Gci = TFS(1,3);      % Control-to-input transfer function
Gco = TFS(2,3);      % Control-to-output transfer function
```

Appendix I: Matlab code for CF superbuck converter

```
%%%%%%%%%%%%%%%%%%%%%%%%%%%%%%%%%%%%%%%%%%%%%%%%%%%%%%%%%%%%%%%%%%%%%%%%%%%%%%%
% Method to predict transfer functions of CF superbuck converter     %
% Tampere University of Technology                                   %
% Department of Electrical Energy Engineering                        %
% Jari Leppäaho / 2011                                               %
%%%%%%%%%%%%%%%%%%%%%%%%%%%%%%%%%%%%%%%%%%%%%%%%%%%%%%%%%%%%%%%%%%%%%%%%%%%%%%%

% Operation point and component values
Uo = 23; Iin = 0.962; Du = 0.57; fs = 400e3; L1 = 485e-6; L2 = 455e-6;
Ce1 = 1.1e-6; Ce2 = 3.1e-6;

% Parasitics
rc1 = 0.08; rc2 = 0.08; rL1 = 0.9; rL2 = 0.9; rds = 0.3; rd = 0.4;
Ud = 0.4;

% State-space model parameters
R1 = (1-Du)*(rc1 + rds) + Du*(rc2 + rd) + rL1;
R2 = (1 - Du)*rc1 - Du*rc2; R3 = rc1 + rc2 + rL2;
R4 = rc1; U1 = Uo + Ud + ((1-Du)*rc2 - Du*rc1 + Du*rL2 + rd - rds)*Iin;
U2 = (rc1 + rc2)*Iin; U3 = rc1*Iin;

s = tf('s');

% Coefficient matrices
Am = [0, 0, -(1-Du)/Ce1, -1/Ce1;
      0, 0, Du/Ce2, -1/Ce2;
      (1-Du)/L1, -Du/L1, -R1/L1, -R2/L1;
      1/L2, 1/L2, -R2/L2, -R3/L2]
Bm = [1/Ce1, 0, Iin/Ce1;
      0, 0, Iin/Ce2;
      (1-Du)*R4/L1, 0, -U1/L1;
      R4/L2, -1/L2, U2/L2]
Cm = [1, 0, -(1-Du)*R4, -R4;
      0, 0, 0, 1]
Dm = [R4, 0, U3;
      0, 0, 0]

% State-Space model (SSM) and system transfer function matrix (TFS)
SSM = ss(Am,Bm,Cm,Dm); TFS = tf(SSM);

% Transfer Functions
Zin = TFS(1,1);      % Input impedance
Gio = TFS(2,1);      % Input-to-output transfer function
Toi = TFS(1,2);      % Output-to-input transfer function
Yo = -TFS(2,2);      % Output admittance
Gci = TFS(1,3);      % Control-to-input transfer function
Gco = TFS(2,3);      % Control-to-output transfer function
```

Appendix J: Matlab code for CF boost converter

```
%%%%%%%%%%%%%%%%%%%%%%%%%%%%%%%%%%%%%%%%%%%%%%%%%%%%%%%%%%%%%%%%%%%%%%%%%%%%%%%
% Method to predict transfer functions of CF boost converter                   %
% Tampere University of Technology                                             %
% Department of Electrical Energy Engineering                                  %
% Jari Leppäaho / 2011                                                         %
%%%%%%%%%%%%%%%%%%%%%%%%%%%%%%%%%%%%%%%%%%%%%%%%%%%%%%%%%%%%%%%%%%%%%%%%%%%%%%%

% Operation point and component values
Uo = 6; Iin = 1; Du = 0.6; IL = Iin/(1-Du); fs = 400e3; Ts = 1/fs;
L1 = 47e-6; C1 = 5e-6;

% Parasitics, modified for synchronous mode
rc = 0.004; ri = 0.1; rds = 0.015; rd = 0.015; Ud = 0.0;

% State-space model parameters
Uc = (((1-Du)*rds + Du*rd + (1-Du)*rc + ri)*IL - (1-Du)*rc*Iin +
Du*Ud+Uo)/(1-Du)

s = tf('s');

% Coefficient matrices
Am = [-(ri + Du*rd + (1-Du)*rds + (1-Du)*rc)/L1, (1-Du)/L1
       -(1-Du)/C1, 0]
Bm = [((1-Du)*rc)/L1, -1/L1, (-(rd - rds - Du*rc)*IL - Uc - Ud)/L1
       1/C1, 0, IL/C1]
Cm = [-(1-Du)*rc, 1
        1, 0]
Dm = [rc, 0, rc*IL
       0, 0, 0]

% State-Space model (SSM) and system transfer function matrix (TFS)
SSM = ss(Am,Bm,Cm,Dm);
TFS = tf(SSM);

% Transfer Functions
Zin = TFS(1,1);      % Input impedance
Gio = TFS(2,1);      % Input-to-output transfer function
Toi = TFS(1,2);      % Output-to-input transfer function
Yo = -TFS(2,2);      % Output admittance
Gci = TFS(1,3);      % Control-to-input transfer function
Gco = TFS(2,3);      % Control-to-output transfer function
```

Appendix K: Matlab code for PCM CF boost converter

```
%%%%%%%%%%%%%%%%%%%%%%%%%%%%%%%%%%%%%%%%%%%%%%%%%%%%%%%%%%%%%%%%%%%%%%%%%%%%%%%
% Method to predict transfer functions of PCMC CF boost converter    %
% Tampere University of Technology                                   %
% Department of Electrical Energy Engineering                        %
% Jari Leppäaho / 2011                                               %
%%%%%%%%%%%%%%%%%%%%%%%%%%%%%%%%%%%%%%%%%%%%%%%%%%%%%%%%%%%%%%%%%%%%%%%%%%%%%%%

% Operation point and component values
Uo = 6; Iin = 0.96; Du = 0.69; Du2 = (1-Du); IL = Iin/Du; fs = 400e3;
Ts = 1/fs; L = 15e-6; C1 = 5e-6; C2 = 33e-6;

% Parasitics, synchronous mode
rc1 = 0.004; rc2 = 0.004; ri = 0.1; rds1 = 0.015; rds2 = 0.015;

% State-space model parameters
R1 = Du2*rds2 + Du*rds1 + Du*rc1 + ri;
U1 = (Uo/Du)+(rds2+ri)*Iin/(Du^2);
Uc1 = Uo/Du + ((Du*Du2*rc1 + Du2*rds2 + Du*rds1 + ri)*Iin)/(Du^2);

% Peak-current-mode control
Mc = 0.5e6; Rs = 33/100;
Fm = 1/(Ts*(Mc + ((Du2-Du)*(Du*Uo + (ri + rds2)*Iin))/(2*L*Du^2)));
qL = 1 - (Du*Du2*Ts/(2*L))*(rc1 + rds1 - rds2);
qC1 = Du*Du2*Ts/(2*L); qin = Du*Du2*Ts*rc1/(2*L);

s = tf('s');

% Coefficient matrices
Am = [-(R1+(Fm*qL*U1))/L, (Du-(Fm*qC1*U1))/L, 0
      -(Du-(Fm*qL*IL))/C1, (Fm*qC1*IL)/C1, 0
      0, 0, -1/(rc2*C2)]
Bm = [(Du*rc1-(Fm*qin*U1))/L, -1/L, (Fm*U1)/L
       (1+(Fm*qin*IL))/C1, 0, -(Fm*IL)/C1
       0, 1/(C2*rc2), 0]
Cm = [((Fm*qL*rc1*IL)-Du*rc1), (1+(Fm*rc1*IL)), 0
      1, 0, 1/rc2]

Dm = [(rc1 + (Fm*rc1*IL*qin)), 0, -Fm*rc1*IL
      0, -1/rc2, 0]

% State-Space model (SSM) and system transfer function matrix (TFS)
SSM = ss(Am,Bm,Cm,Dm);
TFS = tf(SSM);

% Transfer Functions
Zin = TFS(1,1);      % Input impedance
Gio = TFS(2,1);      % Input-to-output transfer function
Toi = TFS(1,2);      % Output-to-input transfer function
Yo = -TFS(2,2);      % Output admittance
Gci = TFS(1,3);      % Control-to-input transfer function
Gco = TFS(2,3);      % Control-to-output transfer function
```

Appendix L: Matlab code for solving effect of non-ideal source and load

```
%%%%%%%%%%%%%%%%%%%%%%%%%%%%%%%%%%%%%%%%%%%%%%%%%%%%%%%%%%%%%%%%%%%%%%%%%%%%%%%
% Method to include the effect of non-ideal source and load into the %
% nominal transfer functions of CF converter (H parameters)          %
% Tampere University of Technology                                   %
% Department of Electrical Energy Engineering                        %
% Jari Leppäaho / 2011                                               %
%%%%%%%%%%%%%%%%%%%%%%%%%%%%%%%%%%%%%%%%%%%%%%%%%%%%%%%%%%%%%%%%%%%%%%%%%%%%%%%

%%% EFFECT OF NON-IDEAL SOURCE, i.e. ideal current source I_ins with Ys
r_dyn = 100;    % Example value of low-frequency impedance of
                % PV generator, i.e. dynamic resistance
                % (operation-point  dependent)
Ys = (1/r_dyn); % Operation-point dependent admittance of
                % PV generator (can substituted with measured response)

Zin_oco = Zin + (Gio*Toi/Yo);   % Input impedance at
                                % open-circuited output
Zin_inf = Zin + (Toi*Gco/Gci);  % Ideal input impedance
Zin_S = Zin/(1 + Ys*Zin);       % Source-affected input impedance
Gio_S = Gco/(1 + Ys*Zin);       % Source-affected input-to-output
                                % transfer function
Toi_S = Toi/(1 + Ys*Zin);       % Source-affected output-to-input
                                % transfer function
Yo_S = -(1 + Ys*Zin_oco)*Yo/(1 + Ys*Zin); % Source-affected
                                          % output impedance
Gci_S = Gci/(1 + Ys*Zin);       % Source-affected control-to-input
                                % transfer function
Gco_S = (1 + Ys*Zin_inf)*Gco/(1 + Ys*Zin); % Source-affected
                                           % control-to-output
                                           % transfer function

%%% EFFECT OF NON-IDEAL LOAD, i.e. ideal battery voltage e_o with ZL
r_bat = 1;      % Example value of the low-frequency impedance of
                % battery
ZL = r_bat;     % Impedance of battery (can be substituted with
                % measured response)
Yo_sci = Zin + (Gio*Toi/Yo);   % Output admittance at
                               % short-circuited input
Yo_inf = Zin + (Toi*Gco/Gci);  % Ideal output admittance

Zin_L = (1 + ZL*Yo_sci)*Zin/(1 + ZL*Yo); % Load-affected
                                         % input impedance
Gio_L = Gio/(1 + ZL*Yo);       % Load-affected input-to-output
                               % transfer function
Toi_L = Toi/(1 + ZL*Yo);       % Load-affected output-to-input
                               % transfer function
Yo_L = -Yo/(1 + ZL*Yo);        % Load-affected output impedance
Gci_L = (1 + ZL*Yo_inf)*Gci/(1 + ZL*Yo); % Source-affected
                                         % control-to-input
                                         % transfer function
Gco_L = Gco/(1 + ZL*Yo);       % Load-affected control-to-output
                               % transfer function
```

Appendix M: Measurement setup, lamp unit and PV module

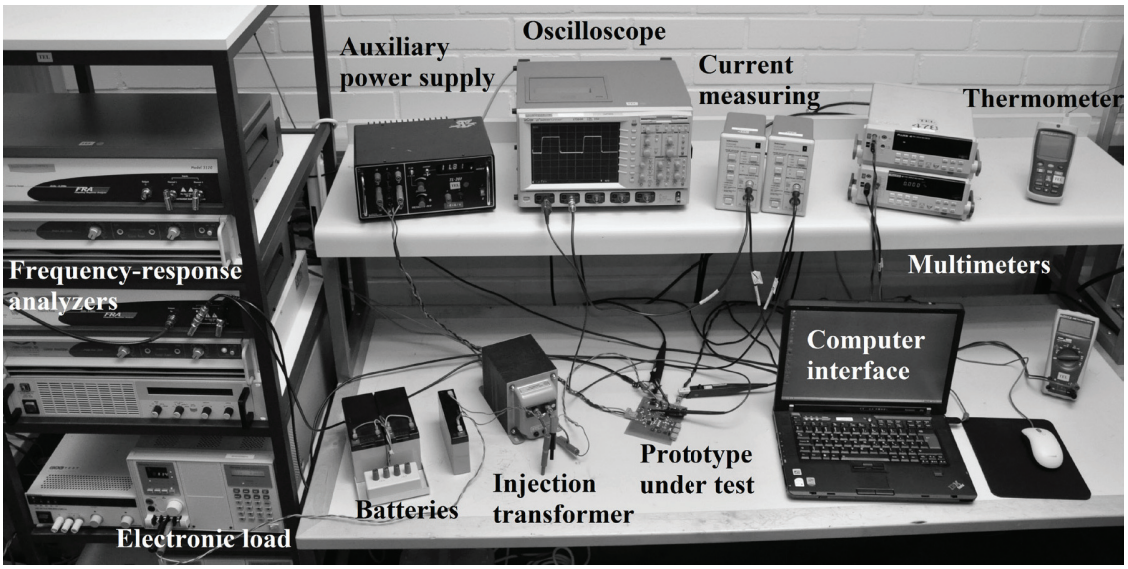

a)

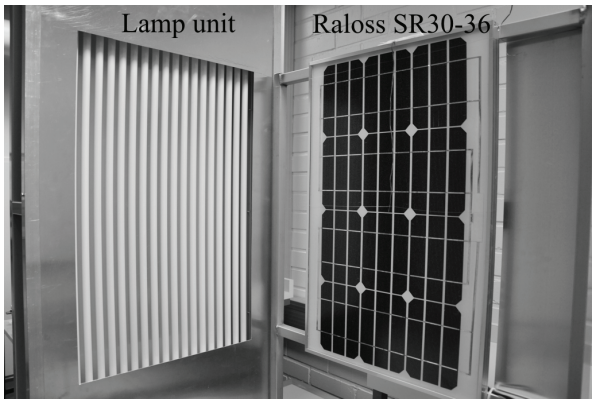

b)

Fig. M.1 a) Measurement setup in laboratory and b) lamp unit and PV module used in the experiments

Appendix N: Experimental converter prototypes

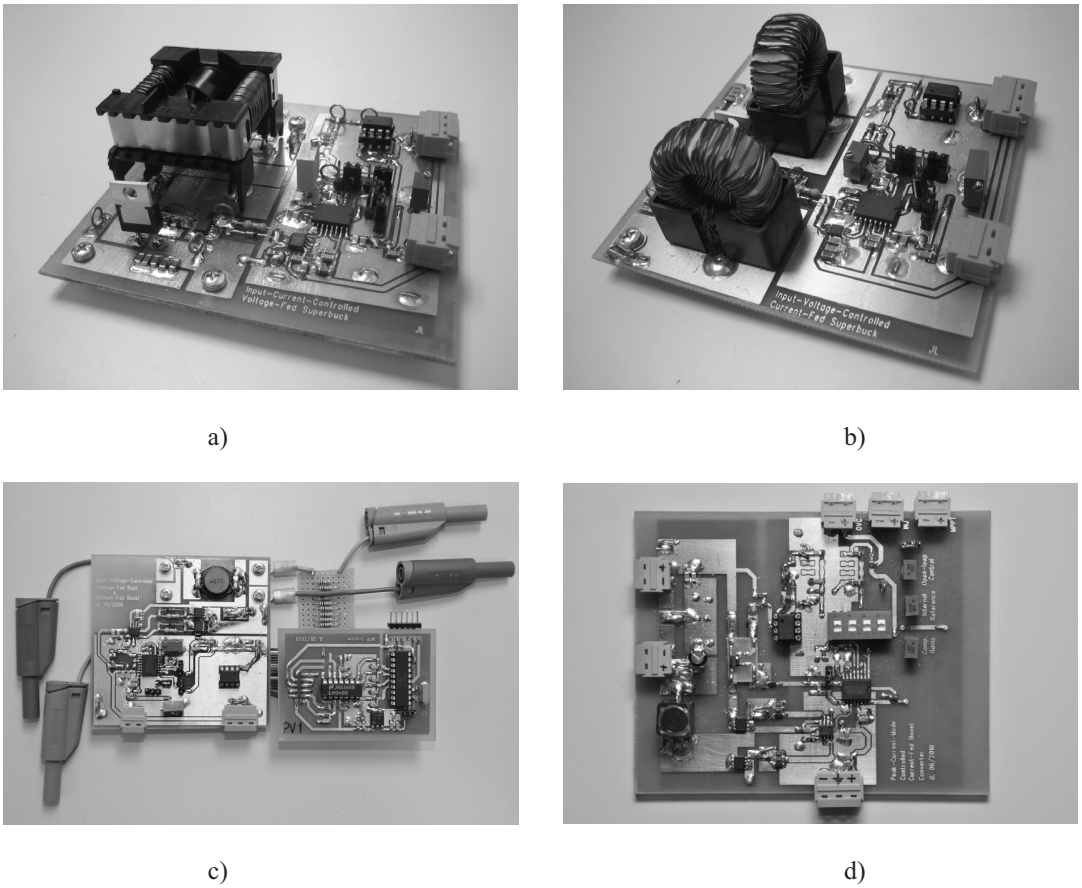

a) b)

c) d)

Fig. N.1 a) Input-current-controlled VF superbuck converter, b) input-voltage-controlled CF superbuck converter, c) buck-derived PV converter with MPP-tracker and c) PCM-controlled buck-derived PV converter

Appendix O: Control block diagrams of the tested converters

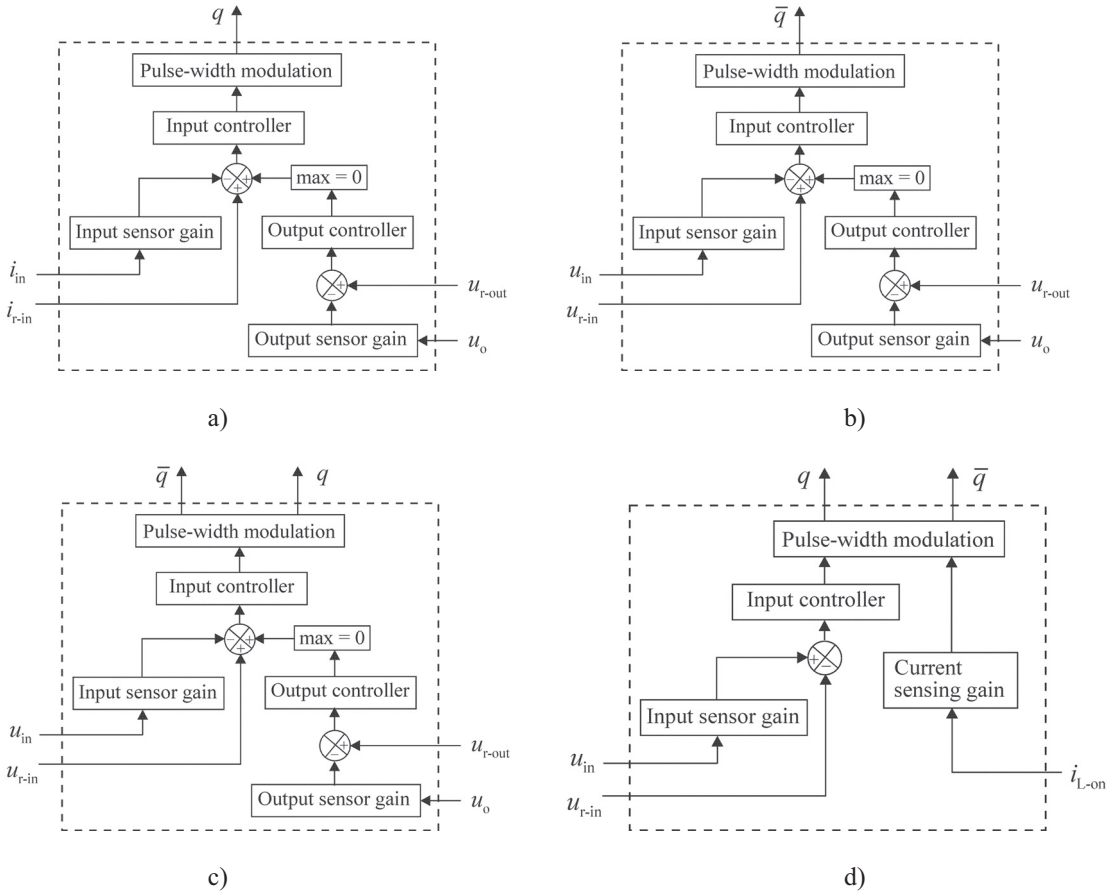

Fig. O.1 Control block diagrams of a) VF superbuck converter, b) CF superbuck converter, c) buck-derived PV converter (i.e., CF boost) and c) PCM-controlled buck-derived PV converter (i.e., CF boost)

Publications

Tampereen teknillinen yliopisto
PL 527
33101 Tampere

Tampere University of Technology
P.O.B. 527
FI-33101 Tampere, Finland

ISBN 978-952-15-2667-1
ISSN 1459-2045